Identified, putative pacemaker neurons of the medial septum lead the hippocampal network during theta activity

Doctoral dissertation

Dr. Balázs Hangya

Semmelweis University
János Szentágothai School of Ph. D. studies

Supervisor: Dr. Zsolt Borhegyi senior research fellow, Ph.D.

Official opponents: Dr. Anita Kamondi professor, Ph.D.
Dr. Zoltán Somogyvári senior research fellow, Ph.D.

Chairman of terminal exam committee: Dr. András Csillag professor, D.SC.
Members of terminal exam committee: Dr. György Karmos professor, Ph.D.
Dr. Árpád Dobolyi senior research fellow, Ph.D.

Budapest
2009

Table of contents

Abbreviations

a: nucleus accumbens

A: anterior

ab: angular bundle

ac: autocorrelogram

al: alveus

AP: ascending phase

B: baseline

BI: burstiness index

bst: bursting

CA: cornu ammonis; anterior commissure in Figure 7

cAMP: cyclic adenosine monophosphate

CCA: corpus callosum

CCK: cholecystokinin

cGMP: cyclic guanosine monophosphate

CGRP: calcitonin gene-related peptide

ChAT: cholin acetyltransferase

CNBD: cyclic nucleotide binding domain

CO: optic chiasma

CWT: Continuous Wavelet Transform

DBB: diagonal band of Broca

DF: preferred direction of flow

DG: dentate gyrus

EC: entorhinal cortex

EEG: electroencephalogram

fi: fimbria

GABA: gamma-aminobutyric acid

GAD: glutamate decarboxylase

gcl: granule cell layer of the dentate gyrus

HCN: hyperpolarization activated and cyclic nucleotide gated non-selective cation channel

HCN-IR: HCN-immunoreactive

HDB: horizontal limb of the diagonal band of Broca

hf: hippocampal fissure

int: interneuron

int(a/o): interneuron from the stratum oriens/alveus

int(pyr): interneuron from the pyramidal layer

IS: interneuron-selective interneurons

ISI: interspike interval

LFP: local field potential

LHRH: luteinizing hormone-releasing hormone

LIA: large amplitude irregular activity

lm: light micrograph

ml: molecular layer of the dentate gyrus

MS: medial septum

MS-DBB: medial septum - diagonal band of Broca complex

MVL: mean vector length

Nb: Neurobiotin

nbst: non-bursting

ND: not detected

NPY: neuropeptide Y

NT: not tested

NTE: normalized transfer entropy

nucl: nucleus

O-LM: oriens lacunosum moleculare (associated) cell

Para: parasubiculum

pcl: pyramidal cell layer of the hippocampus

pl: polymorphic layer of the dentate gyrus

Pre: presubiculum

PV: parvalbumin

PV-IR: parvalbumin-immunoreactive

pyr: pyramidal neuron

R: ripple

REM: rapid eye movement

RMS: root mean square

SD: standard deviation

SIA: small amplitude irregular activity

sl: stratum lucidum of CA3

sr: stratum radiatum of the hippocampus

sl-m: stratum lacunosum moleculare of the hippocampus

SP: substance P

SPW: sharp wave-ripple complex

Sub: subiculum

T: trough

TBS: Tris-buffered saline

TE: transfer entropy

TP: tail pinch

TPI: theta propensity index

VDB: vertical limb of the diagonal band of Broca

VIP: vasoactive intestinal polypeptide

Introduction

Mnemonic functions of the hippocampus critically rely on its interaction with subcortical regions, particularly on reciprocal connections with the medial septum (MS). Information transmission between the MS and the hippocampus was assumed to be fundamentally different during the two major hippocampal activity patterns, the 4 to 10 Hz theta rhythm and the large amplitude irregular activity (Borhegyi et al., 2004). A large body of experimental and modeling data points to the critical role of the MS in synchronizing the hippocampal network during theta oscillation (Wang, 2002). However, a direct evidence for septal pacing of hippocampal theta is still lacking. Furthermore, the classical view of medial septal theta formation has recently been debated based on an in vitro study suggesting intrahippocampal theta genesis (Manseau et al., 2008). Here we review the basic anatomical and physiological aspects of the septo-hippocampal system, with a special emphasis on the formation of hippocampal theta activity.

The hippocampus

The hippocampus plays a pivotal role in the formation and maintenance of declarative memory traces (i.e., episodic and semantic memory; Squire, 1992) and in spatial navigation (O'Keefe, 1976). Recent evidence indicates that all of these hippocampal functions are mediated via the sequential activation of dynamically changing hippocampal cell assemblies (Pastalkova et al., 2008). Population level activity of these hippocampal ensembles can be manifested in a highly regular, 4 to 10 Hz oscillatory pattern of the local field potential, the so-called theta rhythm, associated to exploration, orientation and rapid eye movement (REM) sleep (Vanderwolf et al., 1977). This report focuses on the subcortical control of hippocampal theta-synchronization, hence we provide a brief overview of hippocampal anatomy and population activity patterns in the following sections.

Anatomy of the hippocampus

The hippocampus is part of the so-called hippocampal formation, which also includes the dentate gyrus, the presubiculum, the parasubiculum and the entorhinal cortex. The hippocampus proper is further divided to three regions, named CA1, CA2 and CA3 (from the subiculum to the hilus) after the traditional term 'cornu ammonis' (Fig. 1A, Fig. 6) (De Garengeot, 1742; Andersen et al., 2007), identified by Rafael Lorente de Nó (Lorente de Nó, 1934). The distinction between these areas is based on cytoarchitectonic differences (Ramon y Cajal, 1893), which are accompanied by different connectivity patterns (see below).

Cytoarchitectonic organization

Its highly regular laminar organization made the hippocampus an ideal candidate of neuroanatomic and neurophysiologic research over the past decades (Fig. 1B-C). The pyramidal cells, which form the main output source of the hippocampus and provide the 90% of all hippocampal neurons, are comprised in the pyramidal layer. Deep to this layer a thin, fiber-rich layer can be found, called stratum oriens. It contains the proximal basal dendrites and axons of the pyramidal cells as well as some of the recurrent connections in the CA3 and Shaffer collateral connections in the CA1. Below the stratum oriens is the narrow, fiber-containing alveus. In CA3, the stratum lucidum, a thin, relatively cell-free layer is located above the pyramidal layer, which contains the mossy fiber inputs from the dentate gyrus. Superficial to this layer in CA3 and to the pyramidal layer in CA2 and CA1, the relatively fiber-rich layer stratum radiatum can be identified. It contains the pyramidal neurons' apical dendrites, CA3 to CA3 associational connections and CA3 to CA1 Shaffer collateral connections. Stratum lacunosum moleculare, the most superficial layer of the hippocampus, comprises the branching segments of pyramidal apical dendrites. It also contains incoming fibers from the entorhinal cortex as well as other brain regions (e.g. nucl. reuniens) (Andersen et al., 2007; Paxinos, 2004). The hippocampus contains a great variety of interneurons, located mostly in the strata pyramidale, radiatum and lacunosum moleculare (Freund and Buzsaki, 1996; Klausberger and Somogyi, 2008).

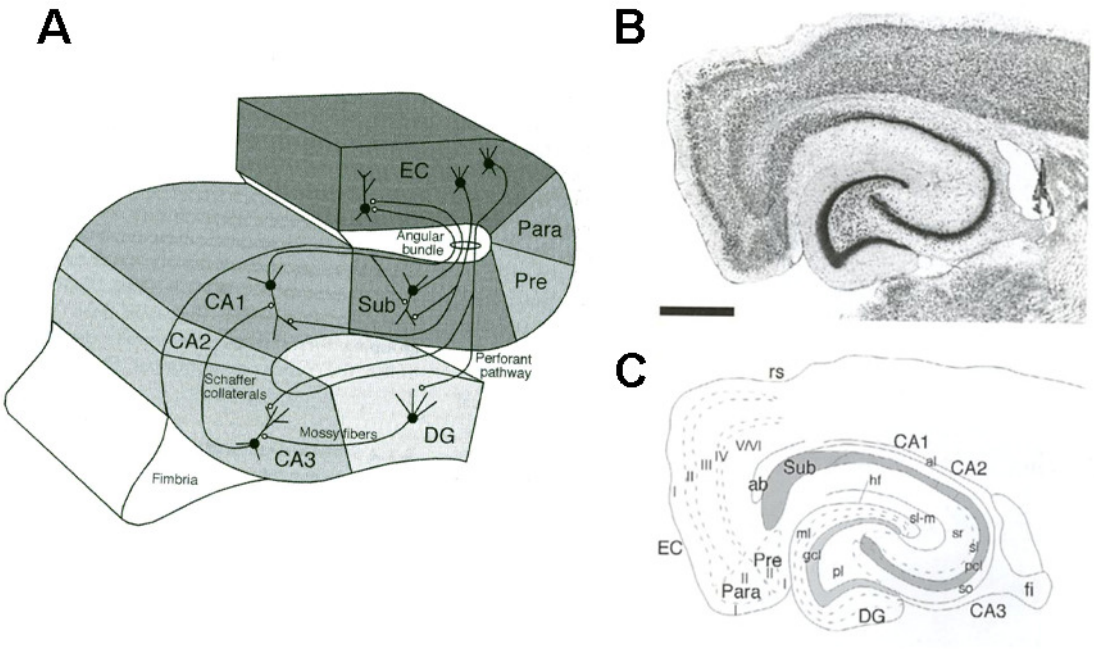

Figure1. Anatomy of the hippocampus. A: Schematic view of the hippocampal formation and its basic structural connectivity. **B**: Nissl staining of a horizontal section from the rat hippocampus. **C**: Line drawing of the same view displaying hippocampal regions and layers. ab, angular bundle; al, alveus; CA, cornu ammonis; DG, dentate gyrus; EC, entorhinal cortex; fi, fimbria; gcl, granule cell layer of the dentate gyrus; hf, hippocampal fissure; ml, molecular layer of the dentate gyrus; Para, parasubiculum; pcl, pyramidal cell layer of the hippocampus; pl, polymorphic layer of the dentate gyrus; Pre, presubiculum; sl, stratum lucidum of CA3; sr, stratum radiatum of the hippocampus; sl-m, stratum lacunosum moleculare of the hippocampus; Sub, subiculum. Roman numbers: cortical layers. Scale bar: 500 μm. *Source: Andersen et al., 2007*.

Neurons of the hippocampus

The principal cells of the hippocampus are the glutamatergic pyramidal neurons, which constitute the vast majority of neurons in the hippocampus. They represent the main output of the hippocampus towards the entorhinal cortex and the lateral septum. Pyramidal cells in different areas of the hippocampus have distinct connectivity

patterns, as we discuss it shortly. Also, pyramidal cells in the CA1 region are, on average, smaller than that of the CA2 and CA3 (Andersen et al., 2007).

Although GABAergic interneurons constitute only ten percent of all hippocampal neurons, they play a key role not only in the stabilization of the hippocampal network, but also in the precise timing of pyramidal cell activity (Cutsuridis et al., 2009; Somogyi and Klausberger, 2005). Hippocampal interneurons form an extremely heterogeneous population based on their morphologic, neurochemical and electrophysiological properties (Freund and Buzsaki, 1996; Klausberger and Somogyi, 2008). Here, we provide a brief review of the most common types of hippocampal interneurons.

Interneurons in the class of *perisomatic inhibitory cells* target the cell bodies, proximal dendrites or axon initial segments of the pyramidal cells. They have a pivotal role in controlling pyramidal neuron output. Somata of basket cells are located in the pyramidal layer (Fig. 2). Their dendritic trees extend to the stratum oriens, stratum radiatum and stratum lacunosum-moleculare. Basket cells receive inhibitory input from intra- and extrahippocampal sources, whereas their excitatory inputs mainly arise from hippocampal pyramidal neurons. These cells provide efficient inhibitory connections to pyramidal cell somata and proximal dendrites. Two major classes of basket cells express cholecystokinin (CCK) or parvalbumin (PV). CCK-containing basket cells express a large repertoire of neuromodulatory receptors, require extensive integration of excitatory inputs to reach firing threshold and might participate in the modulation of pyramidal cell action potential timing. PV-immunopositive basket cells have few receptors for neuromodulatory molecules, are quickly recruited by excitatory input and transmit effective inhibition of principal cell activity (Karson et al., 2009; Freund, 2003; Freund and Katona, 2007).

Another characteristic type of perisomatic inhibitory cells is the so-called axo-axonic (or chandelier) cell, also located in, or adjacent to, the pyramidal layer. Dendritic trees of the axo-axonic cells span all layers of the hippocampus, whereas their axons terminate on the axon initial segments of pyramidal neurons (Freund and Buzsaki, 1996).

Dendritic inhibitory cells target principal neuron dendrites and are designed to control the efficacy of excitatory input on pyramidal neurons. The oriens lacunosum

moleculare (associated) cell (O-LM), expands its axonal arbor to the stratum lacunosum molculare, where the entorhinal afferents terminate (Lacaille et al., 1987). The soma and the dendrites of these cells are located in those layers in which the recurrent collaterals of the pyramidal neurons can be found. In CA3, this comprises all strata except lacunosum moleculare, whereas in the CA1, it confines to stratum oriens (Freund and Buzsaki, 1996).

Somata of the bistratified cells are inside or close to the pyramidal layer. Multipolar dendritic arbor of the latter cells expands the stratum oriens and the stratum radiatum, but usually do not reach the stratum lacunosum moleculare. Bistratified cells send axon collaterals to the stratum oriens as well as to the deep portion of the stratum radiatum, where they terminate on the dendritic spines and dendritic shafts of the pyramidal neurons (Andersen et al., 2007).

An additional type of dendritic inhibitory cells is the neurogliaform cell. Their cell bodies are in the stratum lacunosum moleculare. Also, most of their axonal and dendritic processes can be found in the same layer, albeit they may penetrate the stratum radiatum. Neurogliaform cell axons innervate the apical dendritic tuft of pyramidal neurons (Klausberger and Somogyi, 2008).

Recently, a new type of hippocampal interneurons has been described by Fuentealba and colleagues (Fuentealba et al., 2008). The cell bodies of “Ivy cells” are found in the stratum pyramidale. They innervate the basal and oblique dendrites of pyramidal cells, express nitric oxide synthase and neuropeptide Y.

Interneuron-selective interneurons (IS) are located in all layers of the hippocampus and can be identified based upon their calretinin content. IS neurons selectively innervate other hippocampal interneurons (Freund and Buzsaki, 1996).

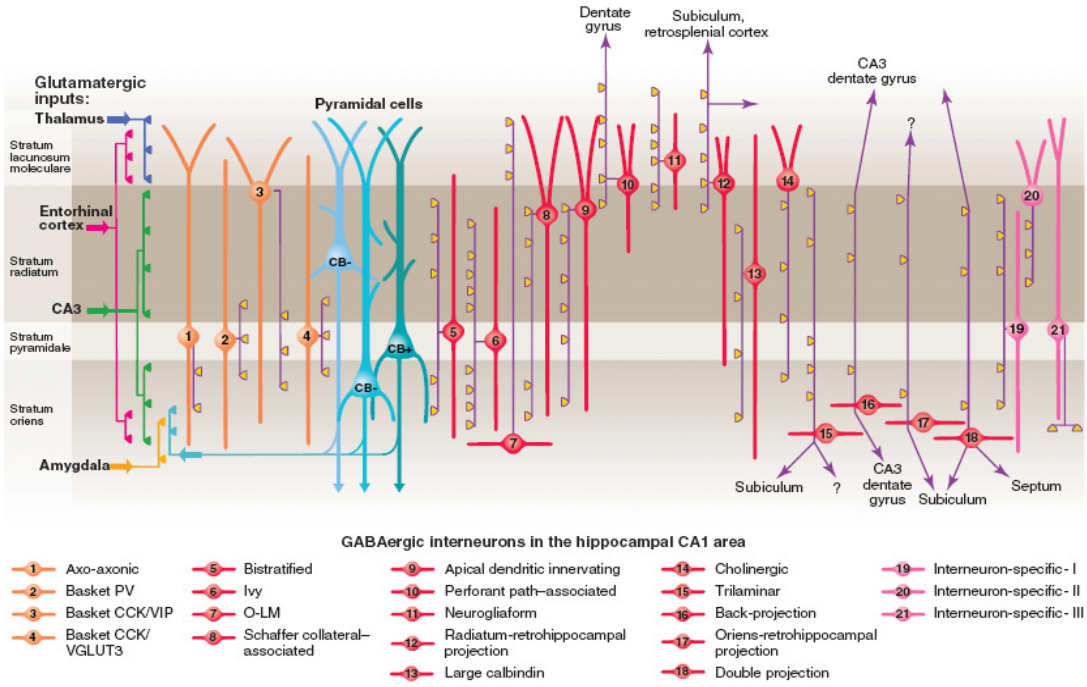

Figure 2. Types of hippocampal interneurons and pyramidal cells. Orange, cell bodies and dendrites of perisomatic inhibitory cells; red, dendritic inhibitory cells; pink, IS interneurons; blue, pyramidal cells; purple, axons; yellow, synaptic terminations. Glutamatergic excitatory inputs to the hippocampus are indicated on the left.

Source: Klausberger and Somogyi, 2008

Hippocampal connectivity

Hippocampal circuitry is dominated by the so-called trisynaptic loop. The first synapse is formed on the granule cells of the dentate gyrus by the perforant path input arising from the entorhinal cortex (Ramon y Cajal, 1893). This pathway originates mainly from the second layer of the medial and lateral entorhinal cortex and terminates in the outer molecular layer of the dentate gyrus. Fibers arising from the lateral entorhinal cortex occupy the outer third of the molecular layer, whereas those coming from the medial entorhinal cortex penetrate the middle third (van Strien et al., 2009). Perforant path axons also give collaterals to the CA3 and CA2 regions of the hippocampus, where they terminate in the stratum lacunosum-moleculare with a similar laminar distribution profile as in the dentate gyrus (Andersen et al., 2007). The second synapse of the trisynaptic loop is established by the axons of the dentate granule cells, which are called mossy fibers. They produce large terminals (up to 8 μm in diameter) on

the proximal apical dendrites of CA3 pyramidal cells, forming the stratum lucidum, a narrow layer between stratum pyramidale and stratum radiatum unique to the CA3 area (Swanson et al., 1978; Acsady et al., 1998). Additionally, mossy fibers innervate a great variety of hippocampal interneurons (Acsady et al., 1998; Szabadics and Soltesz, 2009). The third synapse of the loop is formed between the Schaffer collaterals of CA3 pyramidal cell axons and the proximal apical and basal dendrites of CA2 and CA1 pyramidal neurons in the stratum radiatum and the stratum oriens (Ishizuka et al., 1990; Li et al., 1994). Return projections from the hippocampus to the entorhinal cortex originate in the CA1 but not in the CA2 and the CA3 (Naber et al., 2001). These fibers terminate mostly in the deep layers (V and VI) of the entorhinal cortex. The CA1 also gives rise to a subicular projection (Amaral et al., 1991). Additionally, layer III pyramidal neurons of the entorhinal cortex projects directly to the CA1 via the temporoammonic pathway, where they innervate the distal dendrites of CA1 pyramidal cells (Speed and Dobrunz, 2009).

The hippocampus is extremely rich in intrinsic connections. Additional to the Schaffer collaterals already mentioned, CA3 to CA3 (and CA2) associational connections are formed by the recurrent collaterals of CA3 pyramidal neurons in the stratum radiatum and the stratum oriens (Ishizuka et al., 1990; Li et al., 1994). CA1 to CA1 associational connections are much less pronounced and are restricted to the stratum oriens. In the rat, CA3 pyramidal neurons give rise to a dense commissural projection to the contralateral CA3, CA2 and CA1 (Blackstad, 1956). Similar to ipsilateral CA3 to CA3, CA2 or CA1 connections, these fibers also terminate on proximal dendrites of pyramidal neurons in the stratum radiatum and the stratum oriens. Commisural connections are less pronounced in the monkey and the human brain.

The main output structure of the hippocampal formation is the entorhinal cortex, which maintains reciprocal connections with a wide range of neocortical areas. In a sharp contrast, CA2 and CA3 are not connected with any neocortical regions. CA1, besides its reciprocal connection with the entorhinal cortex mentioned above, sends pyramidal axons to the perirhinal and postrhinal cortices. These areas also project back to the CA1. Additionally, the CA1 field is recirpocally connected with the amygdaloid complex (Pikkarainen et al., 1999; Pitkanen et al., 2000). Besides excitatory output, the

hippocampus sends long-range GABAergic projections to the subiculum, the medial septum and the retrosplenial cortex (Jinno et al., 2007).

The dominant subcortical input of the hippocampal formation arises from the medial septum - diagonal band of Broca (MS-DBB) complex. Septal GABAergic and cholinergic fibers terminate in the stratum oriens, and, to a lesser extent, in the stratum radiatum of all fields of the hippocampus. Hippocampal pyramidal neurons also project back to the septal complex (see The medial septum subsection for further details).

CA2 receives inputs from the posterior hypothalamus, especially from the nucl. supramammillaris and the nucl. tuberomammillaris. These fibers distribute in and near the stratum pyramidale and terminate mostly on principal cells (Magloczky et al., 1994). Nucl. reuniens and probably other midline thalamic nuclei send excitatory input to the CA1 pyramidal cells and interneurons. Additionally, the hippocampus receives noradrenergic, serotonergic and dopaminergic brain stem input from the locus coeruleus, the dorsal and median raphe nuclei and the ventral tegmental area, respectively (Andersen et al., 2007).

Electrophysiology of the hippocampus

Hippocampal activity patterns

Two dominant types of hippocampal activity states can be distinguished based on the population activity of hippocampal cells, also reflected in different patterns of local field potential (LFP) (Whishaw and Vanderwolf, 1973; Vanderwolf, 2001). Large amplitude, irregular activity (LIA) can be observed during consummatory behavior, quiet sitting, grooming and slow wave sleep. In contrast, during exploration, orientation and REM sleep, a highly regular, 4 to 10 Hz oscillation called theta rhythm appears (Vanderwolf et al., 1977; Buzsaki et al., 1983; Buzsaki, 2002).

Theta oscillation. Hippocampal theta oscillation was discovered by Jung and Kornmuller (1938) in the rabbit hippocampus. The first description of behavioral correlates of the theta rhythm was provided by Grastyan et al. (1959), who observed hippocampal theta oscillation during the early orientation phase of a reward discrimination task. By this time, a large body of evidence indicates that hippocampal theta oscillation is closely related to most learning and memory functions of the

hippocampus (see Buzsaki et al., 2002 and references therein). At least two types of theta oscillation exist in rodents. Theta synchronization linked to arousal or attention can be discriminated upon pharmacological (sensitive to atropine, resistant to urethane) and physiological (lower frequency with a spectral peak between 6 and 7.5 Hz in freely moving animals) bases (Fig. 3A-B). The other type is associated to voluntary movements, e.g. walk, slow run, head or limb movements (resistant to atropine but sensitive to urethane, characterized by higher frequency with a spectral peak between 7 and 9 Hz) (Kramis et al., 1975). Theta during REM sleep shares some characteristics with both above types and might be considered as a third form of hippocampal theta-band field activity. The medial septum is essential for the formation of all types of hippocampal theta (see "The medial septum" subsection for details). Besides the septum, the entorhinal cortex may also participate in the generation of the atropine-resistant type of theta oscillation. Other brain regions as the supramammillary area and the raphe nuclei were also suggested to take part in this process (Vertes and Kocsis, 1997; Buzsaki, 2002).

Three possible functions of hippocampal theta has been suggested (Andersen et al., 2007). First, hippocampal theta may serve as a general synchronization framework, providing a basis for correlated activity in distant hippocampal and, probably, also extrahippocampal areas. Second, hippocampal theta oscillation might provide a clocking system for hippocampal neurons, which theory is supported by the precise timing of hippocampal interneurons relative to hippocampal theta (Klausberger and Somogyi, 2003) and the phase precession of hippocampal place cells (O'Keefe and Recce, 1993). Third, theta might also act as a regulator of hippocampal long term potentiation and thus that of encoding and retrieval of hippocampal memory traces. Accordingly, it was suggested that different phases of the theta cycle provide windows for different directions of communication between the hippocampus and the entorhinal cortex (Hasselmo, 2005).

The detection of theta oscillation in humans faced several problems. First, emergence of a coherent oscillatory pattern requires not only synchronized rhythmic neuronal activity, but also appropriate anatomical configuration. Differences in location and cytoarchitecture between rodent and human hippocampus might account for worse detectability of theta oscillation in the human EEG. Also, most human studies dealt with

scalp electrodes, collecting data from a wide range of the cortex filtered by the skull and the scalp, which might distort the signals (Buzsaki, 2006; Andersen, 2007). However, Kahana and colleagues demonstrated the existence of hippocampal theta oscillation in the human hippocampus during navigation in a virtual reality maze using invasive recording technique (Fig. 3C) (Kahana et al., 1999; Cantero et al., 2003; Caplan et al., 2003; Ekstrom et al., 2005; Ekstrom et al., 2007). Additionally, a regular oscillation with a frequency between 1.5 and 3 Hz was proposed as the counterpart of rodent theta rhythm during human REM sleep in a study of Bodizs and colleagues (Bodizs et al., 2001).

Large amplitude irregular activity. During low arousal states (e.g. eating, drinking, grooming and slow wave sleep), an irregular local field activity can be recorded from the hippocampus that lacks a clear spectral peak characteristic to theta oscillation (Fig. 3A-B). Instead, a pink noise spectrum appears, which is dominated by low frequencies of the delta range (0.5 to 4 Hz) and below. During LIA activity, large amplitude sharp waves can be detected in the hippocampal LFP, most frequently in slow wave sleep and during quiet sitting. Each sharp wave lasts 50-100 ms and has its peak amplitude in the stratum radiatum that can reach 1 mV (Andersen et al., 2007). Around the peak of sharp waves, short duration, high frequency (120 to 200 Hz) oscillations appear called ripples (Fig. 3D). During ripples, the majority of interneurons discharge synchronously along with approximately ten percent of hippocampal pyramidal neurons. Ripples were suggested to originate from the CA3 region and to be transmitted to the CA1 via the Schaffer collaterals (Csicsvari et al., 1999; Csicsvari et al., 2000).

O'Keefe and Nadel (1978) proposed that LIA is a resting state of the hippocampus characterized by the lack of specific activity (i.e., theta oscillation). However, an increasing body of evidence suggest that LIA, and particularly sharp wave-ripple complexes, have a fundamental role in hippocampus-related memory consolidation processes. Thus, memory traces collected during theta activity can be selectively strengthened during sharp waves (Buzsaki, 1989; Skaggs and McNaughton, 1996; Nakashiba et al., 2008; Nakashiba et al., 2009). Moreover, the transfer of information from the hippocampus to the neocortex may as well occur during LIA (Siapas and Wilson, 1998; Molle et al., 2006; Clemens et al., 2007).

Other hippocampal LFP patterns. Short periods of small amplitude irregular activity (SIA) is infrequently detected, mainly as a transition between other hippocampal LFP patterns (Jarosiewitz and Skaggs, 2004). Hippocampal theta activity is frequently accompanied by gamma (above 20 Hz) or sometimes with beta (10 to 20 Hz) band activity, in a manner that theta oscillation modulates the amplitude of the beta/gamma rhythm (usually referred to as "theta-nested gamma") (Csicsvari et al., 2003). Gamma oscillation might participate in the coupling between the CA1 and the CA3 fields as well as between the CA3 and the entorhinal cortex, providing a framework for effective communication between those areas (Montgomery and Buzsaki, 2007). Recently, a novel type of hippocampal non-theta activity different from LIA and SIA has been described, which was termed hippocampal slow oscillation, based on its similarities with the neocortical slow wave activity (Wolansky et al., 2006).

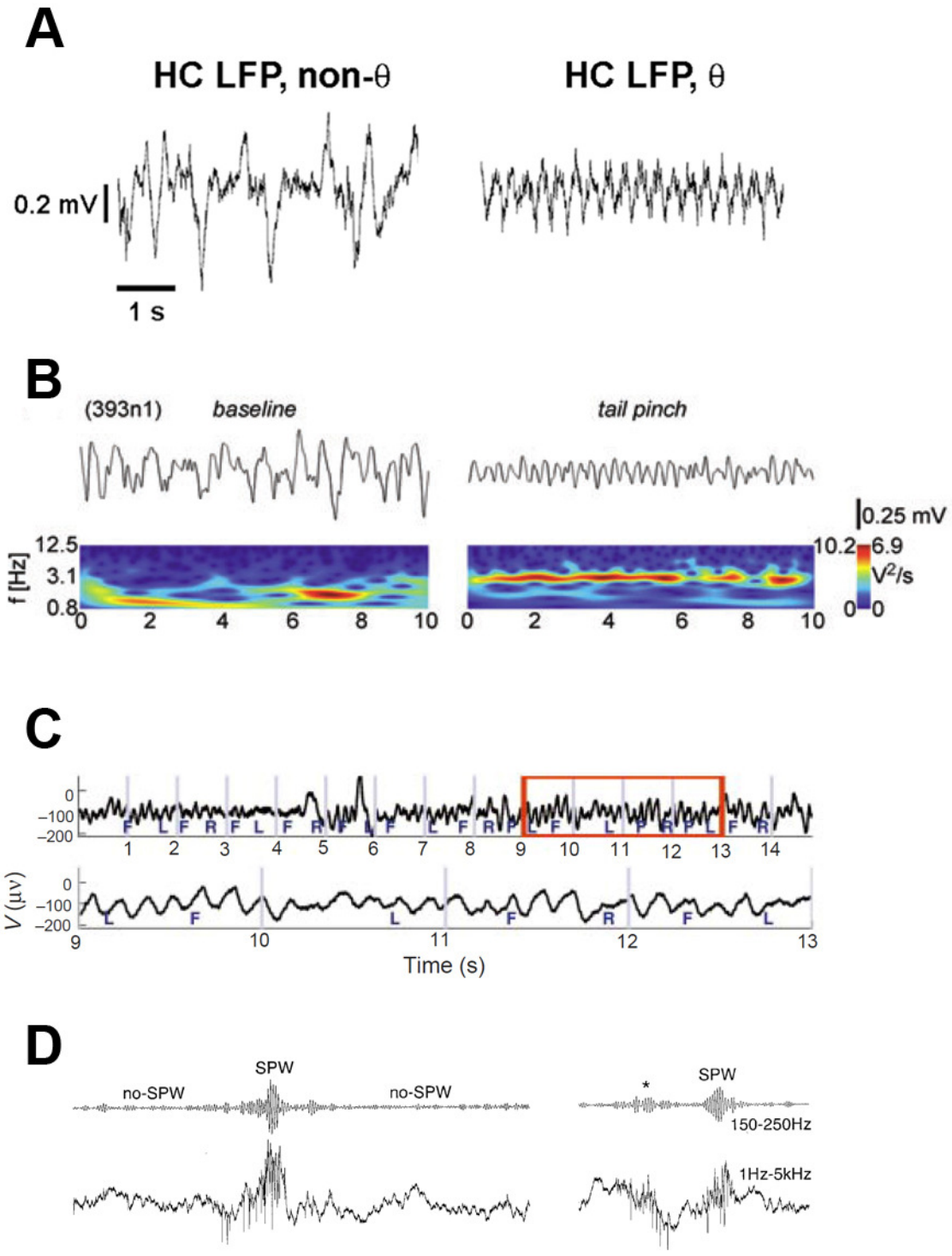

Figure 3. Hippocampal LFP patterns. **A**: LIA (left) and theta (right) activity recorded from the rat CA1 stratum pyramidale under urethane anesthesia. *Source: Hangya et al., 2009*. **B**: The same types of activity patterns as in panel A with corresponding wavelet power images (see Materials and Methods). *Source: Varga et al., 2008*. **C**: Intracranial

EEG recording from the human hippocampus during navigation in a virtual maze. Theta oscillation marked by the red rectangle is enlarged in the lower plot. *Source: Kahana et al., 1999*. **D**: Raw (lower) and filtered (upper) trace of rat hippocampal LFP showing sharp wave-ripple complexes. HC, hippocampal; SPW, sharp wave-ripple complex. *Source: Csicsvari et al., 1999.*

Behavior of hippocampal neurons during different activity patterns

Hippocampal pyramidal cells can be distinguished from the interneurons based on their firing pattern and action potential characteristics (Fig. 4). Pyramidal cells fire at a low average rate (usually < 1 Hz), exhibit long duration action potentials and often show complex spikes, that is, a brief train of action potentials within a short interval with a decreasing amplitude, increasing spike duration and interspike interval. In contrast, interneurons fire at a higher average rate (typically between 10 and 100 Hz with the exception of the slow-firing Ivy cells, see Fuentealba et al., 2008), show short duration action potentials and do not exhibit complex spikes (Csicsvari et al., 1998; Csicsvari et al., 1999).

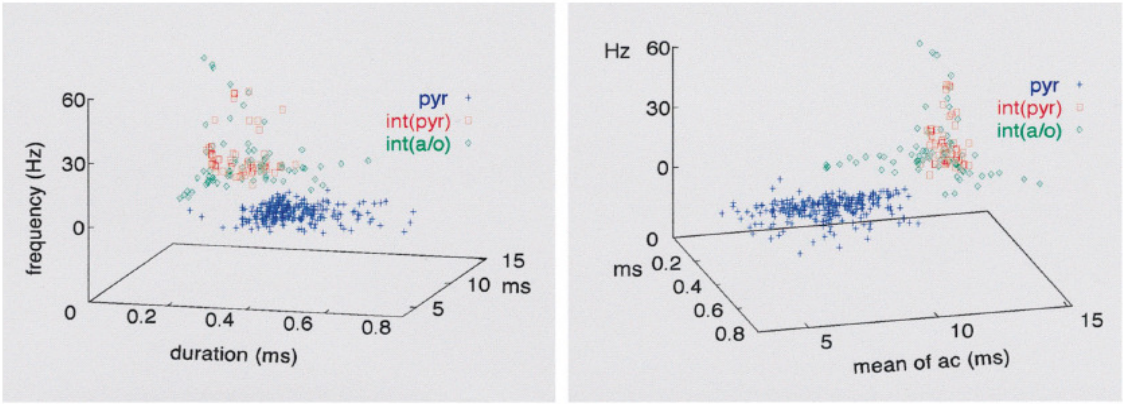

Figure 4. Identification of hippocampal interneurons and pyramidal cells from extracellular recordings. Pyramidal cells and interneurons were separated along three dimensions: spike duration measured at 25% spike amplitude, firing frequency and the mean of the spike autocorrelogram. ac, autocorrelogram; int(a/o), interneuron from the stratum oriens/alveus; int(pyr), interneuron from the pyramidal layer; pyr, pyramidal cell. *Source: Csicsvari et al., 1999.*

In freely moving rodents, pyramidal cell firing has a clear behavioral correlate. Most of the pyramidal cells fire only in exact locations of the physical environment, thus contributing to spatial coding (O'Keefe and Nadel, 1978). Thus, hippocampal pyramidal neurons are often called "place cells", while the piece of the environment where they are active is termed "place field". As already mentioned, place cell firing is phase coupled to the ongoing theta oscillation. Pyramidal cells fire in more and more advanced phases of the theta cycle as the animal traverses the neurons place field, a phenomenon called phase precession. This process might contribute to the coding of physical distances (Geisler et al., 2007). Besides place cells, some hippocampal pyramidal cells show a firing pattern that correlates with the direction to which the animal is headed (so-called "head direction cells"). More head direction cells can be found in the dorsal presubiculum (Ranck, 1984).

Hippocampal interneurons often show a consistent phase relationship with theta oscillation (Fig. 5; phasic cells in the classification of Colom and Bland, 1987). For example, CCK-containing basket cells fire on the rising phase, axo-axonic cells are associated to the peak and PV-immunopositive basket cells fire on the descending phase of theta recorded from the pyramidal layer (Klausberger and Somogyi, 2003). This observation is in agreement with the hypothesis that these perisomatic inhibitory cells contribute to the hyperpolarizing phase of pyramidal cell membrane potential oscillation (Freund and Buzsaki, 1996). Conversely, dentritic targeting interneurons, such as O-LM cells, tend to fire on the trough of the theta cycle (Klausberger and Somogyi, 2003), concurrent with the excitation conveyed by the entorhinal cortex. Interneurons phase coupled to theta oscillation either show burst firing (i.e., clearly separable clusters of action potentials, see also Materials and Methods) or display a theta-modulated activity without distinguishable bursts (i.e., they show rhythmic firing rate changes at specific phases of the theta cycle). Some interneurons display tonic firing with increased frequency during theta rhythm (tonic theta-on cells in Colom and Bland, 1987). Interneurons with a decrease of firing rate or complete cessation of spiking at theta onset were also, albeit infrequently, detected (theta-off cells in Colom and Bland, 1987).

It was also observed that most types of interneurons show characteristic behavior during ripples. PV-containing basket cells and bistratified cells are activated, axo-axonic

cells and O-LM cells are inhibited, whereas CCK-containing basket cells do not show a change in firing rate (Fig. 5) (Klausberger and Somogyi, 2008).

Although most of the interneurons are more or less constitutively active, their firing rate can also be modulated by the physical environment. Thus, interneuron firing also carries some spatial information and it was recently suggested that interneurons might as well contribute to spatial processing (Wilent and Nitz, 2007).

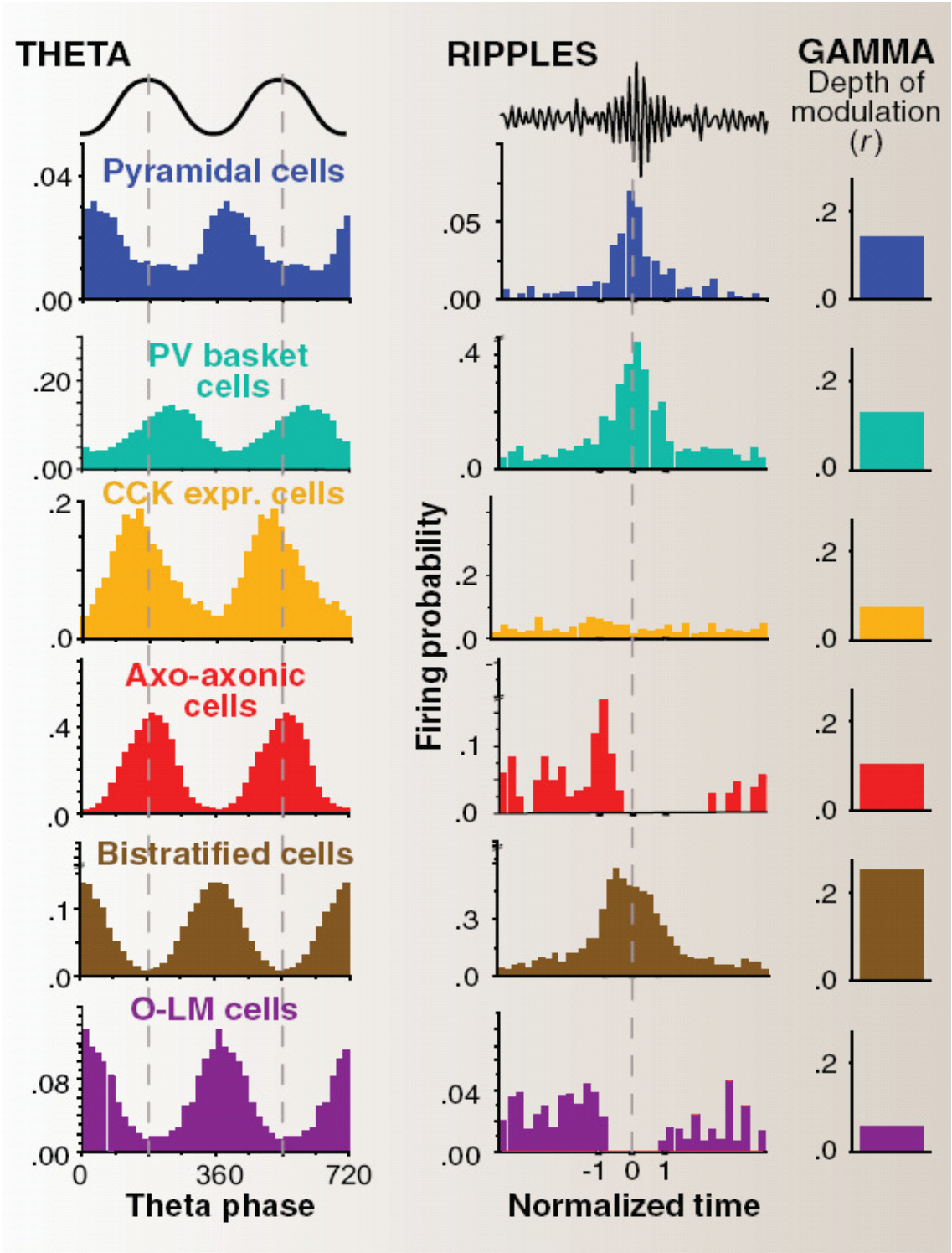

Figure 5. Relationship between interneuron firing and hippocampal LFP patterns. Firing histograms of different types of hippocampal interneurons during theta oscillation (left) and ripples (middle) are shown. Depth of modulation of firing by hippocampal gamma oscillation is indicated on the right. *Source: Klausberger and Somogyi, 2008*.

The medial septum

The medial septum (MS) is the most rostral part of the cholinergic system of the basal forebrain. The MS receives afferent input from various brain regions as the hippocampal formation, the amygdala, the ventral pallidum, the lateral septum, the lateral hypothalamus, the supramammillary area, the dorsal thalamus and from several brainstem nuclei (ventral tegmental area, substantia nigra, raphe nucei, locus coeruleus) (Swanson and Cowan, 1979; Montagnese et al., 2008). It also spreads its activity to a wide range of brain structures via its efferent connections to the hippocampus, the subiculum, the entorhinal cortex, the amygdala, the lateral hypothalamus, the mediodorsal thalamus, the habenular nuclei, the mammillary complex, the supramammillary area, the ventral tegmental area and the raphe nuclei (Swanson and Cowan, 1979; Meibach and Siegel, 1977; Montagnese et al., 2004). Through its widespread connections, medial septum participates in a great variety of neuronal processes such as the modulation of arousal and attention, the coordination of hormonal processes (aggressive and sexual behavior), thermoregulation, fear learning and, via its bidirectional connection with the hippocampus, the control of hippocampal memory functions (Borhegyi et al., 2004; Calandreau et al., 2007; Srividya et al., 2007; de Almeida et al., 2005; Merchenthaler et al., 1984). Since the septo-hippocampal pathway was in the main focus of our study, we review the role of the MS in the formation of declarative memory traces associated to the hippocampal theta oscillation. The utmost importance of the medial septum in this process is indicated by the fact that lesion of the analogous area in the human brain, which is most frequently caused by jet bleeding after rupture of an aneurysm on the anterior communicating artery, leads to the classical symptoms of the Korsakoff syndrome (i.e., retrograde and anterograde amnesia, confabulation). Additionally, Alzheimer's disease is accompanied by the loss of cholinergic basal forebrain neurons projecting to the hippocampus (Craig et al., 2008) and the activation of the MS was shown to reverse age-related encoding deficits in a spatial navigation task (Sava and Markus, 2008).

Anatomy of the medial septum

Cytoarchitectonic organization

The medial septum - diagonal band of Broca (MS-DBB) is a midline structure located in the area of the lamina terminalis and the septum pellucidum, rostral to the third ventricle (Fig. 6). It is surrounded by the corpus callosum (from rostral and above), the anterior commissure (from caudal) and the lateral ventricles (from each side). The region is part of the cholinergic system of the basal forebrain. The MS-DBB complex is divided to the VDB, which comprises the MS proper and the vertical limb of DBB, and the HDB (horizontal limb of DBB). Based on neurochemical markers, neurons in the VDB form an onion-like structure, which serves a bases for distinguishing inner, outer and a thin outermost layer of the VDB, which separates the MS-DBB complex from the lateral septum (Paxinos, 2004; Kiss et al., 1990a; Kiss et al., 1990b).

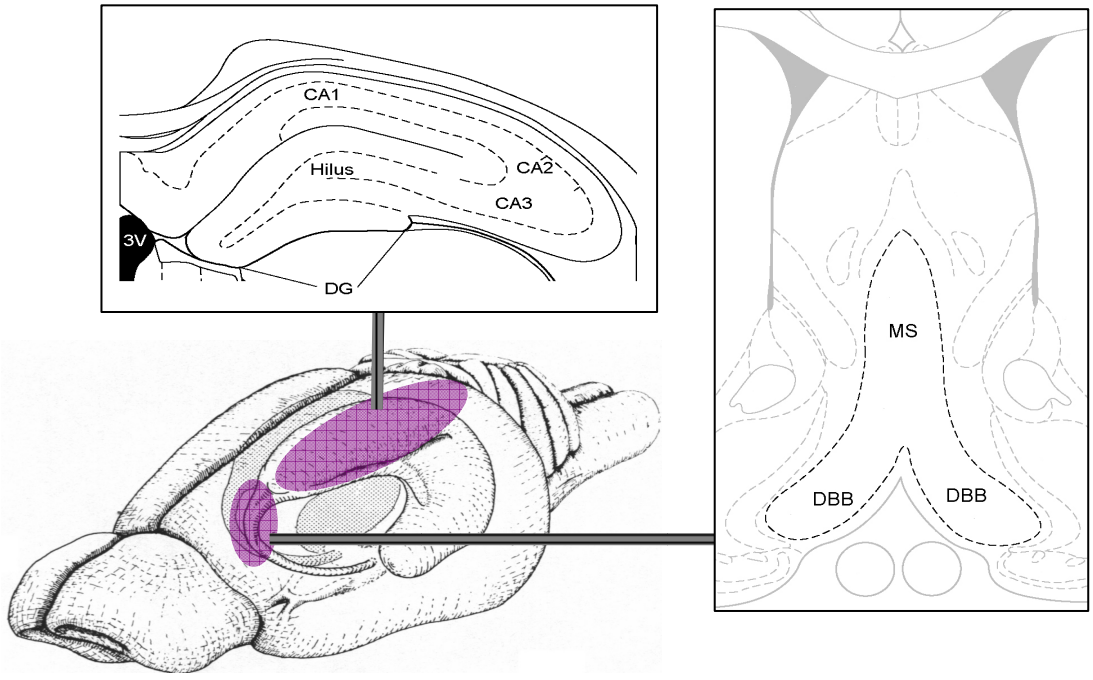

Figure 6. Localization of the rat hippocampus and medial septum. *Source: Cheung and Cardinal, 2005; Paxinos and Watson, 1998.*

Neurons of the medial septum

MS neurons are divided to two major, non-overlapping populations, the cholinergic neurons expressing cholin acetyltransferase (ChAT) and the GABAergic neurons containing glutamate decarboxylase (GAD). GABAergic neurons occupy the innermost layer of the MS in the midline, which is surrounded by the cholinergic neurons of the outer layer (Fig. 7) (Kiss et al., 1990a; Kiss et al., 1990b). Also, large cholinergic neurons can be found among GABAergic cells along the midline. The cholinergic group, which forms one of the major projecting populations of the MS (Frotscher and Leranth, 1985), can be divided to a larger and a smaller type, based on ChAT immunoreactivity. Also, two types of GABAergic neurons are distinguished: the ones containing the Ca^{2+}-binding protein parvalbumin (PV) and the group of PV-immunonegative neurons. PV-immunoreactive neurons were shown to project to the hippocampus (Freund, 1989; Borhegyi et al., 2004).

Outer layers and caudal part of the medial septum also contain a considerable population of glutamatergic neurons (Manns et al., 2001; Manns et al., 2003; Sotty et al., 2003). These neurons innervate both the cholinergic and the GABAergic neurons of the MS (Hajszan et al., 2004; Manseau et al., 2005). However, little is known about possible distant targets of septal glutamatergic cells.

Additionally, a population of medial septal neurons expresses luteinizing hormone-releasing hormone (LHRH). These cells participate in the regulation of the ovarial cycle (Merchenthaler et al., 1984).

A great variety of neuropeptides are expressed in different septal neurons. Substance P (SP) -containing cells of the outermost layer project to the CA2 and CA3 regions of the hippocampus. MS neurons expressing somatostatin, neurotensin, met-enkephalin, calcitonin gene-related peptide (CGRP), dynorphin B, vasoactive intestinal polypeptide (VIP), neuropeptide Y (NPY), cholecystokinin (CCK), delta sleep inhibiting peptide were also found (Kiss et al., 1997).

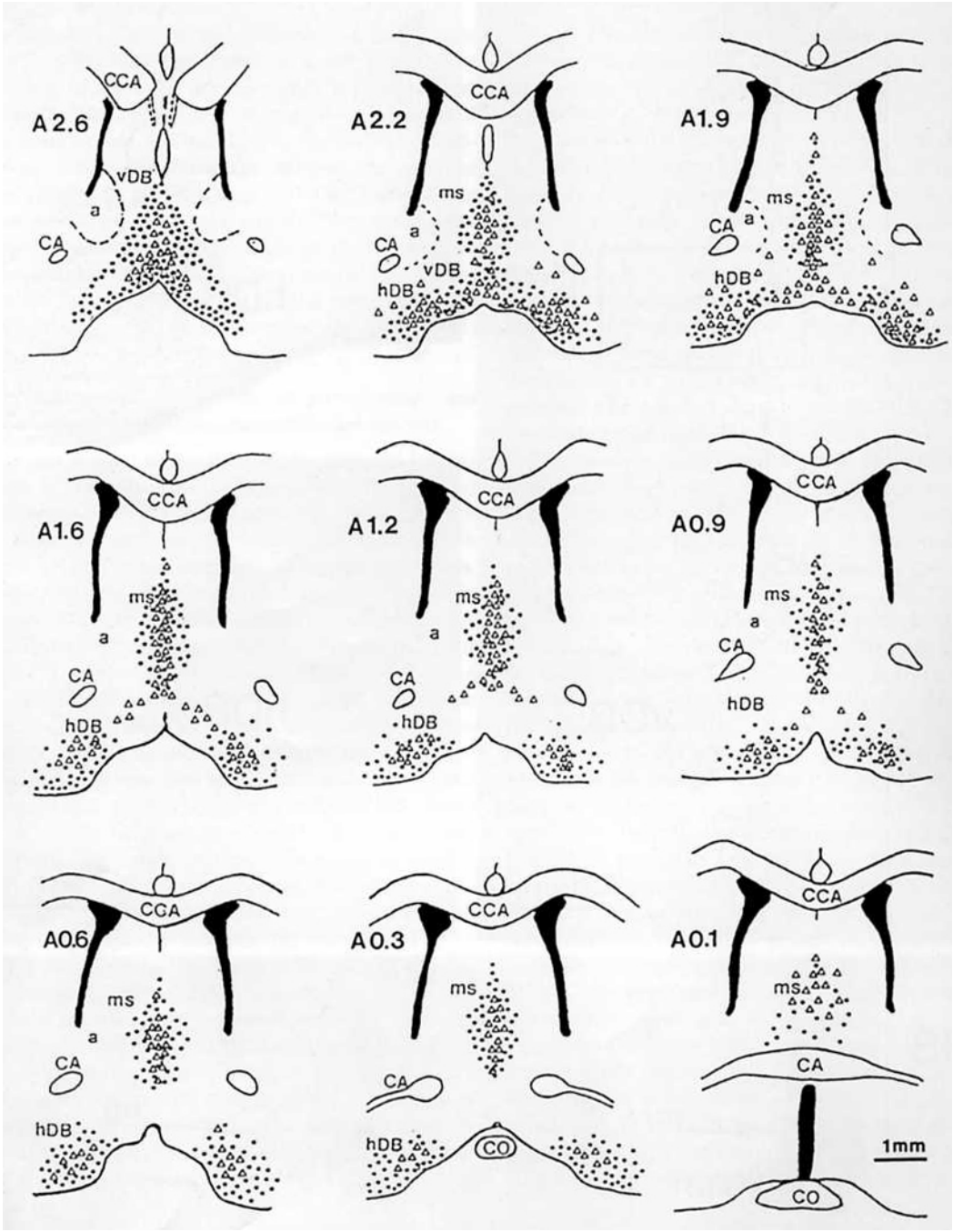

Figure 7. Localization of medial septal GABAergic and cholinergic neurons. Cross-sectional maps in the frontal plane arranged rostro-caudally show the characteristic spatial pattern of PV-immunoreactive (open triangles) and ChAT-immunopositive (closed dots) neurons. Levels at which maps were made are indicated relative to the bregma. A, anterior; CCA, corpus callosum; a, nucleus accumbens; CA, anterior commissure; ms, medial septum; vDB, vertical limb of the diagonal band of Broca; hDB, horizontal limb of the diagonal band of Broca; CO, optic chiasma. *Source: Kiss et al., 1990b*.

The septo-hippocampal pathway

Reports dealing with current source density mapping of hippocampal activity as well as studies of hippocampal single cell activity revealed that dendritic excitation of pyramidal neurons is accompanied by somatic inhibition (Buzsaki et al., 1986; Kamondi et al., 1998). PV-immunoreactive (PV-IR) neurons of the MS selectively innervate hippocampal interneurons, thus contributing to the rhythmic change of somatic and dendritic inhibition (Freund and Antal, 1988; Borhegyi et al., 2004). Besides septal GABAergic innervation, cholinergic cells of the MS send diffuse projection to the hippocampus, influencing both interneurons and pyramidal cells (Fig. 13A). Glutamatergic neurons may also project to the hippocampus; however, identification of extraseptal targets of those neurons needs further investigation. A large body of experimental (Lawson and Bland, 1993; Vertes and Kocsis, 1997) and modeling (Wang, 2002) data show that the MS plays a crucial role in hippocampal theta-synchronization. Lesion or procain-induced anesthesia of the medial septum or separation of the MS from the hippocampus abolishes all forms of theta oscillation in the hippocampus (Rawlins et al., 1979; Smythe et al., 1991). However, the hippocampo-septal back-projection has recently been proved to be essential for synchronizing the medial septal and hippocampal circuits (Toth et al., 1993; Wang, 2002). Furthermore, the classic hypothesis of MS drive to hippocampal theta has been challenged by Manseau et al. (2008) based on *in vitro* data suggesting a mechanism of intrahippocampal theta genesis.

Electrophysiology of the medial septum

Activity patterns of different cell types in the MS

Cholinergic septal neurons are slow firing with wide action potentials followed by large amplitude, long lasting afterhyperpolarization *in vitro* (Sotty et al., 2003; Henderson et al., 2005). Recently, *in vivo* activity of these neurons was shown to be characterized by extremely slow, irregular firing, completely unrelated to hippocampal theta oscillation (Fig. 8) (Simon et al., 2006).

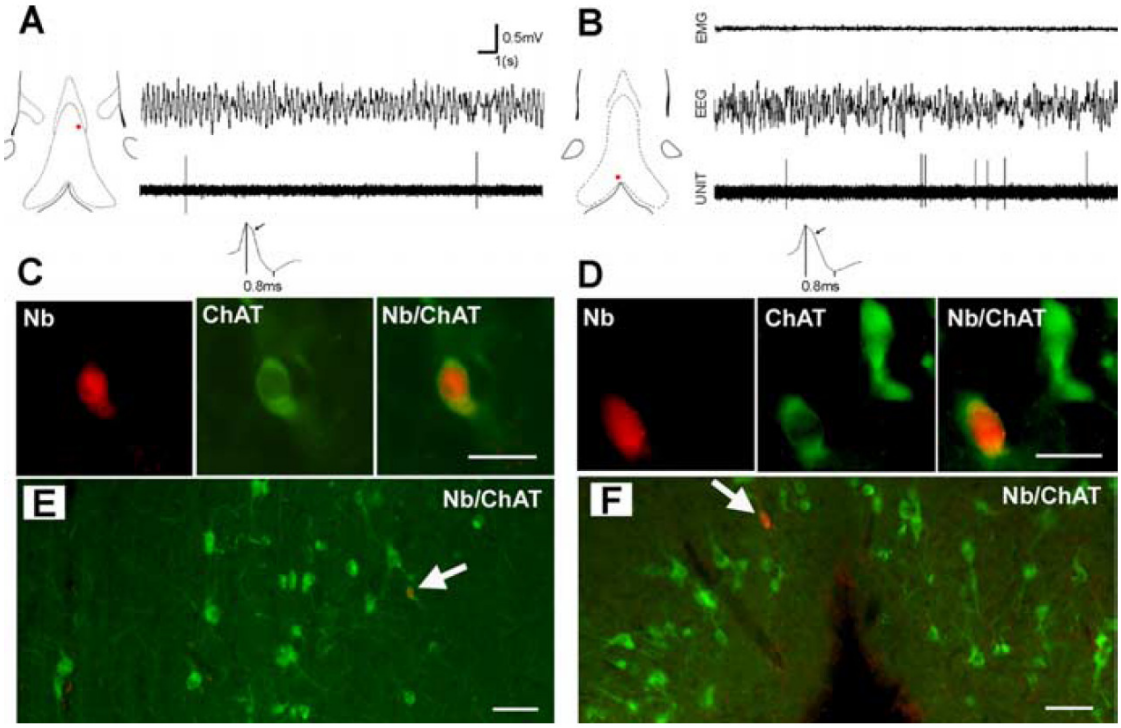

Figure 8. Discharge pattern of medial septal cholinergic neurons. A: Firing pattern of a septal cholinergic neuron in a urethane anesthetized rat during hippocampal theta oscillation. Red dot on the left panel shows the location of the cell. **B**: Activity of a cholinergic neuron in an anesthetic-free rat during hippocampal theta state. Note the low firing rate and long spike duration (0.8 ms) in both cases. **C-D**: Immunohistochemical identification of the neurons revealed ChAT immunopositivity. Scale bar: 20 μm **E-F**: Fluoromicrographs at low magnification. Scale bar: 50 μm. ChAT, cholin acetyltransferase; Nb, Neurobiotin. *Source: Simon et al., 2006.*

Medial septal GABAergic neurons show narrow spikes followed by, if at all, a short, small amplitude afterhyperpolarization *in vitro* (Morris et al., 1999; Sotty et al., 2003). GABAergic cells are capable of fast firing and often display a regular firing pattern with action potential clusters (bursts) phase-locked to the ongoing hippocampal theta oscillation *in vivo* (Fig. 9) (Borhegyi et al., 2004). Another type of theta-related activity shown by septal GABAergic cells is the so-called 'theta-modulated' firing, in which case clearly separable bursts are not observed. Instead, rhythmic changes of firing rate at specific phases of the hippocampal theta cycle can be detected.

Glutamatergic cells exhibit slow firing or cluster firing discharge pattern *in vitro* (Sotty et al., 2003). *In vivo* activity patterns of these neurons are yet to be characterized.

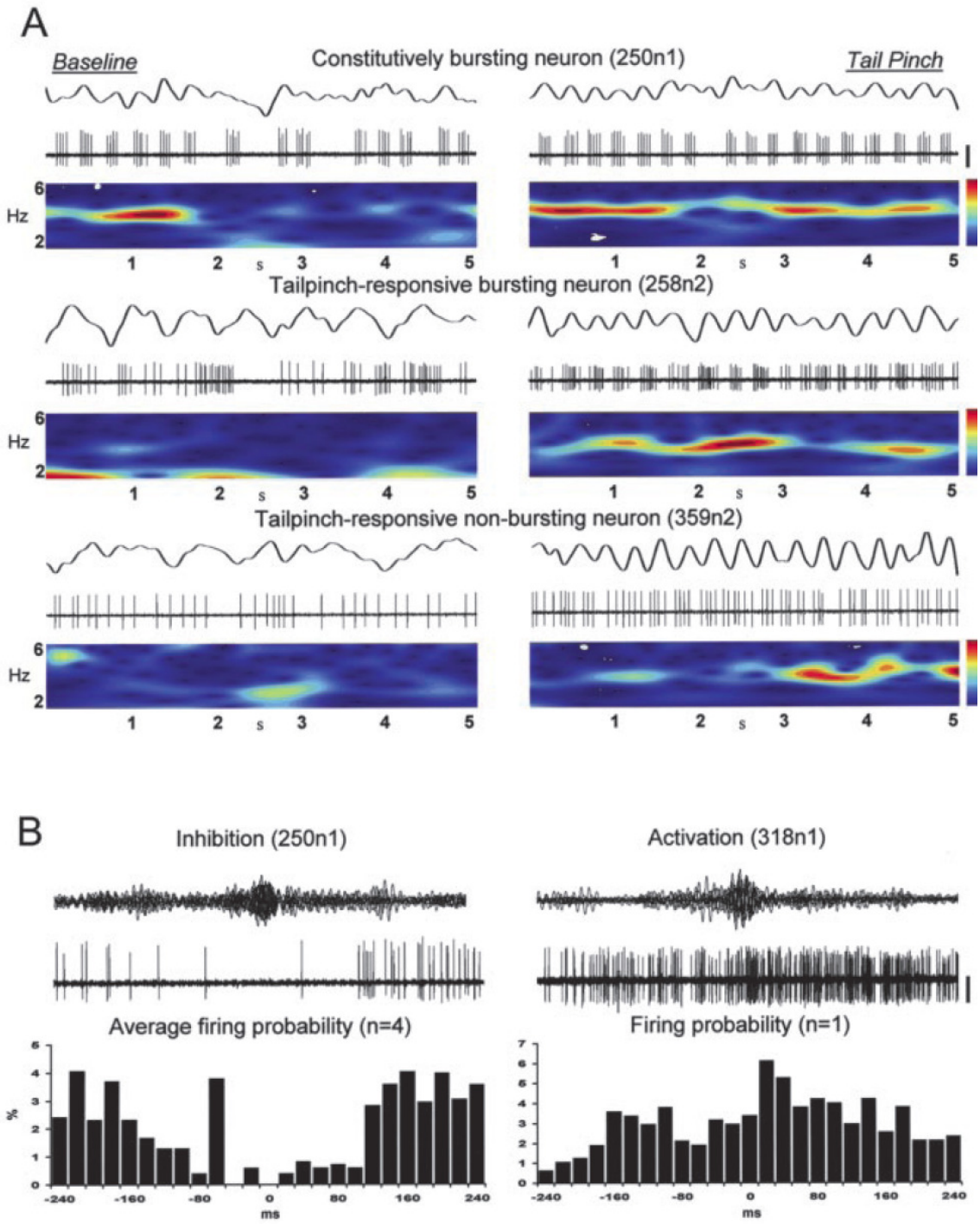

Figure 9. Firing pattern of medial septal PV-IR GABAergic neurons. Discharge pattern of septal PV containing neurons during LIA (A, left), theta oscillation induced by sensory stimulation (tail pinch) (A, right) and ripples (B) in urethane anesthetized

rats are shown. **A**: Filtered LFP and unit traces and cross-wavelet spectra are displayed for three PV-IR neurons. Septal GABAergic cells usually exhibit fast-firing, often theta-bursting activity pattern. Calibration in volts for the LFP-unit traces from left to right (shown as LFP/unit; see black vertical bar at the right of the topmost panel, right column): 250n1, 1.5/2, 1.1/2.2; 258n2, 2.2/1.1, 2.2/1.1; 359n2, 1.7/2, 1/1.7. **B**: Overlaid ripple segments of filtered LFP and unit are displayed in a neuron that was inhibited (left) and in a cell that was activated (right) during hippocampal ripples. Calibration in volts for the traces (shown as LFP/unit; see black vertical bar at right): 250n1, 0.5/1.75; 318n1, 0.65/2.2. *Source: Borhegyi et al., 2004*.

Discharge of MS neurons during different hippocampal activity patterns

During hippocampal theta oscillation, most of the MS neurons (up to 75%) show theta-dependent activity (Fig. 9A). The proportion of theta-related MS neurons drops to 30% after the cease of theta rhythm in the hippocampus (King et al., 1998; Brazhnik and Fox, 1999). Some medial septal neurons maintain theta-rhythmic firing even after complete isolation of the MS (Vinogradova, 1995). Importantly, it was shown by Borhegyi and colleagues that PV-containing septal neurons display a bursting activity tightly phase-locked to the hippocampal theta oscillation. On the population level, PV-IR neurons concentrated around two preferred phase angles on the trough (178 degrees) and around the peak (330 degrees) of the theta cycle (Fig. 10) (Borhegyi et al., 2004).

Three types of MS neurons can be distinguished based on their potential activity changes during hippocampal sharp waves. Some septal cells are blocked, probably via direct inhibition conveyed by the hippocampo-septal GABAergic neurons (Toth et al., 1993). Other neurons are activated, possibly through disinhibition (Fig. 9B). The rest of the MS cells' activity remains unchanged during hippocampal sharp waves (Dragoi et al., 1999).

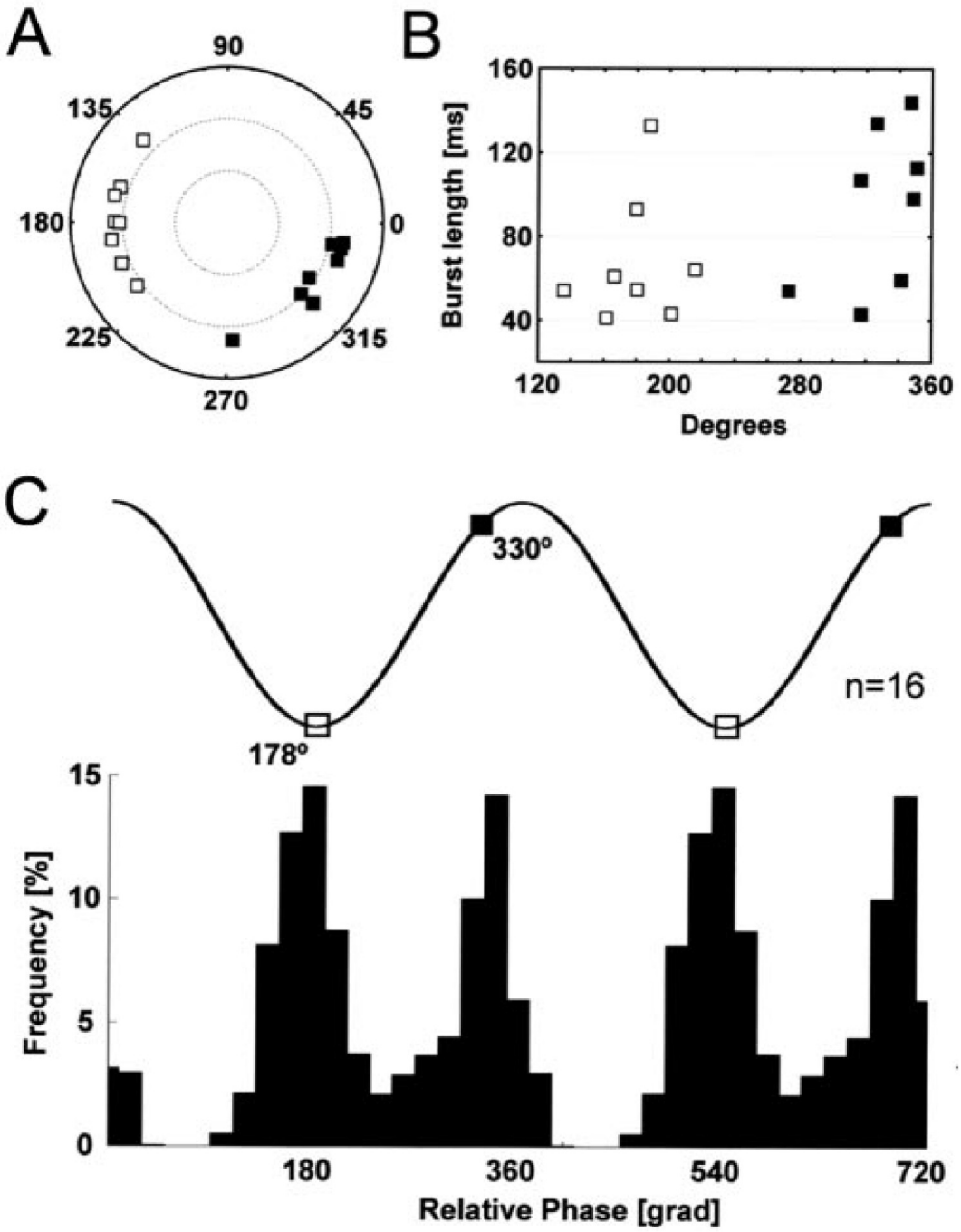

Figure 10. Phase preference of medial septal PV-IR neurons. A: Polar plot showing the preferred phases of PV-containing neurons of the MS. PV-expressing neurons could be separated to two clearly distinguishable groups: these cells showed a preferred phase on the trough (180 degrees) or near the peak (330 degrees) of the hippocampal theta cycle. Long distance from the center on the polar plot indicates high level of phase coupling. **B**: A weak correlation was observed between burst length and preferred theta phase. **C**: Population phase histogram of PV-expressing cells showed two clearly

separable peaks corresponding to the above two groups of PV-IR neurons. *Source: Borhegyi et al., 2004*.

Hyperpolarization activated and cyclic nucleotide gated non-selective cation channel (HCN)

Experimental evidence from a great variety of studies published in the recent decades illustrates that the hyperpolarization activated and cyclic nucleotide gated non-selective cation channel (HCN), and the so-called H-current which it mediates, is central to electric rhythm generating processes in the mammalian organisms (for a review, see Robinson and Siegelbaum, 2003). The HCN channel was first described in the sinuatrial node of the rabbit by Dario DiFrancesco in 1979 (Brown et al., 1979; DiFrancesco, 1986). Because of its unusual characteristics, the discovered cation current was named 'funny current' (Accili et al., 2002).

The capability of the HCN channel of forming cyclic activity and its established role in other rhythm generating brain circuits raises the possibility that neurons of the medial septum expressing HCN could participate in the generation of hippocampal theta oscillation. Since testing this hypothesis was one of the main aims of this study, we briefly discuss the structural and functional properties of the HCN channel.

Structure of the HCN channel

HCN channel operates in a tetramer form of four subunits. Four different types of HCN channel subunit has been described so far (HCN1-4), which are capable of forming both homo- and heterotetramers. All subunits have six transmembrane domains (S1-6). Positively charged aminoacids of the S4 domain act as a voltage sensor. Near the C-terminal, cyclic nucleotide binding domain (CNBD) can be found, which precludes channel opening in the absence of cyclic adenosine monophosphate (cAMP) (Zagotta et al., 2003). The HCN channel shows marked homology with the voltage sensitive potassium channels.

HCN channel can be detected on the pacemaker cells of the heart tissue (sinuatrial node, atrioventricular node) as well as on the somadendritic membrane of

neurons involved in rhythm generating brain networks (e.g. nucleus reticularis thalami, neocortex, medial septum).

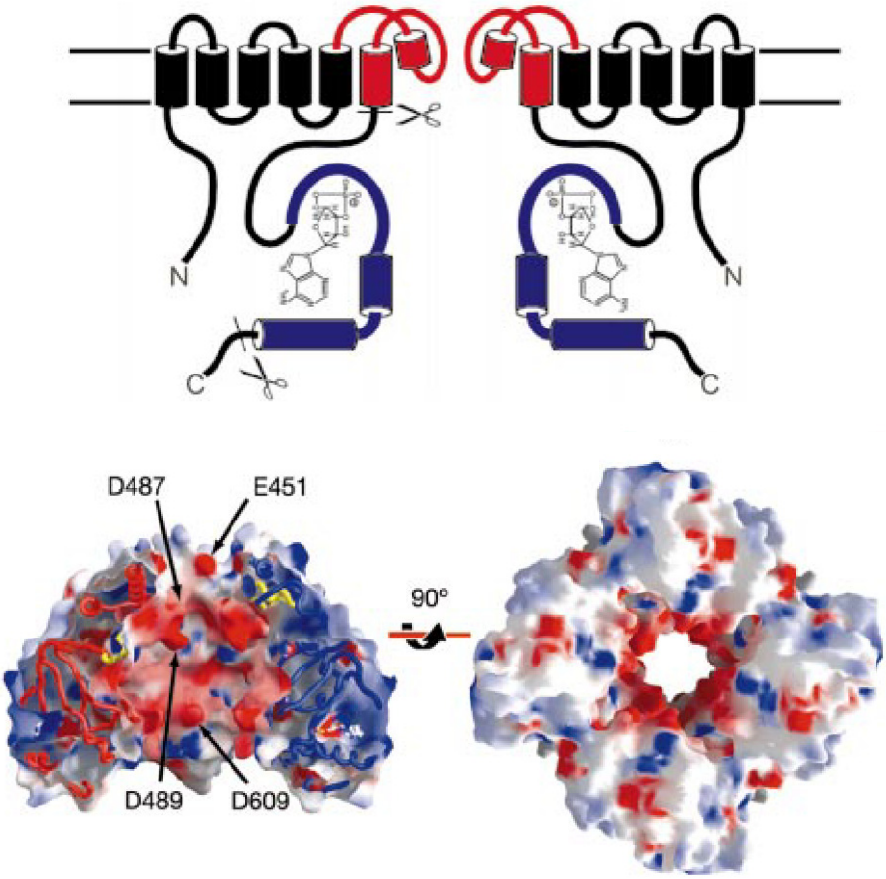

Figure 11. Structure of the HCN channel. Upper: topology of the HCN2 channel. Two of the four subunits are shown. The pore and the S6 transmembrane domains are indicated in red, CNBD is blue. Lower: molecular surface representation of the HCN2 tetramer. Left view is perpendicular to the four-fold axis of the channel and the molecule is sliced along the symmetry axis. Right view is parallel with the four-fold axis from the intracellular surface. *Source: Zagotta et al., 2003*.

Kinetics and regulation of the HCN channel

HCN channel is activated upon hyperpolarization. As the consequence of channel opening, cation-permeability increases and sodium enters the cell paralleled by an outward potassium flux. As a net effect, membrane potential is shifted towards more

depolarized levels. If this depolarization reaches the threshold of action potential generation, a single spike (in heart cells) or a burst of action potentials (in neurons) is emitted, composed of fast depolarization mediated by sodium channels followed by repolarization via the opening of the delayed rectifier potassium channels. Afterhyperpolarization mediated by potassium currents following the action potentials is capable of reopening the HCN channels, thus closing the pacemaker cycle. This type of periodic activity can serve as an electrophysiological basis of rhythm generation.

The activation kinetics of the channel is characterized by a sigmoid I-V curve with an activation time constant varying between 1 and 15 seconds (Fig. 12). Increasing concentrations of cAMP shifts the I-V curve to the right and lowers the activation time constant. According to the recently developed dynamic allosteric model (Wang, 2002), the HCN channel can appear in four states: open ligand-free (O + A), closed ligand-free (A + C), open ligand- (cAMP-) bound (AO), closed ligand-bound (AC) (Fig. 12). Channel opening enhances the affinity of HCN to cAMP, causing the increased cAMP-binding of open channels. This process decreases the proportion of open ligand-free channels, which facilitates the opening of additional HCN channels, thus adding a slow component to the inward cation current. This model explains the observation that, in the presence of low cAMP concentrations (0,01 μM), the H-current is composed of a fast and a slow process. However, at high cAMP concentrations (100 μM), HCN channels bind cAMP even in the closed state, thus preventing the evolution of the slow component. The channel is also capable of cyclic guanosine monophosphate- (cGMP-) binding, albeit with an affinity that is an order of magnitude lower than that of the cAMP.

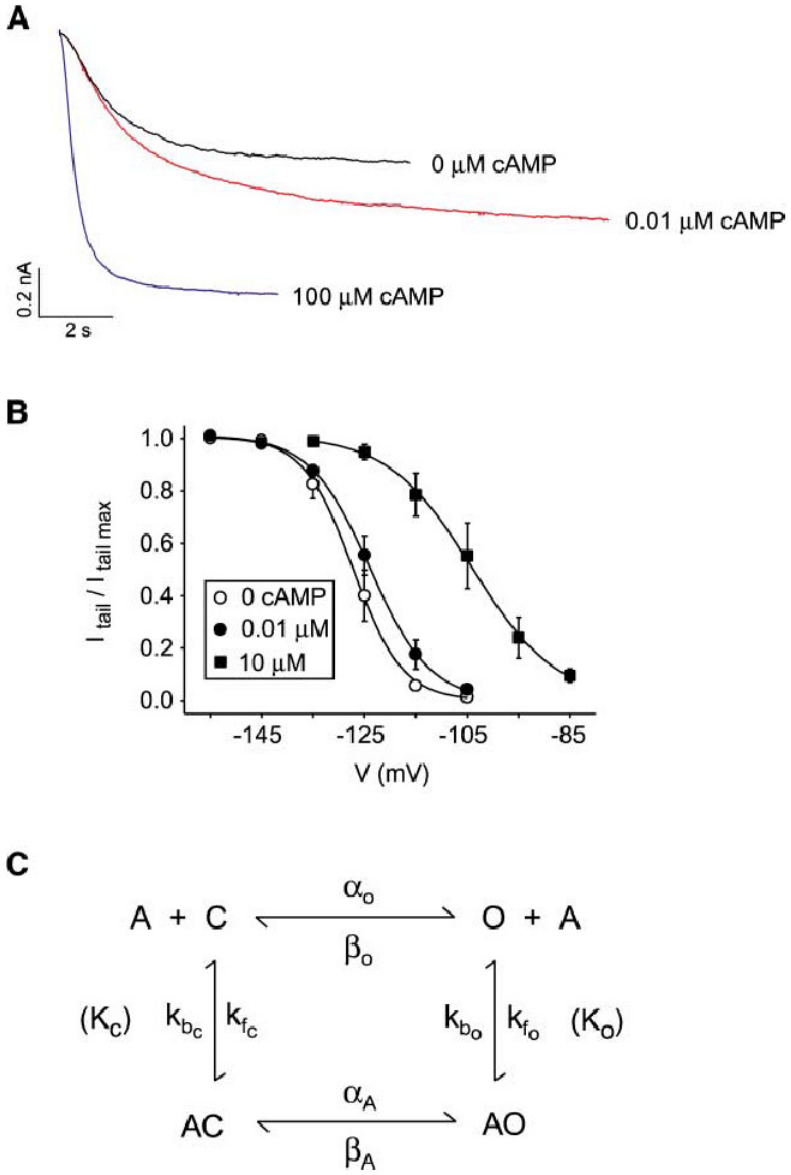

Figure 12. Kinetic effects of cAMP signaling on HCN2. A: Current records in inside-out-patch configuration in response to current steps from a holding potential of -40 mV to -135 mV in the presence of different concentrations of cAMP. **B**: Effect of cAMP on steady-state activation. Normalized tail currents (at -40mV) are plotted as a function of hyperpolarizing voltage. Solid lines show fits of the Boltzmann equation. Bars: SEM. **C**: Cyclic allosteric model for the effect of cAMP binding on HCN gating. Designations of rate constants are indicated on the arrows. See the text for the description of the model. *Source: Wang et al., 2002*.

The role of the HCN channels in electric rhythm generation

H-current is detectable in various tissues including the cardiac muscle, the nervous system, the smooth muscle, different glands and even the flagellum of spermatozoons. HCN channel not only plays an inevitable role in rhythm generation, but also participates in setting the resting membrane potential and regulation of the spread of electric signals.

In the cardiac muscle, it is expressed in the pacemaker cells of the sinuatrial and atrioventricular nodes. The H-current is responsible for the slow diastolic depolarization called prepotential or pacemaker potential. In pacemaker cells, HCN is activated by the afterhyperpolarization of the action potentials, causing a slow depolarization that finally leads to the opening of the T- and, subsequently, the L-type calcium-channels, thus initializing a new action potential (Fonyó, 2002). The H-current is evolutionary conserved, serving as a key component of electric rhythm generation in lower species also. It was shown that HCN is responsible for the rhythmic contractions of the dorsal tube in *Hirudinea* (Robinson and Siegelbaum, 2003). HCN is also expressed in the smooth muscle cells of the alimentary tract. It participates in the generation of periodic muscle contractions in the gastrointestinal system of mammals (basal electric rhythm) and also in the digestive system of lobsters (Robinson and Siegelbaum, 2003).

The role of HCN channels was examined in details in thalamocortical relay neurons. When the depolarization mediated by the HCN channel reaches the threshold of the T-type calcium channels, a calcium spike emerges, during which a series of action potentials is generated. Inactivation of the T-type calcium channels is followed by hyperpolarization, which reopens the HCN channels, generating rhythmic burst firing (McCormick and Pape, 1990; Rosenbaum and Gordon, 2004; Sherman and Guillery, 2000). HCN-mediated currents were shown to play an important role in the generation of the 0.5 to 4 Hz delta oscillations and also in the formation of the 7 to 15 Hz spindle activity. Moreover, the slow rhythmic activation and deactivation of HCN channels might be responsible for the periodic occurrence of thalamic spindles (Destexhe et al., 1996; Lytton et al., 1996).

Similar rhythm generating mechanisms were described in the inferior colliculus (Koch and Grothe, 2003) and in the respiratory neurons of the ventrolateral medulla (Mironov et al., 2000). HCN can also be found in hippocampal pyramidal cells and in a

subset of hippocampal interneurons (e.g. O-LM cells), thus it may play a role in the generation of hippocampal oscillations (Hu et al., 2002).

Besides pacemaker processes, the HCN channel also plays a role in the regulation of the resting membrane potential, thus setting the excitability of neurons. Furthermore, firing pattern can also be modulated via the HCN channel, e.g. shifting the membrane potential to more depolarized levels can turn rhythmic firing to a tonic mode. In cerebellar Purkinje cells, the H-current holds the membrane potential at a relatively depolarized level, causing spontaneous tonic firing of the cells (Raman et al., 1999; Nolan et al., 2004b). HCN can also be detected on dendritic processes of various neurons, where it participates in the regulation of signal propagation (George et al., 2009).

HCN in the medial septum

In the medial septum, HCN channels were found on the somadendritic membrane of a subset of the GABAergic neurons, whereas none of the examined cholinergic neurons contained HCN. HCN1 and HCN2 subunits were shown to completely colocalize in the MS. Among the neurons immunoreactive for HCN, both PV-IR and non-PV cells were present. Based on the analysis of 486 immunolabeled neurons, 21% of PV-IR cells colocalized with 55.8% of the HCN1-expressing neurons. HCN-immunoreactivity was also detectable among hippocampus-projecting medial septal cells (Fig. 13) (Varga et al., 2008).

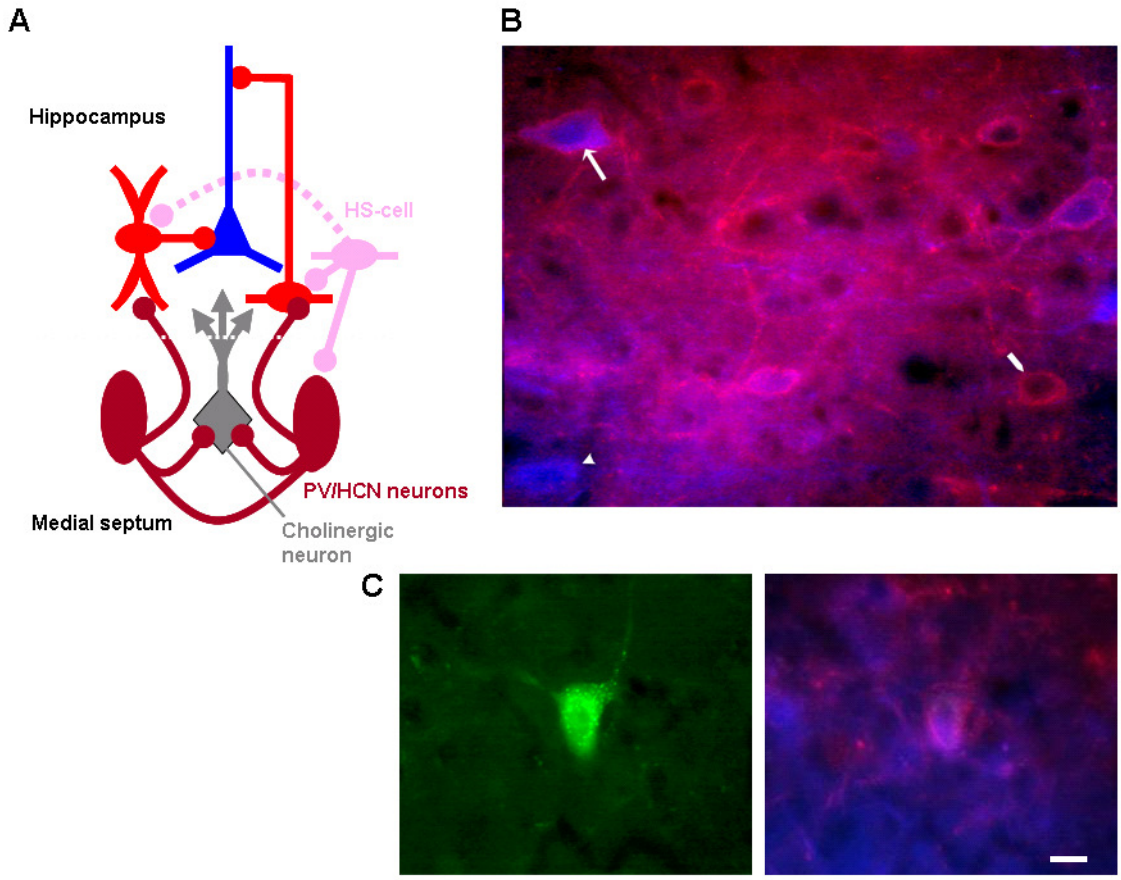

Figure 13. HCN-immunopositive neurons in the medial septum. A: Schematic representation of the septo-hippocampal circuitry. **B**: Double immunolabeling for PV (blue) and HCN (blue). The arrow points to double immunopositive MS neuron, the arrowhead marks a PV-IR non-HCN cell and the thick white line indicates a neuron containing HCN only. **C**: Retrograde labeling experiment. Fluoroscent microsphere (green) was injected into the hippocampus, and sections of the MS containing the retrogradely labeled neurons were immunostained for PV (blue) and HCN (red). Left: A retrogradely labeled MS cell is shown. Right: This neuron was immunopositive for both PV and HCN. Scale bar: 10 µm. *Source: Varga et al., 2008.*

Aims

Synchronization of the septo-hippocampal system was demonstrated during the major hippocampal activity states, the regular theta rhythm and the large amplitude irregular activity. Previous experimental and modeling data suggest that the MS provides rhythmic drive to the hippocampus, and hippocampo-septal feedback synchronizes septal pacemaker units. In this process, septal neurons expressing parvalbumin were proposed to play a fundamental role. However, the state-dependent alterations of septo-hippocampal interaction and its possible imbalance leading to septal or hippocampal dominance were not yet investigated. Furthermore, even the theory of medial septal theta formation has recently been questioned and an intrahippocampal theta generating mechanism was suggested.

Here we set out to uncover if the sequence of events during theta formation and the direction of information transmission supports the classic view of septal drive or the challenging theory of hippocampal pacing of theta. Also, we aimed to reveal whether medial septal neurons expressing parvalbumin and/or the putative pacemaker channel HCN play a role in the theta-frequency synchronization of the septo-hippocampal system. We asked the following questions:

Do the firing characteristics of PV- and/or HCN-expressing cells support their hypothesized role in theta genesis?

Does the timing of events in the septo-hippocampal system suggest a septal or a hippocampal lead on the course of theta synchronization?

Is there any asymmetry in the bidirectional information transfer between the MS and the hippocampus?

To address these questions, we analyzed the temporal relationship of activity between medial septal neurons, particularly those ones that express PV and/or HCN, and hippocampal local field potential recorded from urethane anaesthetized rats.

Additionally, we performed information theoretical analysis on theta-band information of MS single-neuron activity and hippocampal local field potential.

Materials and Methods

Animal handling

Male Wistar rats of 200-400 g body weight were used (Charles River Kft., Budapest, Hungary or bred in the own dedicated specific pathogen-free animal facility of the Institute). Experiments were performed according to the guidelines of the Institutional Ethical Codex and the Hungarian Act of Animal Care and Experimentation (1998, XXVIII, section 243/1998), which conforms to the regulation of animal experiments by the European Union. Animals were kept under a 12-12 hour light-dark cycle, water and food was available *ad libitum*. All efforts were made to minimize pain and suffering and to reduce the number of animals used.

Contributions

Dr. Viktor Varga performed all surgery and data recording except a part of hippocampal unit recordings that were accomplished by Dr. Balázs Hangya. All anatomical procedures in identification of juxtacellularly labeled neurons by immunohistochemistry methods are the work of Dr. Zsolt Borhegyi. Dr. Balázs Hangya performed all data analysis reported in this study except firing pattern analysis of HCN-immunopositive neurons, which was the joint work of Dr. Balázs Hangya and Dr. Viktor Varga.

Data recording

Rats were anesthetized using 0.37 ml of 40% or 0.7 ml of 20% urethane per 100 g body weight. Anesthetic was administered intraperitoneally. Body temperature was held on 36˚C by a heating pad connected to a rectal probe (Harvard Apparatus, Holliston, MA, USA). The animal was placed in a stereotaxic device (Kopf Instruments, Tujunga, CA, USA), and a window above medial septum as well as a small hole above the right hippocampus was drilled. In cases of hippocampal unit recordings, a left hippocampal window was prepared. Hippocampal local field potential (LFP) was recorded using monopolar tungsten microelectrodes with 0.8-3 MΩ *in vitro* impedance (FHC Inc. Bowdoin, ME, USA), or by a stainless steel wire fixed to the skull by dental

cement (Harvard Dental GmbH, Berlin, Germany). LFP was recorded from the CA1 pyramidal layer. When using tungsten electrodes, stratum pyramidale was identified by the increase in multiunit activity and the appearance of complex spikes (see The hippocampus subsection) between 1.9 and 2.2 mm from the brain surface during electrode descent. A mechanical microdrive was used to set the position of the tungsten electrode (Hugo Sachs Elektronik, March-Hugstetten, Germany). The recorded signal was amplified and band pass filtered between 0.3 Hz and 2 or 5kHz (Bio-Amp; SuperTech, Pécs, Hungary) and digitized at 10 kHz (micro1401 mkII; Cambridge Electronics Design, Cambridge, UK).

Medial septal unit activity was recorded concurrently with hippocampal LFP by the juxtacellular technique using glass microelectrodes (pulled from borosilicate glass capillaries, 1.5 mm outer diameter, 0.86 or 0.75 mm inner diameter; Sutter Instruments, Novato, CA, USA) with 20-40 MΩ *in vivo* impedance. Electrodes were filled with 0.5 M NaCl and 3% biocytin (Sigma-Aldrich Kft., Budapest, Hungary) or 2% Neurobiotin (Vector Laboratories, Burlingame, CA). A piezoelectric microdrive (6000 ULN; Burleigh Instruments, Fishers, NY or ISS-8200, EXFO, Quebec City, Quebec, Canada) was used to move the unit recording electrode. Septal single cell activity was amplified by a DC amplifier (Axoclamp 2B; Axon Instruments, now Molecular Devices, Sunnyvale, CA, USA), filtered between 0.1 and 5 kHz by a signal conditioner (SuperTech) and digitized at 10 kHz (Cambridge Electronics Design). Hippocampal theta was elicited by sensory stimulation (tail pinch with a pinching clip) and/or occurred spontaneously. Recording period was followed by juxtacellular labeling of the neuron (Pinault, 1996) by injecting a positive current through the electrode in a 200 ms on-off duty cycle on the top of a low-intensity negative current (0.4-1.5 nA). Labeling period lasted from 5 up to 10 minutes.

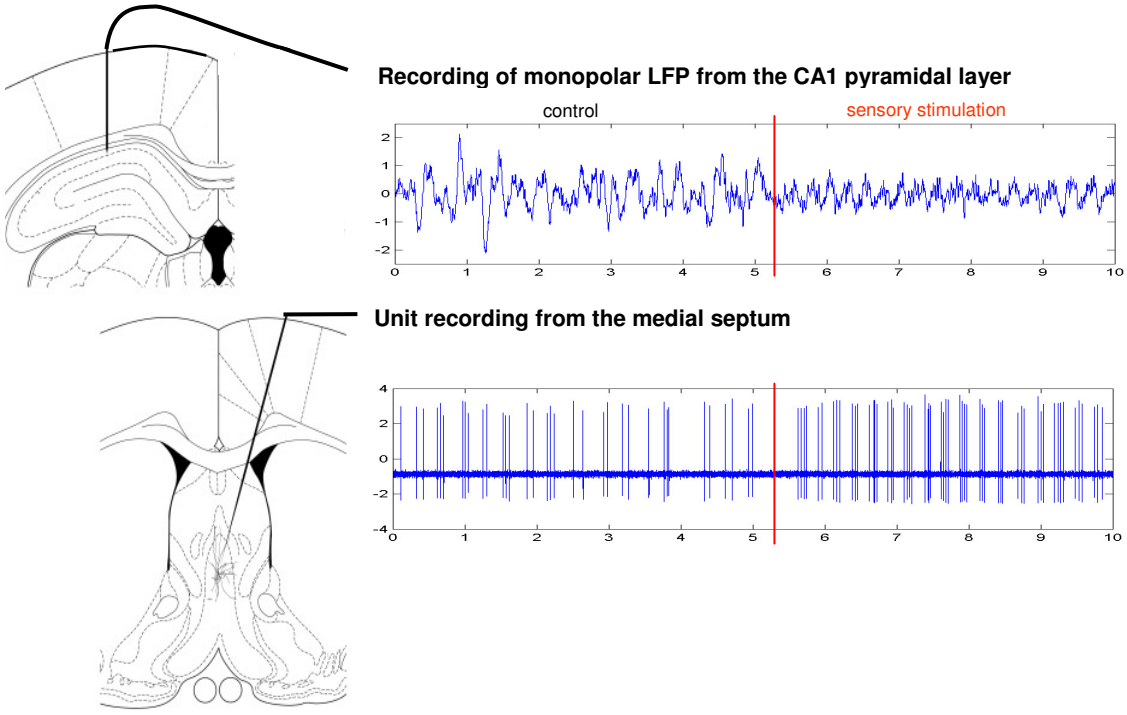

Figure 14. Data recording. LFP from the pyramidal layer of the CA1 region and single cell activity from the medial septum (or, in some cases, from the hippocampus; see Results) were recorded concurrently. Hippocampal theta oscillation either appeared spontaneously or was elicited by sensory stimulation (tail pinch).

Identification of juxtacellularly labeled neurons

After data recording, labeling, and a survival period of 10 to 120 minutes, the animals were perfused transcardially with a fixative containing 0.05% glutaraldehyde, 4% paraformaldehyde and 0.2% picric acid in 0.1 M phosphate buffer (PB; pH=7.4). Brains were removed and the block containing the septum was cut and postfixed in glutaraldehyde-free fixative overnight. Coronal sections of 60 µm thick were cut on a vibratome from the tissue blocks. After washes in PB (three times for 20 minutes each) the sections were transferred into Tris (Sigma)-buffered saline (TBS), pH 7.4, and, from this step, all of the washes and serum dilutions were performed in TBS (0.02% saponin (Sigma) was added to antibody solutions to enhance penetration). The sections were incubated with streptavidin-conjugated Alexa 488 (1:3000; Molecular Probes, now

Invitrogen, Carlsbad, CA, USA) for 2 hours to identify the biocytin- or Neurobiotin-labeled neuron by fluorescent microscopy (Axioscope; Zeiss, Oberkochen, Germany). The wavelength for filter sets absorption and emission (in nm): 365 bandpass / 420–460, 450–490 / 512–542, 546 ± 12 / 590 long pass. The section containing the labeled cell was incubated in PV (mouse anti-parvalbumin dilution: 1:1000, Swant) and HCN (guinea pig anti-HCN1, kind gift from prof. Ryuichi Shigemoto (Notomi and Shigemoto 2004), dilution: 1:500) primaries overnight at room temperature, followed by a secondary antibody (Alexa350 conjugated goat anti-mouse (1:50, Invitrogen - Molecular Probes) or Alexa594 goat anti-guinea pig (1:200, Invitrogen - Molecular Probes)) for 2 hours. The sections were mounted on slides, coverslipped (Vectashield) and examined by fluorescent microscopy. The result was documented by digital camera (DP-70; Olympus Optical, Tokyo, Japan). HCN1-immunoreactive neurons are referred as HCN-immunoreactive throughout this report. HCN1 and HCN2 were shown to completely colocalize in the MS (Varga et al., 2008). Representative examples of labeled medial septal neurons are shown in Figure 19. The number of identified neurons used in the analysis of time delays and in the information theory analysis (mutual information and transfer entropy calculations) as well as the overlap of these neurons with the ones used for the studies of Borhegyi et al. (2004) and Varga et al. (2008) are indicated in Table 1.

Table 1: Identification of medial septal neurons

	all cells	Z-shift	MI	Z-shift & MI
PV/NT*	14	13	9	8
PV/HCN**	12	12	9	9
PV/non-HCN	0	0	0	0
non-PV/NT***	3	3	3	3
non-PV/HCN**	6	6	4	4
non-PV/non-HCN****	8	7	4	3
NT/NT	157	146	50	39
NT/HCN**	2	2	2	2
NT/non-HCN	0	0	0	0
hippocampal	27	27	7	7

* included in Borhegyi et al., 2004

** included in Varga et al., 2008

*** one of those included in Borhegyi et al., 2004

**** three of those included in Varga et al., 2008

PV: parvalbumin-immunoreactive; non-PV: parvalbumin-immunonegative; HCN: HCN-immunoreactive; non-HCN: HCN-immunonegative; NT: not tested (NT in the first position indicates that the cells were not tested for PV, whereas NT in the second position denotes that the neurons were not tested for HCN); all cells: number of all analyzed neurons; Z-shift: number of neurons included in the Z-shift analysis (including those that were subjected to the MI analysis as well); MI: number of cells included in the MI calculations (including those that were subjected to the Z-shift analysis as well); Z-shift & MI: number of cells included in both analyses (the overlap between columns 2 and 3).

Data analysis

Wavelet spectrum

Our signals recorded in the time-domain were decomposed in the time-frequency domain using Continuous Wavelet Transform (CWT), as published in Torrence and Compo (1998). Medial septal (or hippocampal) unit recording was first discriminated (i.e., converted to a zero-one series with ones at the localizations of spikes and zeros elsewhere) and convolved with a sinc ($sin(x)/x$) kernel before wavelet transform. Hippocampal LFP and sinc-convolved unit were down-sampled at 1000 Hz, standardized (normalized to zero mean and unitary standard deviation) and then decomposed to 189 scales with equivalent Fourier frequencies varying from 0.5 Hz to 500 Hz, which corresponded to the Nyquist frequency (Fig. 18B).

Every signal sampled at discrete time points can be decomposed to a set of sine waves of different frequencies using the discrete Fourier transform. Wavelet transform also takes its bases on this theorem; however in this case, the signal is decomposed to scaled and shifted versions of a finite waveform (the wavelet) (Fig 15). The use of a finite wavelet instead of a theoretically infinite sine wave results in the good temporal resolution of the CWT method. The wavelet coefficients at a given time point indicates the extent to which the different (i.e., scaled and translated) wavelets are represented in the signal. Scales can be easily interpreted as frequencies (similar to the case of decomposition to sine waves), whereas the shifting parameter indicates the phase of the

wavelet. Thus, CWT results in a matrix that indicates the magnitude and phase of the frequency components of the signal at each time point.

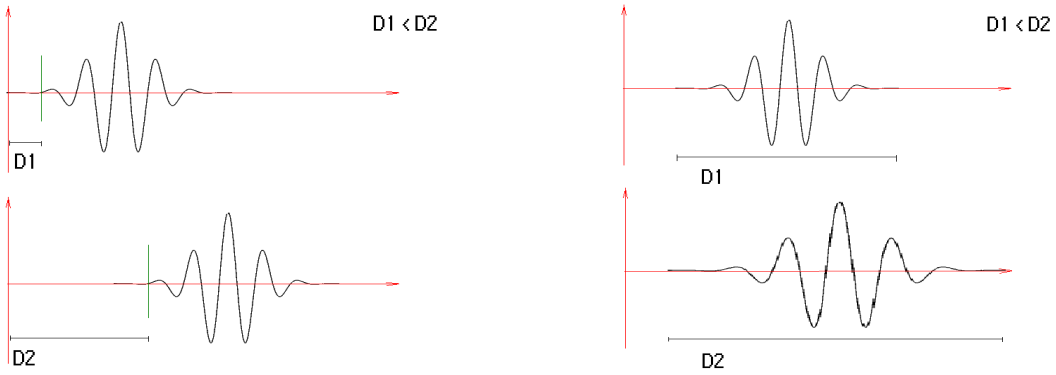

Figure 15. The Morlet wavelet. This figure illustrates the effect of shifting (left) and scaling (right) on the Moret wavelet.

We give a brief description of the mathematical application of CWT. Assume to have an evenly sampled time series x_n (n = 0,1,...,N-1) with δt sampling time. In order to calculate CWT, a "mother" wavelet function has to be chosen, $\Psi_0(\eta)$, which depends on the non-dimensional time parameter η. In the present study, Morlet wavelet was applied, consisting of a plane wave modulated by a Gaussian envelope of unit width:

(1) $$\Psi_0(\eta) = \pi^{-1/4} e^{i\omega_0\eta} e^{-\eta^2/2},$$

where ω_0 constant was taken to be 6 according to Farge, 1992. Wavelet coefficient at a given time-scale pair (n,s) was defined by the convolution of the recorded time series x_n and the scaled and translated wavelet function:

(2) $$W_n(s) = \sum_{n'=0}^{N-1} x_{n'} \Psi^* \left[\frac{(n'-n)\delta t}{s} \right],$$

where * denotes complex conjugate and Ψ is a version of Ψ_0 that is normalized to have unit energy, which can be defined via the following equation:

(3) $$\Psi\left[\frac{(n'-n)\delta t}{s} \right] = \left(\frac{\delta t}{s} \right)^{1/2} \Psi_0 \left[\frac{(n'-n)\delta t}{s} \right],$$

from which

(4) $$W_n(s) = \sum_{n'=0}^{N-1} x_{n'} \left(\frac{\delta t}{s} \right)^{1/2} \Psi_0 \left[\frac{(n'-n)\delta t}{s} \right]$$

holds. Scales can be easily translated into Fourier frequencies; spectral power and phase at a given time-frequency point are defined as the absolute power and the argument of the appropriate complex wavelet coefficient (Muthuswamy and Thakor, 1998; Misiti, 2000).

Selection of analyzed segments

Selection of theta and non-theta segments was based on the analysis of the wavelet power spectrum of the hippocampal LFP. For the analysis of firing behavior of HCN-expressing septal neurons, theta segments were distinguished based on the ratio of wavelet power in the theta (2.5 to 6 Hz) and in the delta (0.5 to 2.5 Hz) frequency band. Theta episodes were defined as the segments where the above ratio reached a threshold of mean + 0.5 standard deviation SD. Frequency band boundaries were chosen according to the observation that urethane anesthesia lowers the limits of the traditional frequency bands (Leung, 1985; Clement et al., 2008). For the analysis of temporal delays and information theory measures, a stricter definition of theta segments was applied as follows. Maximum location of wavelet power spectrum along scales was calculated for each time point. Time segments where the above defined point-wise maxima fell consecutively in the theta band were considered as theta segments. Complementary, non-theta segments were defined as segments where spectral maxima fell consecutively out of the theta band. Two hundred ms long edges were left from the beginning and the end of all theta and non-theta segments. In order to compare mutual information during theta and non-theta segments, we needed a proper definition for large amplitude irregular activity. Since information processing during sharp wave-ripple complexes is believed to be substantially different from other non-theta activity patterns (Csicsvari et al., 1999), we had to exclude those episodes from the analysis. Sharp wave-ripple segments were detected after filtering the LFP between 90 and 145 Hz (Klausberger et al., 2003) using high-order finite impulse response filters, and calculating the root mean square (RMS) of the filtered signal in 100-point (10 ms) non-overlapping windows. The detection threshold for ripples was mean + 5 standard deviation of the RMS of the signal; the beginning and end of ripples were determined at RMS values of mean + 1 SD. Segments of large amplitude irregular activity were

defined as non-theta non-sharp wave segments (except 4 recordings in the firing analysis of HCN-containing MS cells, in which a maximum of 2 ripples occurred in the analyzed non-theta segments); they are referred to as “non-theta” segments hereinafter. Only segments longer than 5 seconds were taken into account. For most of the analysis, the longest theta and non-theta segments were chosen.

Firing pattern analysis of HCN-expressing neurons of the medial septum

Theta modulation of unit firing was quantified by the relative theta power of the unit autospectrum. The autospectrum was calculated by generating the power spectral density estimate of the autocorrelation function (bin size: 10 ms) of the discriminated unit (see above) using the Welch method as implemented in the pwelch function of Matlab (frequency-resolution: 0.2 Hz; the central 512 points of the autocorrelogram were used in the spectral calculations). State-dependent firing rate of medial septal and hippocampal neurons was also computed.

Theta modulated firing was also analyzed in the time domain by introducing a measure called the theta propensity index (TPI). TPI was determined as the time during which the wavelet power maxima of the unit fell in the theta band divided by the time while the wavelet power maxima of the LFP was in theta band. For this calculation, the entire recording segment was used in each neuron. A value <1 shows that the unit was weakly theta modulated (non-bursting or tonic cells), a TPI near 1 indicates that the theta bursting of the unit was strictly coupled to the theta rhythm in the LFP (tail pinch responsive cells), TPI > 1 shows that the unit was theta modulated during both theta and non-theta episodes of the hippocampal LFP (strongly theta-modulated, non-theta-associated theta bursting or constitutive bursting cells).

All pair-wise comparisons were done by Mann–Whitney U test. Interdependence of firing pattern and HCN immunoreactivity was tested by $\chi 2$-test. Anatomical group and physiological parameter interactions were further investigated using repeated measures ANOVA with anatomical identity as the grouping variable and hippocampal state (non-theta, theta, ripple) as the repeated measures factor. Threshold of significance

was set to a level of 0.05. The statistical tests were carried out using Statistica (Statsoft Inc., Tulsa, OK, USA).

Identification of theta-bursting medial septal neurons

In order to separate septal neurons showing bursting activity pattern with frequency of bursts falling in the theta range (i.e. theta-bursting neurons), we applied the slightly modified version of the semi-automatic procedure published in Borhegyi et al. (2004). Hierarchic cluster analysis on interspike intervals (ISI) using Euclidean distance measure and Ward's amalgamation rule was performed (Dekhuijzen and Bagust, 1996). Cluster tree (dendrogram) was cut iteratively at different linkage distances in order to have 2 to 7 clusters and the cluster containing the smallest ISI (which obviously corresponded to the cluster of intraburst intervals for bursting neurons) was selected in each case. In each iteration, a recurrence plot was produced showing every ISI against the previous ISI. If any of the iterated clustering processes succeeded to separate the intraburst intervals (as the cluster containing the smallest interval) on the recurrence plot, we considered the neuron as theta-bursting.

In the case of bursting neurons, a burstiness index (BI) was calculated as the number of intraburst spikes relative to the number of all spikes of the neuron. Average number of spikes in bursts, intraburst firing frequency and burst duration were also computed.

Identification of hippocampal interneurons

Hippocampal interneurons were differentiated from principal cells based on the following assumptions: interneurons fire at higher rate (mean firing rate: 6.52 ± 6.21 Hz (mean ± SD), peak firing rate calculated in 5 second non-overlapping windows: 10.78 ± 8.37 Hz), produce narrower spikes (width at maximal amplitude: 0.58 ± 0.37 ms) and did not fire complex spikes (equivalent to low threshold bursts; Csicsvari et al., 1999; Fuentealba et. al, 2008; see also "The hippocampus" subsection of the Introduction).

Calculating phase angles

Phase values for medial septal (or hippocampal) action potentials as correlated to hippocampal LFP were defined using the *analytic signal* method (Gabor, 1946). Hilbert transform of the LFP (*x(t)*) was calculated:

$$(5) \qquad x_H(t) = \frac{1}{\pi} \lim_{c \to \infty} \int_{-c}^{c} \frac{x(\tau)}{t - \tau} d\tau ,$$

from which the complex valued analytic signal can be obtained:

$$(6) \qquad \varsigma(t) = x(t) + i x_H(t).$$

Phase values can be defined as the angles of $\zeta(t_k)$ values where t_k denotes the localization of the *k*th medial septal (or hippocampal) action potential (Rosenblum et al. 1996, 2001; Schafer et al. 1999).

For the phase analysis of medial septal HCN-immunoreactive neurons, a different method of phase value calculation was applied based on the instantaneous phase values of the crosswavelet spectrum of the unit and the LFP. The algorithm is discussed in details in the studies of Borhegyi et al. (2004) and Varga et al. (2008).

Phase preference analysis of HCN-containing neurons of the medial septum

For each neuron, the phase histogram was determined and tested against the null hypothesis of circular uniformity by Rao's spacing test (Rao, 1972; Rao, 1976) and Watson's test for uniformity (Watson, 1961). Then, the circular mean and the mean vector length were determined, the latter analogous to coupling strength (0: no coupling; 1: maximal coupling) (Fisher, 1993).

To test whether the identified anatomical classes show group-level phase preference, a cumulative phase histogram of each anatomical group was generated from balanced pooled samples of phase values. Phase preference of anatomical groups was analyzed by the same statistical tests as the individual neurons (see above). In case of the double immunoreactive group of neurons containing both PV and HCN, the distribution of phase angles was bimodal, which was verified by fitting the distribution with the mixture of two von Mises probability density functions (Fisher, 1993). The

mixing ratio, error of estimate, mean phases and mean vector length values of the fitted distributions were calculated. The phase distributions of anatomical classes were compared using Watson's test for homogeneity.

Z - shift methods

The null hypothesis of Rayleigh's test is that phase angle values show uniform distribution on the circle while the alternative hypothesis stands for phase preference, that is, unimodal non-uniform phase angle distribution (Fisher, 1993). In our case, the value of Rayleigh's Z-statistic indicates the strength of phase coupling (or degree of non-uniformity) between unit events and hippocampal field potential. After fixing hippocampal LFP in the time domain, unit was shifted relative to the field activity by different τ (time) values (-1 second < τ < 1 second). Subsequently, we calculated Rayleigh's Z-statistics (proportion to degree of phase-locking) for all time-shifts (τ). Z-statistics was given by the following equation:

(7) $$Z = n\overline{R}^2,$$

where R denotes the mean resultant length of the given phase series Φ_j (j = 1,...,n):

(8) $$\overline{R} = \left| \frac{1}{n} \sum_{j=1}^{n} e^{j\phi_j} \right|.$$

The probability that the null hypothesis of uniformity holds can be calculated as follows:

(9) $$p = e^{-Z}\left[1 + \left(2Z - Z^2\right)/(4n) - \left(24Z - 132Z^2 + 76Z^3 - 9Z^4\right)/(288n^2)\right];$$

for $n \geq 50$, $p = e^{-Z}$ approximation is appropriate. (However, the exact p value was calculated in the present study in all cases, regardless of the value of n.) Z-shift was defined as the τ value by which shifting unit relative to LFP results in maximal phase-locking (the highest value of the Z-statistics; Fig. 16 and 17). In Figure 16C, the highest peak of the Z-value in the function of time lags corresponds to strongest phase coupling. It appears in the positive halfplane, which implies that the action potential series have to be shifted with a positive value to get maximal phase preference, thus unit leads LFP activity. Vice versa, highest peak in the negative halfplane would infer the lead of the LFP signal over unit activity. Medial septal or hippocampal units that failed to reach a

significant level of phase preference at any delay values ($p > 0.005$, Rayleigh-test) were excluded from this analysis. Thus, Z-shift algorithm is applicable for units with significant phase preference (at least after the application of a given delay), that is, for theta-bursting cells, or neurons showing frequency-changes at specific phases of the theta cycle ("theta-modulated cells"). However, it is inappropriate for neurons with theta-independent firing pattern, e.g. for tonic or irregularly firing cells. Using this method we were able to determine the time delay between corresponding events in the medial septal or hippocampal unit and hippocampal field activity (Siapas et al., 2005). Comparisons between anatomical groups were performed with Mann-Whitney U-test. Results presented on box-whisker plots show median, interquartile range and non-outlier range.

Additionally, the analysis of Z-shifts was repeated using Rao's spacing test, which tests circular uniformity against all other circular distributions, thus being more general than Rayleigh's test. However, Rayleigh's test is more sensitive in detecting unimodal deviation from uniformity. For the details on calculating Rao's statistics, see Rao, 1972 and 1976. The two tests provided statistically similar results, thus we confine ourselves to the presentation of the results from Rayleigh's analysis.

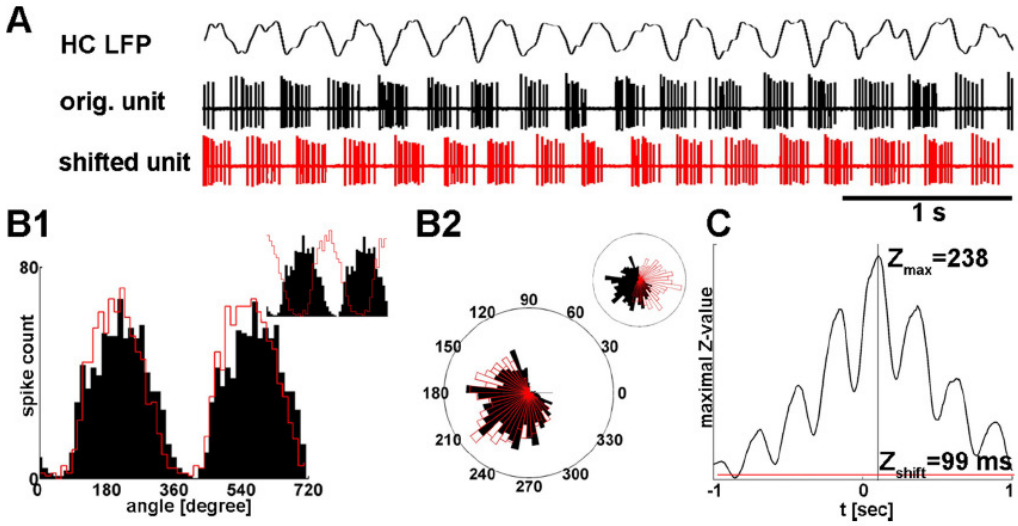

Figure 16. Illustration of Z-shift methods on a medial septal neuron. A: Z-shift analysis of the longest theta segment of a recording is demonstrated. Five second long epoch from the hippocampal LFP band-pass filtered between 2 and 8 Hz is shown above medial septal unit activity. Red action potential series correspond to the MS unit

delayed by Z-shift, the optimal time lag by which shifting the unit activity results in the strongest phase locking. **B1**: Circular distribution of phase values of septal action potentials relative to hippocampal theta oscillation is displayed in black for two theta cycles (zero phase was associated to the trough of the theta cycle). Red line indicates phase angle distribution of the shifted medial septal action potentials, centered to overlap with the original distribution. (Relation of the two histograms without centering is shown on the inset.) Histogram of shifted unit is slightly more focused than the original, which indicates higher level of phase preference. Rayleigh's Z-statistic is sensitive enough to measure such mild differences reliably. **B2**: The same phase histograms are shown on rose diagram; inset displays rose diagram without centering the histogram of shifted action potentials. **C**: Rayleigh's Z-statistic is plotted against different time lags from -1 to 1 second. Red line shows the level of significant phase locking at p = 0.005. Maximum location of the function is Z-shift, the optimal delay to reach the highest "synchrony" between LFP and septal unit, while maximal Z-value describes the strength of the maximal coupling.

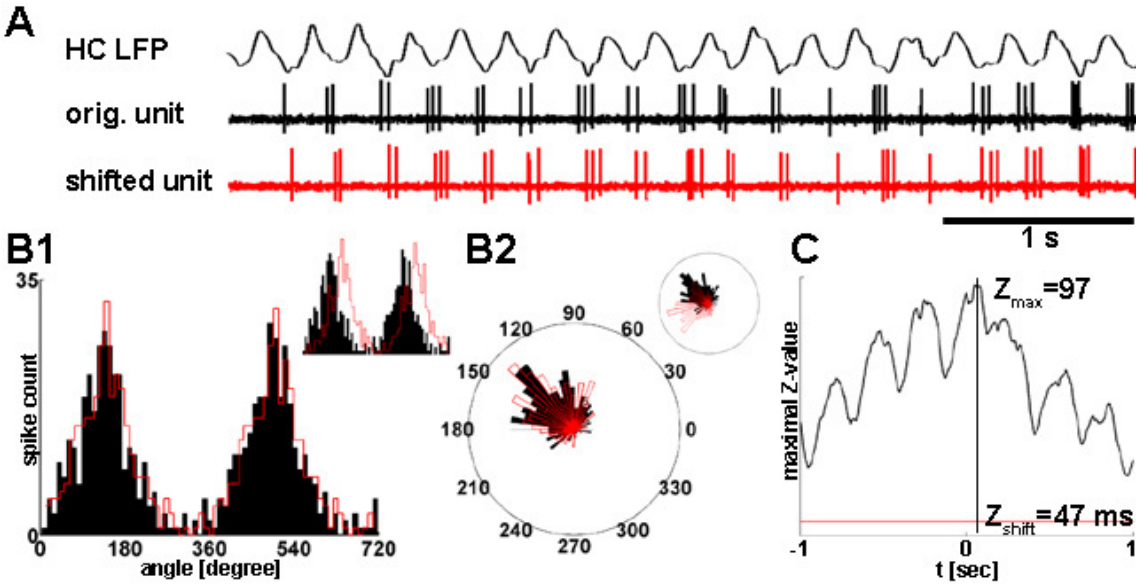

Figure 17. Illustration of Z-shift methods on a hippocampal neuron. This figure demonstrates the Z-shift algorithm for a putative hippocampal interneuron in the same way as Figure 16 does for a medial septal neuron. Organization and notations follow those of Figure 16.

Information theoretical approach

Mutual information

The information theoretical method operates as follows. After calculating wavelet spectra of both signals, wavelet power matrices were cut into 1-second-long segments for scales from 2.5 to 6 Hz in order to get time-frequency windows. Distribution of wavelet power values falling into a specified window was estimated with a histogram and entropy of the distribution was defined using Shannon's formula (Shannon, 1948):

(10) $$H(X) = -\sum_i p_i \log p_i$$

where *H(X)* denotes the entropy (or information content) of power value distribution, p_i denotes the relative frequency of the *i*th bin (Fig.18C). The same method was used to compute the entropy of the joint power value distribution of corresponding windows of the two signals (Fig.18D, left plot).

(11) $$I(X,Y) = H(X) + H(Y) - H(X,Y)$$

Equation (11) gives mutual information (*I(X,Y)*), where *H(X)* and *H(Y)* are the entropies of power value distributions in corresponding windows, *H(X,Y)* is the entropy of the appropriate joint distribution (Fig.18D, right plot). The estimation of entropy and mutual information (MI) from histograms can carry certain types of bias. Hence, these estimations were adjusted using the Panzeri-Treves bias-correction method as reported in Panzeri et al. (2007). Balanced pooled samples for group statistics were generated by taking the first 4 MI values of the analyzed segments. Statistical comparisons were accomplished using either Mann-Whitney U-test (comparison between anatomical or physiological groups of cells) or Wilcoxon signed rank test (comparison between real and control data or theta and non-theta segments). Theta-associated changes of MI were judged at the level of p = 0.01 using Mann-Whitney U-test. Results presented on box-whisker plots show median, interquartile range and non-outlier range.

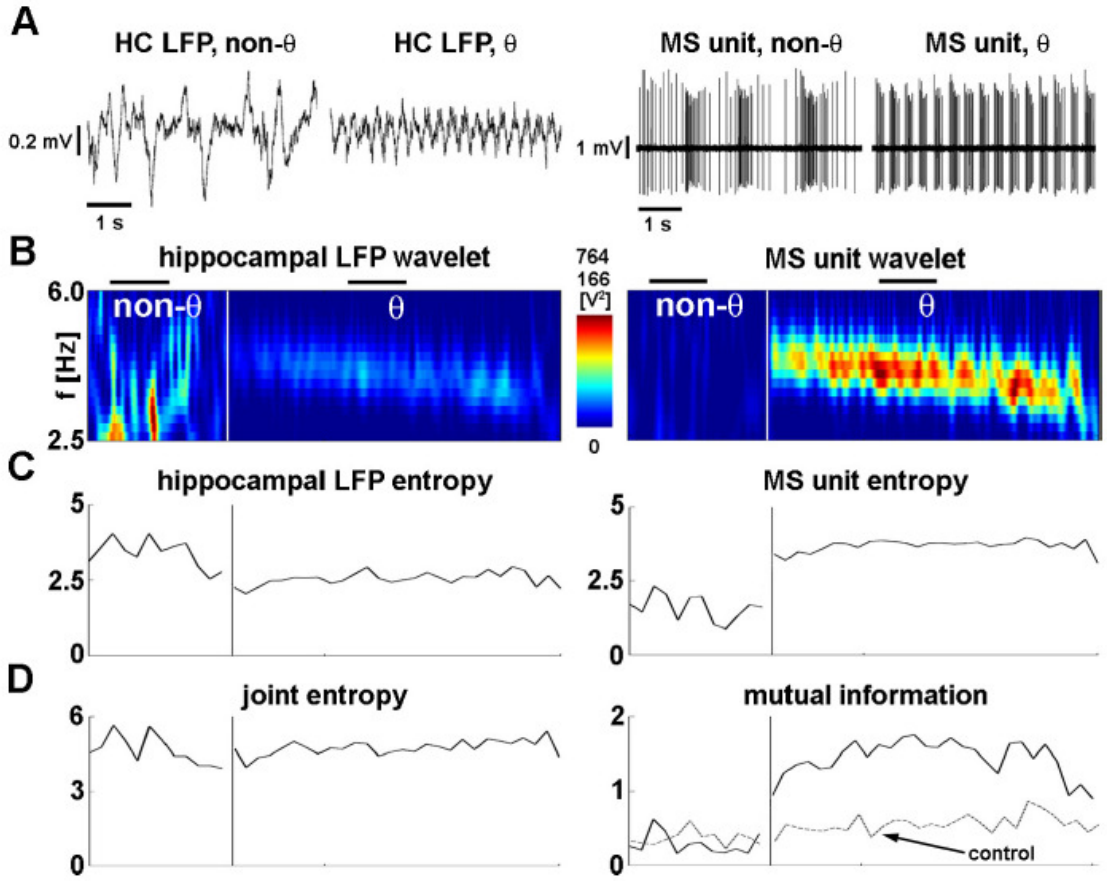

Figure 18. Calculation of wavelet mutual information. **A**: Five second long recordings of hippocampal LFP (left column) and medial septal unit (right column). Within the columns left recordings show non-theta activity and right recordings correspond to theta oscillation. The demonstrated septal neuron exhibits theta-frequency bursting during theta rhythm. **B**: Wavelet power spectra of the hippocampal LFP (left) and medial septal unit activity (right). Time is displayed on the x axis while frequency is showed on y (only the theta-band is displayed). Color-coded values indicate the wavelet power coefficients at given time and frequency. Color-code is indicated on the color-bar between the two plots; upper value above the color-bar shows the upper limit for the LFP and lower value shows the upper limit for unit wavelet power. White vertical line separates non-theta and theta episodes; the segments before and after the white line are the longest non-theta and theta segments, respectively. Horizontal black lines above the LFP wavelet designate the positions of the 5 second long raw data segments shown in A. At the onset of theta, the distribution of spectral components markedly changed in both LFP and unit activity: power density concentrated in the theta

band. Note that even during non-theta, significant amount of power can be observed in the theta band (warm color = high power). **C**: Information content (entropy) of hippocampal LFP (left) and medial septal unit (right). **D**: Joint information content of LFP and unit (joint entropy, left) and amount of common information (mutual information, right). Dashed line shows control mutual information. At the onset of theta oscillation (1) theta frequency range information content of the LFP decreased, (2) information content of unit increased, (3) the joint entropy remained relatively unchanged and (4) the mutual information increased in the presented recording. HC, hippocampus.

Transfer entropy

Transfer entropy (TE) and preferred direction of flow (DF) were calculated as reported in Gourevitch and Eggermont (2007). Let X^F and Y^F denote the theta-band wavelet power values of the LFP and unit wavelet (respectively) falling into the "future" time window $[t,\ t + \tau_F]$ relative to a given time point t. (To simplify the expressions, we omit time-indexing of the variables.) In a similar way, X^P and Y^P denote the wavelet power values of the "past" time window $[t - \tau_P,\ t]$. Equation (12) gives transfer entropy:

$$(12) \qquad TE_{X\to Y} = I(Y^F; X^P \mid Y^P) = H(Y^F \mid Y^P) - H(Y^F \mid X^P, Y^P),$$

where $X|Y$ type notations designate the distribution of X conditional on Y, e.g. $H(Y^F|Y^P)$ denotes the entropy of the future of Y conditional on its past. We can rewrite TE as follows:

$$(13) \qquad TE_{X\to Y} = I(Y^F; (X^P, Y^P)) - I(Y^F, Y^P).$$

Equation (13) shows that TE gives the amount of information on the future of Y provided by the additional knowledge of the past of X over the past of Y.

Following the algorithm of Gourevitch and Eggermont (2007), we calculated control TE by randomly shuffling the interspike intervals of the medial septal unit. Based on this control, we computed normalized transfer entropy (NTE):

$$(14) \qquad NTE_{X\to Y} = \frac{TE_{X\to Y} - TE_{X\to Y}^{shuffled}}{H(Y^F \mid Y^P)}.$$

Finally, we calculated an index of preferred direction of flow (DF):

(15) $$DF_{X\to Y} = \frac{NTE_{X\to Y} - NTE_{Y\to X}}{NTE_{X\to Y} + NTE_{Y\to X}}.$$

DF takes its values between -1 and 1. Negative values indicate septo-hippocampal dominance of information transmission, whereas positive values show hippocampo-septal directional dominance.

We chose identical τ values for future and past time windows. τ value that maximizes NTE was used, as reported in Gourevitch and Eggermont (2007). Sampling bias problem of entropy and mutual information values computed during the calculation of TE and derivatives were corrected using the Panzeri-Treves bias correction algorithm (Panzeri et al., 2007). Like in MI calculations, the first 4 NTE and DF values were used for the generation of pooled samples. Only those neurons were included in TE calculations, where a significantly higher than control MI was detected. To harmonize with the normalizing algorithm of TE published in the study of Gourevitch and Eggermont (2007), the ISI-shuffling method of control generation was applied for the MI values as well (see below). Significant difference between real and control data was judged at a level of $p = 0.01$ (Wilcoxon signed rank test). Comparisons between theta and non-theta segments, bursting and non-bursting neurons and anatomically identified groups of cells were performed using Mann-Whitney U test. Directional NTE values were compared using Wilcoxon signed rank test. Results presented on box plots indicate median, interquartile range and non-outlier range.

Controls

For the mutual information calculations, three types of controls were used. Original hippocampal LFP of the analyzed recording segment was compared to an artificial unit generated by a random Poisson process with frequency adjusted to the original medial septal (or hippocampal) action potential frequency on the chosen segment. In order to further verify the method, two other types of controls were also calculated in all parts of the analysis. First, medial septal (or hippocampal) unit was cut into 1-1.2 second long sections, and these sections were shuffled using a random permutation. Second, interspike intervals of the septal (or hippocampal) action potential series were randomly shuffled. Main results of the study were independent of the choice among the above three types of controls, although the particular statistical tests

comparing real an control data could yield different results in some of the cases (see Figure 29 and 30). For TE calculations, the advantages of the third type of control were documented in the study of Gourevitch and Eggermont (2007), hence in this case we confined ourselves to the use of the latter method of control generation. Significant difference between real and control data was accepted at the level of $p = 0.01$.

Data analysis was implemented in Matlab development environment (MathWorks, Natick, MA) using self-developed and built-in functions. Freely available wavelet program of Christopher Torrence and Gilbert P. Compo (University of Colorado) was utilized for wavelet analysis.

Results

HCN-immunoreactive neurons have firing characteristics ideal for forming a pacemaker group

The hyperpolarization-activated, cyclic nucleotide-gated non-selective cation channel (HCN) plays a key role in various pacemaker mechanisms including rhythmic contractions of the heart muscle and neuronal oscillations. In addition, HCN channel participates in the regulation of electrophysiological properties of neurons by setting neuronal excitability and influencing the propagation of voltage changes. A subset of medial septal GABAergic neurons express HCN channel on their soma-dendritic membrane, which raises the possibility that these neurons participate in the pacing of hippocampal theta oscillation. Does HCN-immunoreactive (HCN-IR) septal neurons have appropriate firing characteristics to fulfill this function, or HCN channel may serve other mechanisms on these cells? To address this question, we analyzed the firing properties of 25 HCN-IR and 12 HCN-immunonegative septal neurons. Examples of anatomically identified medial septal neurons are shown in Figure 19.

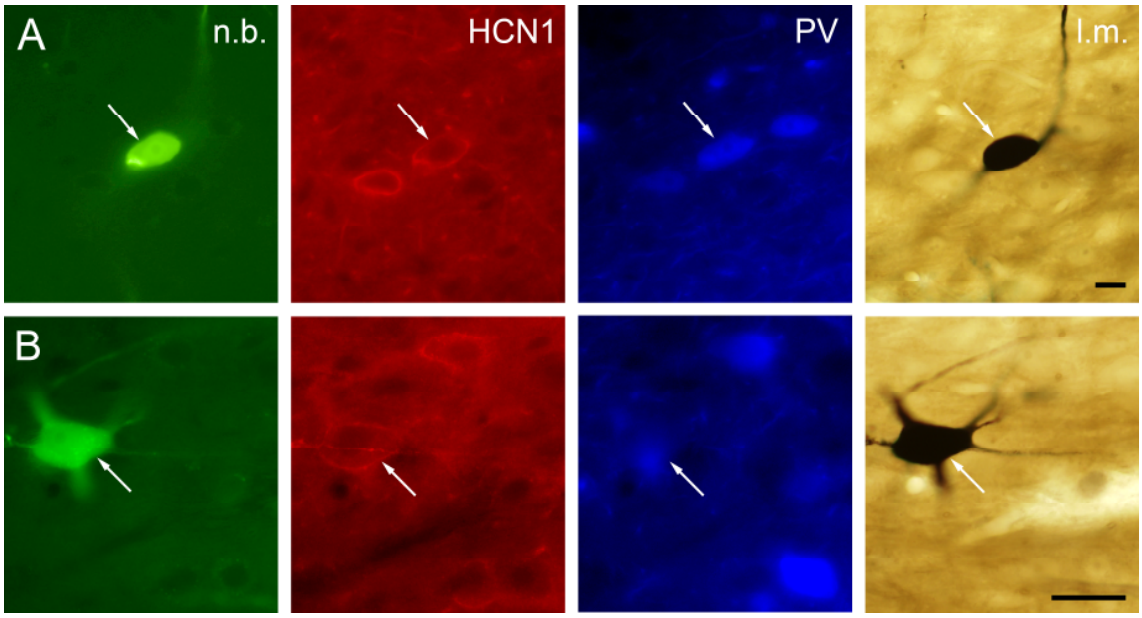

Figure 19. Immunocytochemical identification of juxtacellularly labeled medial septal neurons. Columns from left: Neurobiotin-labeled soma and/or dendrites; HCN1

immunoreactivity; PV immunoreactivity; light micrograph after nickel-intensified DAB reaction. **A**: The white arrows point to a medial septal neuron expressing both HCN1 and PV. **B**: Representative example of an MS neuron containing HCN1 but not PV (the immunoreactivity near the arrowhead belongs to a cell out of focus). PV-immunoreactive elements can also be observed in the vicinity of the labeled cell. Scale bars: 10 μm. nb, Neurobiotin; lm, light micrograph.

HCN-IR neurons show theta-rhythmic firing

Our analysis revealed that all recorded HCN-IR (n = 25) neurons fired in a theta-rhythmic manner (i.e., rate of action potential firing changed rhythmically with a frequency falling into the theta range) during spontaneous and sensory elicited theta oscillation in the hippocampus (Fig. 20). On the contrary, only 4 of 12 HCN-immunonegative neurons showed theta-rhythmic firing associated to hippocampal theta, while one non-HCN neuron fired spike clusters at low, non-theta frequency (Fig. 21) during theta episodes. Degree of theta-rhythmic firing was quantified by calculating the relative theta-band power of unit autospectra. Statistical analysis of relative theta power in HCN-IR and HCN-immunonegative septal cells revealed significant difference between the above groups of cells (significant 'anatomical group'–'hippocampal state' interaction shown by repeated measures ANOVA (groups: HCN versus non-HCN; states: non-theta versus theta; $p < 0.01$, n = 37); significantly higher relative theta power revealed by pairwise comparison of HCN-IR and non-HCN neurons (Mann–Whitney U test; theta segments: $p < 0.001$, non-theta segments: $p < 0.01$; see also Table 2 and Materials and Methods)). Those HCN-IR neurons that were also tested for PV content were subdivided to PV-immunopositive (HCN+/PV+, n = 14) and PV-immunonegative (HCN+/PV-, n = 8) groups. These subgroups did not show any significant difference in the degree of theta-rhythmic firing ($p > 0.05$, see also Table 2).

The overall higher theta content of HCN-IR versus HCN-immunonegative neurons' firing pattern may result from the longer duration of theta rhythm in unit activity arising partly independently from the hippocampal LFP in the former group. Therefore we examined this property by calculating the full length of those segments characterized by theta-rhythmic firing and normalized to the length of the hippocampal

theta episodes for each neuron (TPI, theta propensity index; see Materials and Methods). Neurons spending more time in theta-rhythmic firing mode than the time hippocampus spends in theta state are characterized by TPI > 1. Most of the HCN-IR neurons were shown to have larger than 1 TPI (14 of 25, 56%), whereas only 2 of 12 (16.67%) non-HCN cells had a TPI value > 1. Accordingly, TPI of HCN-IR neurons were significantly higher than that of HCN-immunonegative septal cells ($p < 0.001$, see also Table 2; HCN+/PV+ and HCN+/PV- groups did not differ significantly).

	Firing rate (Hz)			Theta modulation (%)		TPI
Group	B	TP	R	B	TP	
All HCN ($n = 25$)	12.79 ± 8.71	19.25 ± 7.55	14.01 ± 14.54	10.47 ± 11.66	55.10 ± 35.85	1.31 ± 1.37
PV/HCN ($n = 14$)	12.02 ± 8.55	19.82 ± 6.15	14.57 ± 17.59	14.94 ± 22.09	57.07 ± 34.40	1.74 ± 2.29
Non-HCN ($n = 12$)	11.65 ± 11.79	15.15 ± 11.52	7.47 ± 9.11	3.93 ± 4.96	11.38 ± 31.05	0.58 ± 0.73

	Burstiness (%)		Intra-burst F (Hz)		Spikes in burst		Burst length (ms)	
	B	TP	B	TP	B	TP	B	TP
All HCN ($n = 11/24$)*								
Baseline bursting	95 ± 5	99 ± 4	36.9 ± 5.5	48.2 ± 22.7	5.1 ± 2.6	5.6 ± 3.4	108 ± 22.7	98.3 ± 21.2
All bursting	—	98 ± 3**	—	46.7 ± 25.8	—	5.6 ± 3.3	—	98.8 ± 39.3
PV/HCN ($n = 9/14$)*								
Baseline bursting	97 ± 5	99 ± 2	36.9 ± 11.2	44.6 ± 21.4	5.1 ± 1.6	5.6 ± 1.8	108 ± 22	98.3 ± 20.1
All bursting	—	99 ± 2**	—	46.7 ± 21.7	—	5.5 ± 2.9	—	95.9 ± 21.2
Non-HCN ($n = 0/4$)*	ND	0 ± 94**	—	30.9 ± 12.7	—	4.7 ± 2.1	—	114 ± 44.6

Table 2. Firing characteristics of anatomically identified groups. Values are median ± interquartile range. B, baseline = non-theta; TP: tail pinch = theta; R, ripple; TPI, Theta Propensity Index. All HCN, all HCN neurons were included (PV-IR, non-PV and those not tested for PV-content); PV/HCN, the PV-containing subgroup of all HCN cells; ND, not detected, e.g. in case of non-HCN neurons, theta bursts were not observed during non-theta; *, the first number denotes neurons firing in theta bursts during non-theta periods whereas the second number equals to all theta bursting neurons in that category; **, for the calculation of burstiness during theta, all bursting and non-bursting neurons were included (n = 25 HCN, n = 14 PV+/HCN+ and n = 12 non-HCN).

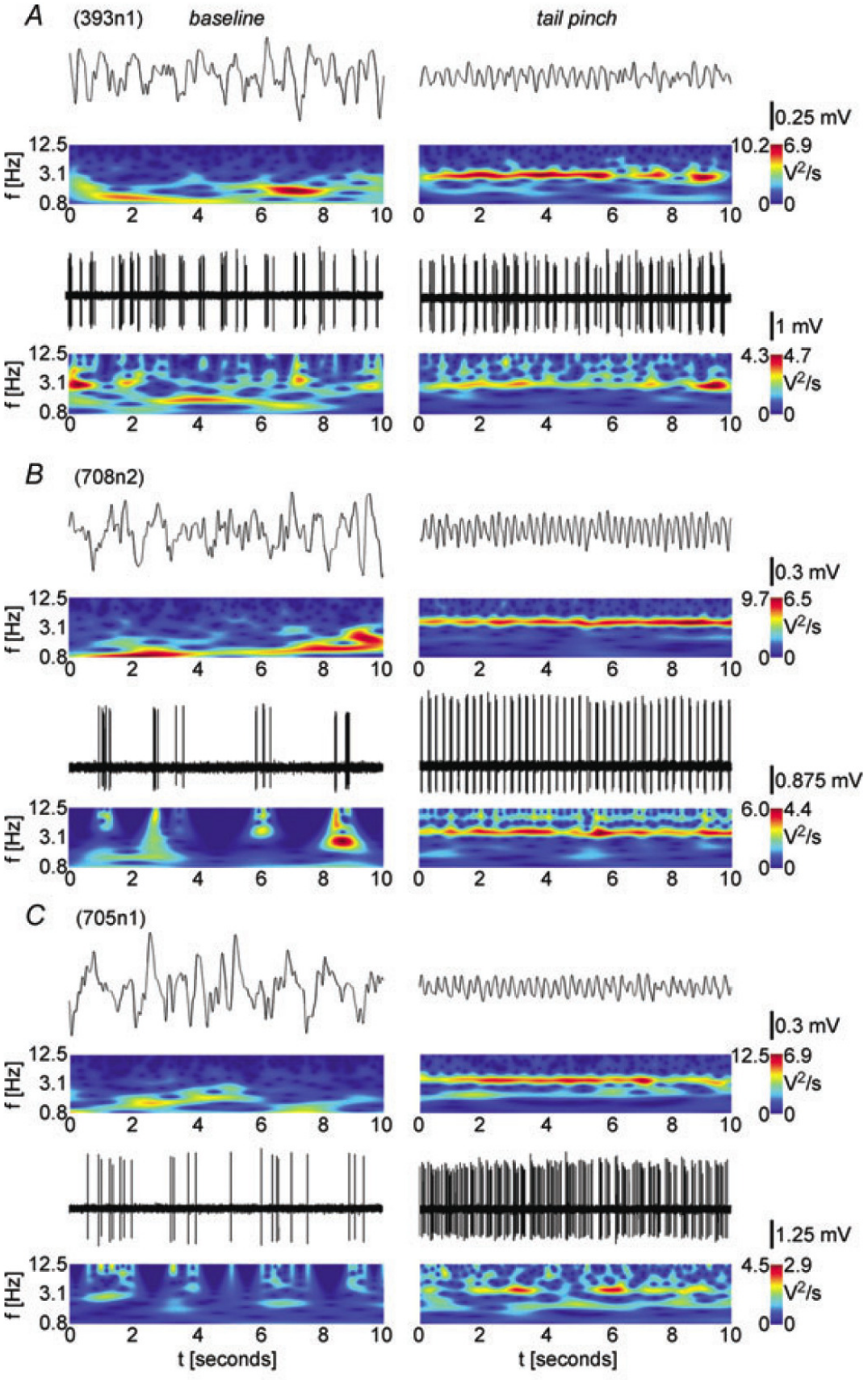
A
(393n1)
baseline
tail pinch
0.25 mV
f [Hz]
12.5
3.1
0.8
10.2
6.9
V²/s
0
0 2 4 6 8 10
1 mV
4.3
4.7
B
(708n2)
0.3 mV
9.7
6.5
0.875 mV
6.0
4.4
C
(705n1)
0.3 mV
12.5
6.9
1.25 mV
4.5
2.9
t [seconds]

Figure 20. Firing characteristics of HCN-IR neurons. Ten second long raw data segments are presented. Wavelet power spectrum of each segment is displayed below raw data trace. Theta band (2.5 to 6 Hz) can be seen in the upper half of the wavelets. Warm colors indicated higher values (see the color bars right to the spectra; the numbers left and right to the color bars show the minimal and maximal values for the wavelets presented on the left and on the right, respectively). **A** shows the activity of an HCN-IR neuron that fired theta-frequency bursts not only during theta episodes (right) but occasionally during hippocampal non-theta activity (left), as also indicated by the spots of warm colors in the theta band of the unit wavelet. (n = 11 HCN-IR neurons showed this behavior.) **B**: Firing pattern of an HCN-IR neuron that fired irregular spike clusters and single spikes during non-theta state (left) and highly regular theta-frequency bursts during theta oscillation (right). (n = 13 HCN-IR neurons exhibit similar firing characteristics.) **C** shows the activity of the only non-bursting HCN-IR cell. This neuron exhibited theta modulated firing during hippocampal theta (right), which is reflected in the high wavelet power coefficients in the theta band.

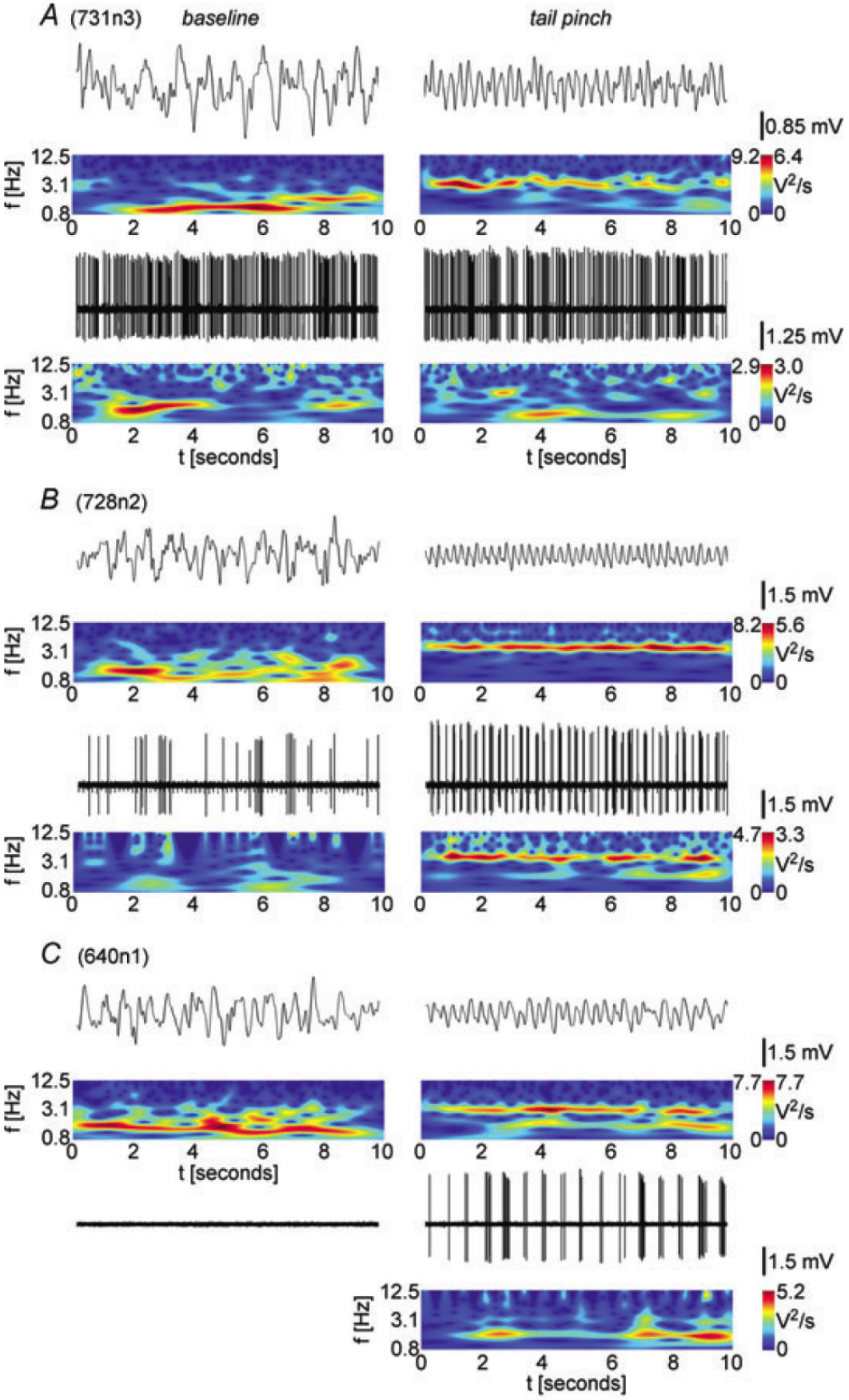
A (731n3)
baseline
tail pinch
0.85 mV
f [Hz]
12.5
3.1
0.8
9.2
6.4
V²/s
0
0 2 4 6 8 10
1.25 mV
2.9
3.0
t [seconds]
B (728n2)
1.5 mV
8.2
5.6
4.7
3.3
C (640n1)
7.7
5.2

Figure 21. Activity of medial septal non-HCN neurons. The organization of the figure and the notations follows those of Figure 20. **A** shows the firing pattern of a non-HCN neuron of the most numerous group (n = 7) that did not show any theta-related activity during either hippocampal non-theta (left) or theta state. **B**: Firing pattern of an HCN-immunonegative cell, which exhibit irregular spiking when no theta in the hippocampal LFP was present (left) and regular theta-bursting during hippocampal theta oscillation (similar to the HCN-IR cell in Fig. 20B). n = 4 neurons belonged to this group. **C**: One non-HCN cell showed very low level of activity during non-theta state, which turned to a low frequency bursting during theta. The neuron fired in every second theta cycle (note the dominant component of the unit wavelet at half of the frequency of that of the LFP wavelet).

HCN-IR neurons fire in highly regular theta-burst mode

Among the neurons firing in a theta-rhythmic manner, two different firing modes can be distinguished. These neurons either emit clearly separable clusters of action potentials (i.e., bursts) with within cluster interspike intervals substantially shorter than the intervals between bursts, or they show rhythmic changes of firing rate without separable bursts (so-called theta-modulated cells). Almost every HCN-IR neuron investigated in this study showed theta-bursting firing pattern (24 of 25, 96%) during hippocampal theta oscillation; the remaining neuron was theta-modulated (Fig. 20). Eleven of the above 24 neurons fired theta-frequency bursts even during non-theta segments of the hippocampal LFP, however, burst firing was often more regular in hippocampal theta state (Fig. 20A). The other 13 cells showed irregular firing pattern in case no theta in the hippocampus was present (Fig. 20B). Four HCN-immunopositive neurons spent the entire recording session in burst mode (so-called constitutively bursting cells). On the contrary, only 4 of 12 (25%) non-HCN neuron fired in theta-burst mode during hippocampal theta (Fig. 21B), one neuron showed low-frequency bursts (Fig. 21C), while the remaining neurons were characterized by irregular spiking (Fig. 21A). None of the non-HCN neurons fired in theta-burst mode associated to hippocampal non-theta episodes. Thus, the presence of HCN channels and theta-bursting firing pattern were highly significantly interdependent ($p < 0.0001$ by $\chi 2$-test, n

= 37). Tendency of burst firing was quantified by the number of within burst action potentials relative to the number of all spikes for each neuron (burstiness index, BI, see Materials and Methods). HCN-IR neurons were found to have significantly higher BI compared with non-HCN cells ($p < 0.001$ for both theta and non-theta segments, see also Table 2).

In summary, firing pattern analysis of the recorded and identified medial septal neurons revealed that regular, theta-rhythmic firing is a dominant attribute of the HCN-expressing group. While a small proportion of HCN-immunonegative neurons also exhibited theta-bursting activity, the majority fired in an irregular pattern.

HCN-IR neurons are strongly phase-locked to hippocampal theta oscillation

Theta-bursting medial septal neurons are usually related to the ongoing hippocampal theta oscillation if present. We examined this relationship by calculating the phase of each action potential relative to hippocampal theta rhythm. Relative phase values were extracted from the crosswavelet spectrum. Subsequently, mean phase and mean vector length (MVL) characterizing the spread around the mean (0: no phase preference, 1: high phase preference) were computed for every theta-bursting neuron (see Materials and Methods).

All theta-bursting neurons showed unimodal phase value distribution and strong phase-coupling to the hippocampal theta oscillation, irrespective of anatomical identity (significant phase-locking with Rao's spacing test at $p < 0.05$ level; high MVL values, see Table 3 and Fig. 22C). Thus, statistically significant difference regarding coupling strength could not be detected either between theta-bursting HCN-IR and HCN-immunonegative neurons (MVL: 0.95 ± 0.06 vs 0.94 ± 0.08; $p > 0.9$; $n = 24$ vs 4) or between the HCN-IR subgroups (HCN+/PV+ and HCN+/PV-: 0.95 ± 0.08 vs 0.94 ± 0.07; $p > 0.9$; $n = 14$ vs 7).

Importantly, phase preference of HCN+/PV+ and HCN+/PV- neurons was strikingly different at the population level (two samples Watson's test, $p < 0.01$, $n = 14$ vs 7). PV-IR group showed a bimodal distribution with two clearly separable peaks at the trough and on the rising segment of hippocampal theta wave, concordant with the

study of Borhegyi et al. (2004). Indeed, a mixture of two von Mises distributions (which is the naturally occurring unimodal circular distribution, analogously to the Gaussian distribution on the line) was successfully fitted on the phase distribution (mean square error of estimate: 3.25×10^{-5}; mean phase: 168.84 degrees and 268.63 degrees, MVL: 0.9 and 0.85, mixing ratio: 0.54). In a sharp contrast, non-PV HCN-IR group exhibited a multimodal distribution spanning the entire unit circle without showing a group level phase preference despite having robust unimodal phase distribution individually (population MVL: 0.02, see Fig. 22). The small number of theta-bursting HCN-immunonegative neurons prevented the statistical comparison of HCN-IR and non-HCN groups.

Table 2. Phase preference of theta bursting neurons

Cell code	Phase (deg)	Mean vector length
HCN/PV		
378n1/T	156	0.89
393n1/T	195	0.97
506n1/T	153	0.98
528n2/T	200	0.95
691n4/T	168	0.95
698n1/T	165	0.84
706n1/T	176	0.87
730n2/T	146	0.97
583n3/AP	258	0.92
631n3/AP	270	0.94
632n1/AP	315	0.96
701n1/AP	292	0.95
708n2/AP	243	0.99
729n2/AP	268	0.88
HCN/NT		
327n2	357	0.96
431n1	251	0.97
451n3	131	0.92
HCN/non-PV		
390n4	73	0.94
449n1	158	0.97
604n2	33	0.99
624n1	201	0.94
626n1	284	0.89
645n1	204	0.97
704n1	326	0.9
PV/non-HCN		
728n2/T	320	0.96
non-HCN/non-PV		
331n4	116	0.92
361n2	117	0.99
391n1	6	0.86

Table 3. Phase preference of theta-bursting neurons. T, trough-preferring group (mean: 168.84 deg); AP, ascending phase, peak preferring group (mean: 268.63 deg); NT, not tested for PV.

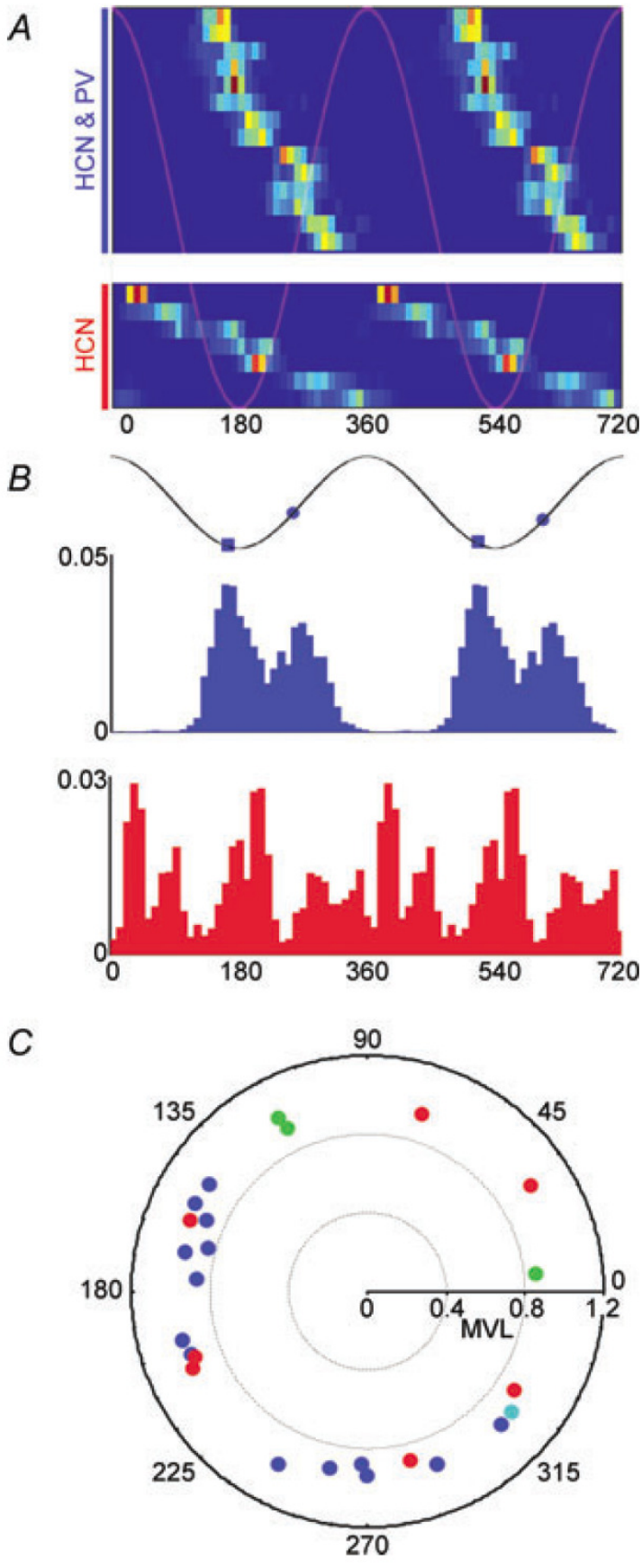
A
HCN & PV
HCN
0
180
360
540
720
B
0.05
0
0.03
0
0
180
360
540
720
C
90
135
45
180
0
225
315
270
0
0.4
0.8
1.2
MVL

Figure 22. Phase preference of HCN-IR neurons of the medial septum. A: Phase histograms of individual neurons. Each row corresponds to a phase histogram, warm colors indicate high bin counts. Two cycles are shown. An idealized theta wave is superimposed in light purple. HCN+/PV+ neurons fired only on the ascending phase of hippocampal theta and tended to form two groups around the trough and before the peak of theta oscillation, whereas HCN+/PV- neurons covered the entire cycle. **B**: Population phase histograms (y axis: firing probability). PV-IR HCN-containing neurons showed a bimodal phase histogram with peaks corresponding to the two groups mentioned above while HCN-IR non-PV neurons exhibited a multimodal phase distribution. **C**: Polar plot showing the mean phase and the MVL (represented as distance from the center) for all individual neurons. Note the grouping of PV-IR neurons (HCN-IR: blue dots and non-HCN: cyan dot) around the trough (180 degrees) and before the peak (360 degrees) of the theta wave. In contrast, HCN+/PV- neurons (red dots) are dispersed around the circle not showing a group-level phase preference. The three non-HCN non-PV neurons are shown in green.

Time delay between medial septal PV/HCN-immunoreactive neurons and hippocampal LFP suggests septal lead

In synchronously operating interconnected neuronal networks, changes in the activity of one network could appear as the perturbation of the other network after a time delay. Temporal difference between correlated alterations of activity may provide new insight into the functional architecture and hierarchy of the septo-hippocampal connection. Thus, we implemented the recently documented circular statistical Z-shift method to unravel the temporal order in the septo-hippocampal system during theta activity. (This algorithm is based on Rayleigh's test for uniformity on the circle; see the Materails and Methods section for additional details.) Although phase coupling of bursting or theta-modulated neurons to the hippocampal LFP is usually observed without shifting the signals, applying a time delay for the unit can change the strength of phase preference. Importantly, phase coupling can even be stronger for the delayed unit as compared to the original action potential series. In case a neuron directly influences the local field potential recorded from the same area, a strong phase coupling

(high Z-value, see Fig.16 and 17) of its action potentials to the concurrent population activity can be observed. However, if a neuron contributes to the LFP in a distant localization, unit activity is better phase-locked to a later segment of the field oscillation. This delay indicates the time needed for the changes in the unit activity to be reflected in corresponding changes in the LFP. Conversely, when a cell's firing is modulated by the population activity in a spatially distinct area, phase preference is maximal between the current unit activity and a previous LFP epoch. Z-shift expresses the time difference by which alterations of hippocampal field oscillation (e.g. minor perturbations) follow (Z-shift > 0) or precede (Z-shift < 0) the corresponding minor changes of septal unit activity. In case maximal phase synchrony appears after shifting the unit forward, lead of the unit over the LFP can be established. In contrast, if strongest phase coupling corresponds to a negative delay, LFP leads unit activity. Recordings in which the longest theta segment was shorter than 5 seconds or the maximal phase coupling was not significant ($p > 0.005$, Rayleigh's test) were excluded, resulting in the analysis of the longest theta segments of 189 septal neurons (Table 1).

Independence of Z-shift values and classical circular statistical parameters

First it was shown that Z-shift is mostly independent from the main statistical parameters determining a circular sample (i.e., a set of angle values; in this case, phase values of septal action potentials relative to hippocampal LFP). Mean angle (equivalent to mean phase in the case of neuronal phase series) and concentration parameter (also called kappa, characterizing the spread around the mean) are standard circular statistics that can describe a unimodal circular distribution (for details see Fisher, 1993). Sample mean angle and maximum likelihood estimate of the concentration parameter were calculated as described in Fisher (1993). To test whether Z-shift is correlated with either of the above statistics, linear regression for Z-shift and estimated kappa as well as linear-circular regression for Z-shift and estimated mean angle was calculated (Fisher, 1993). We could not detect any significant interaction ($p > 0.05$) among the above parameters (similarly to Siapas et al., 2005). Accordingly, Z-shift did not show any structure along the different mean angle values on the Z-shift versus circular mean angle

scatter plot, indicating that time delay and preferred phase relative to the hippocampal theta were independent parameters (Figure 23). On the other hand, Z-shift values appeared to be more focused at higher kappa values on the Z-shift versus kappa scatter plot, which was concordant with the more concentrated Z-shift values at higher maximal Z-values on Figure 24. This relationship suggests that the MS units with higher degree of phase coupling show lower time delay variability.

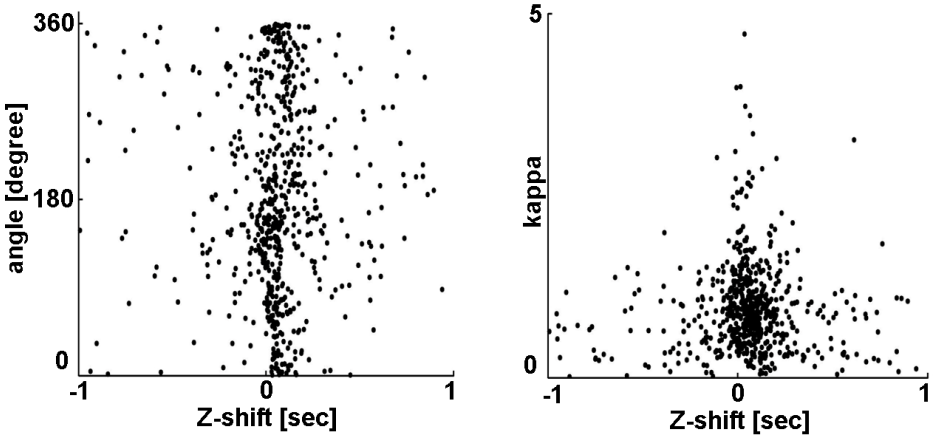

Figure 23. Relationship between Z-shift and classical circular statistical parameters. Scatter plots showing the relation of Z-shift to standard statistics of the phase angle distribution: Z-shift vs. mean angle is shown on the left plot, whereas Z-shift vs. the estimated concentration parameter (kappa) is displayed on the right plot. No correlation between Z-shift and preferred phase angle could be observed, while Z-shift showed less variability at higher kappa values.

Z-shift analysis suggests septal lead

Next, we analyzed temporal delays between septal and hippocampal signals. Most of the time lags calculated for MS neurons (117 of 189, 61.9%, 72 of 117 theta-bursting) fell between 0 and 200 ms (below 0 ms: 50 of 189, 26,5%, 23 of 50 theta-bursting; above 200 ms: 22 of 189, 11.6%, 8 of 22 theta-bursting; median for all 189 neurons: 58 ms; interquartile range: -1.75 to 129.75 ms), especially those with higher maximal Z-values. The latter indicates stronger phase preference and longer distance from the x axis (Fig. 24). This finding implies that events during theta oscillations in the

activity of septal neurons precede those of the hippocampal field with a median of 58 ms, especially for highly regular, strongly theta phase-locked MS cells.

Thirty-three neurons were immunopositive for PV or HCN or both among the neurons included in the Z-shift analysis. Twelve of those neurons were immunopositive for both HCN and PV, representing the overlap between the PV-IR and HCN-IR population; 13/33 additional neurons were proved to be immunopositive for PV, whereas 8/33 were shown to contain HCN (Table 1). PV-immunoreactive neurons (25 of 189; 12 of 25 immunoreactive for HCN; Fig.3.) showed a median delay of 79 ms (Table 4), which was significantly different from zero ($p = 4.424 \times 10^{-27}$) and from the delay characterizing PV-immunoneagtive MS cells ($p = 0.0168$, Fig. 24A). Median delay of PV-immunonegative neurons (16 of 189) was 11.5 ms, which was not significantly different from zero ($p = 0.168$). Thus, only the MS cells containing PV preceded hippocampal LFP. Additionally, PV-IR neurons formed a more consistent group characterized by a significantly smaller standard deviation (PV-IR SD: 82.10 ms, PV-immunonegative SD: 304.60 ms; $p = 5.226 \times 10^{-8}$, F-test) of the individual delay values. Alike PV-IR neurons, HCN-immunoreactive cells (20 of 189; 12 of 20 immunoreactive for PV) were characterized by a longer delay with a median identical to that of PV-IR cells as opposed to HCN-immunonegative MS neurons (7 of 189) (HCN-IR median: 79 ms, HCN-immunonegative median: -78 ms; $p = 0.005904$, Fig. 24B). Both medians were significantly different from zero ($p = 6.146 \times 10^{-6}$ and $p = 0.0084$ for HCN-immunopositive and - immunonegative groups, respectively). Thus, HCN-IR neurons preceded, whereas HCN-immunonegative cells followed hippocampal LFP. Standard deviation of time lags in the HCN-IR group was significantly smaller than in the HCN-immunonegative group (HCN-IR SD: 82.20 ms, HCN-immunonegative SD: 454.49 ms; $p = 1.752 \times 10^{-8}$, F-test). Both PV-IR and HCN-IR neurons were more strongly phase-coupled to hippocampal theta than the PV- or HCN-immunonegative cells showed by the higher maximal Z-values on Figure 24. Moreover, phase modulation was markedly small in the latter cell group, further supporting our observations reported above that strength of phase coupling distinguishes HCN-immunoreactive and HCN-immunonegative cells.

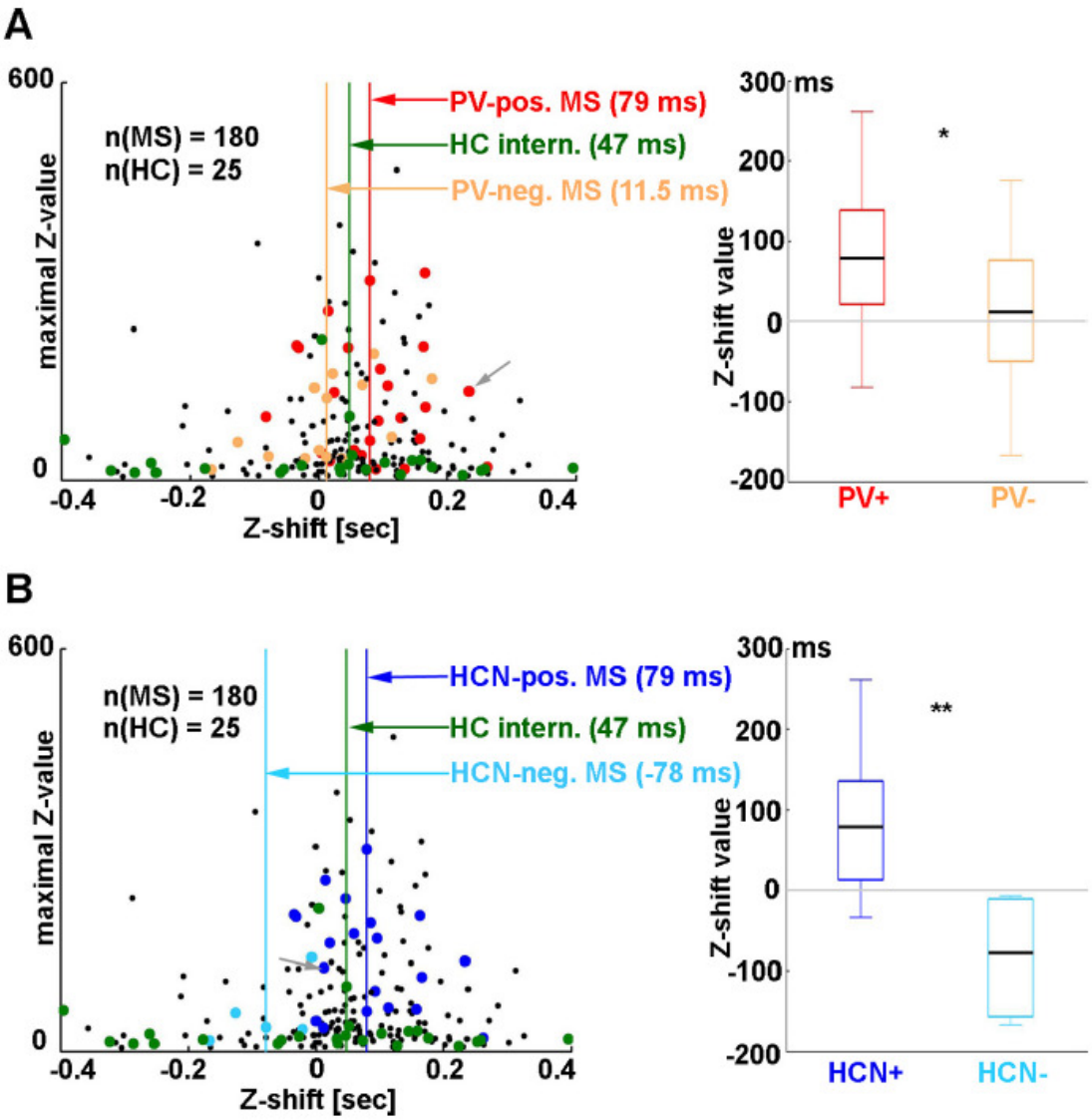

Figure 24. Activity of PV/HCN-IR neurons precedes hippocampal LFP activity. A: Z-shift analysis of medial septal and hippocampal neurons. Every dot designates the longest theta segment of a neuron on the Z-shift vs maximal Z-value plane (left). Red: identified PV-IR neurons of the MS; orange: septal non-PV cells; black: unidentified septal neurons; green: putative hippocampal interneurons. Color-coded vertical lines indicate medians of Z-shift values for identified septal anatomical groups and putative hippocampal interneurons. The grey arrow points to data of the neuron shown in Figure 19A. Most of the points corresponding to septal cells (red, orange and black) fell on the positive halfplane, indicating that changes in their activity preceded hippocampal LFP. Right: the distribution of Z-shift values of medial septal PV-IR and non-PV cells are presented as box plots. PV-containing cells exhibited significantly higher Z-shift values

compared with the ones that were shown not to express PV. **B**: Dark blue: HCN-IR medial septal neurons; light blue: septal non-HCN cells; black: unidentified septal neurons; green: putative hippocampal interneurons; grey arrow: data from the neuron presented in Figure 19B. HCN-IR MS cells preceded putative hippocampal interneurons and HCN-immunonegative cells. Right: comparison of Z-shift value distribution of HCN-expressing and non-HCN neurons. HCN-immunopositive cells showed significantly higher Z-values. Some points fell out of the range of the left plots presented on this figure (9 MS neurons and 2 hippocampal cells); Figure 25A-C shows the Z-shift values of all analyzed cells. *: $p < 0.05$, **: $p < 0.01$, ***: $p < 0.001$.

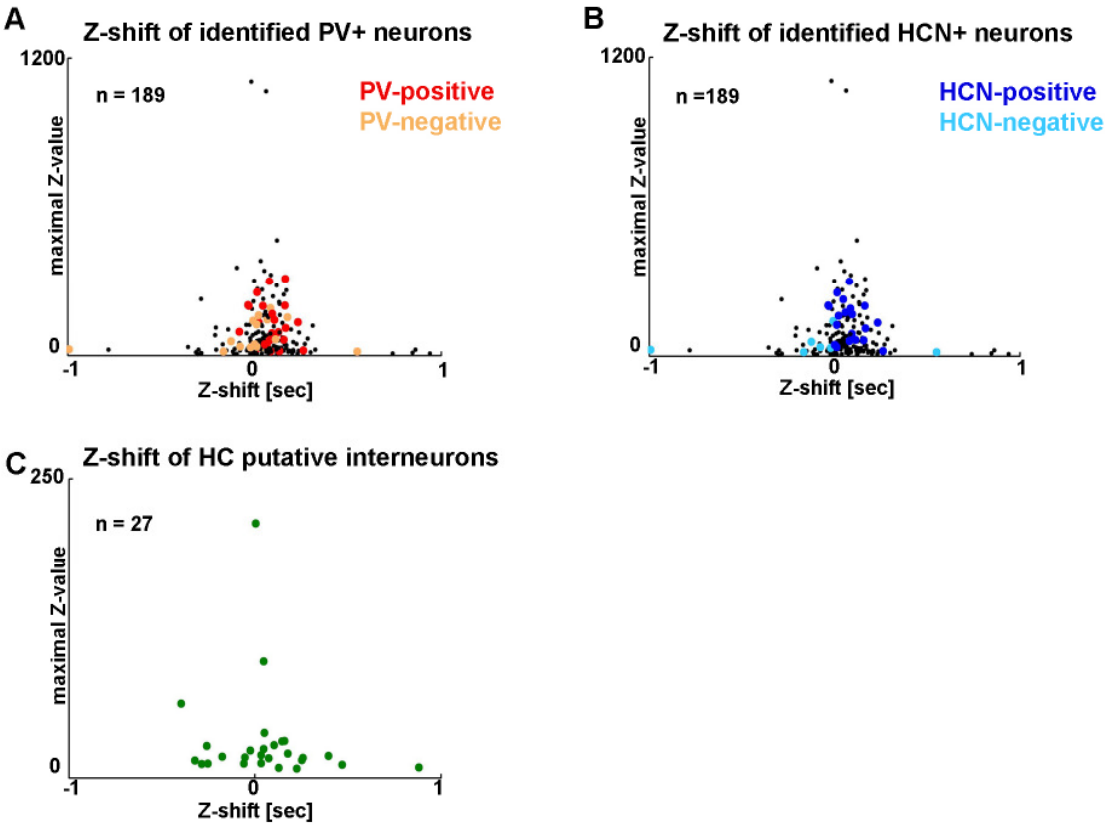

Figure 25. Z-shift results. A and **B** shows Z-shift of all analyzed MS neurons on the Z-shift vs. maximal Z-value plane. Color-coding of identified cells on Figure 24 applies for this figure as well. **C:** Z-shift values of all putative hippocampal interneurons included in the present study.

	median	n
PV+	79	25
PV-	11,5	16
HCN+	79	20
HCN-	-78	7
all	58	189
HC	47	27

Table 4: Median time lags between identified neuronal groups and hippocampal LFP. all, all medial septal neurons including identified and unidentified cells; HC, putative hippocampal interneurons.

Analysis of all theta segments yielded similar results

The above results are strengthened by the observation that, at the population level, the same results were obtained irrespective of analyzing all theta segments of all neurons (Fig. 26), or only the longest theta segments of septal neurons (Fig. 24), or theta segments with maximal Z-value (the strongest phase-coupling; Fig. 27). The antecedence of PV/HCN-IR neuron firing relative to hippocampal LFP activity indicates that changes in the spiking of these neurons may influence theta rhythm in the hippocampus.

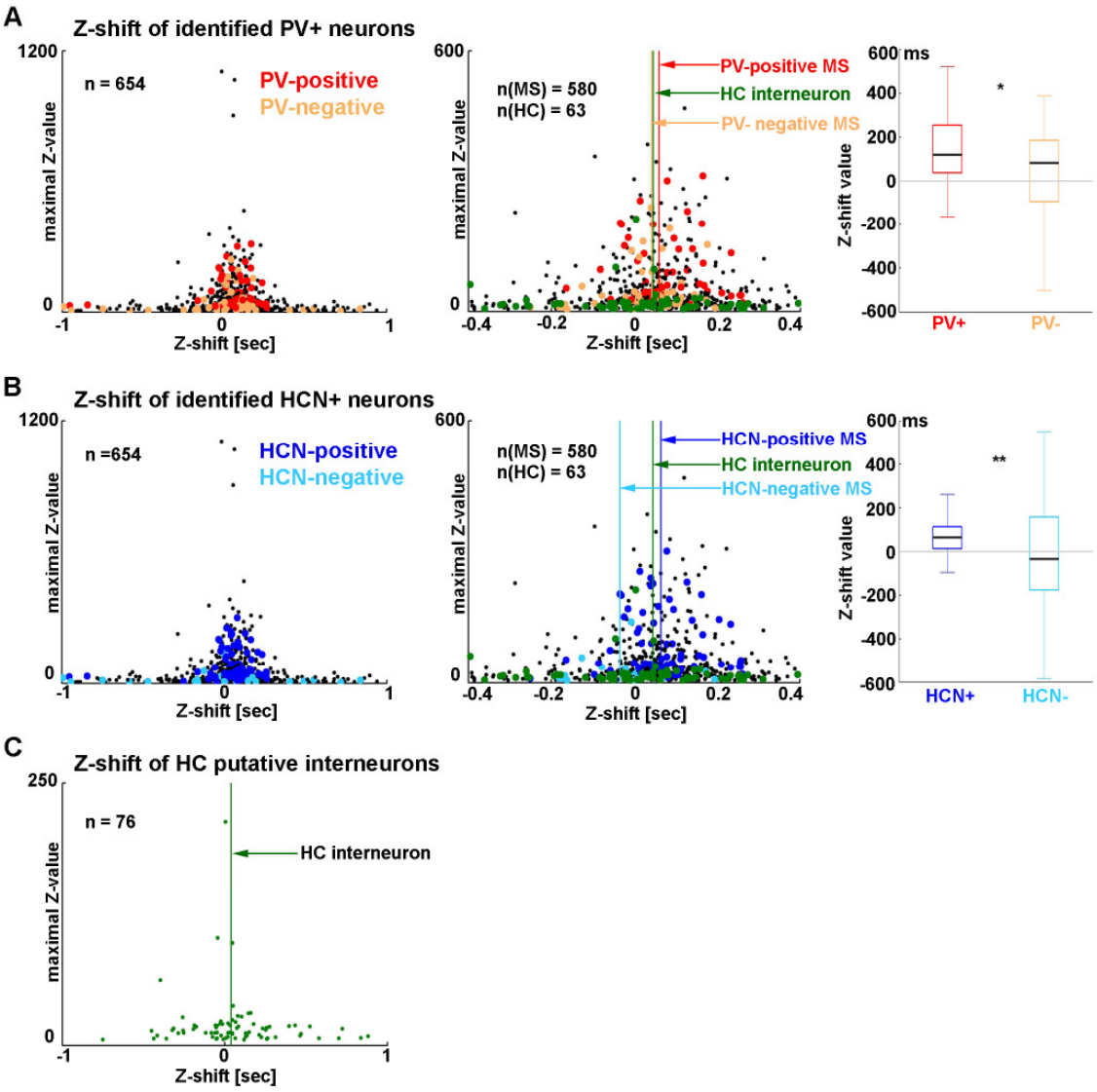

Figure 26. Z-shift values for all theta segments. This figure includes all theta segments of the analyzed recordings. Color-coding of Figure 24 also applies for this figure. **A**: Z-shift values for identified PV-IR and PV-immunonegative MS neurons. Left panel shows all analyzed cells, middle panel displays the enlargement of the central part of the left plot, and includes hippocampal neurons. Z-shift distributions of PV-IR and PV-immunonegative neurons are compared in a box plot (right). **B**: Similar demonstration of identified HCN-IR and HCN-immunonegative MS neurons. **C**: Z-shift values calculated for putative hippocampal interneurons.

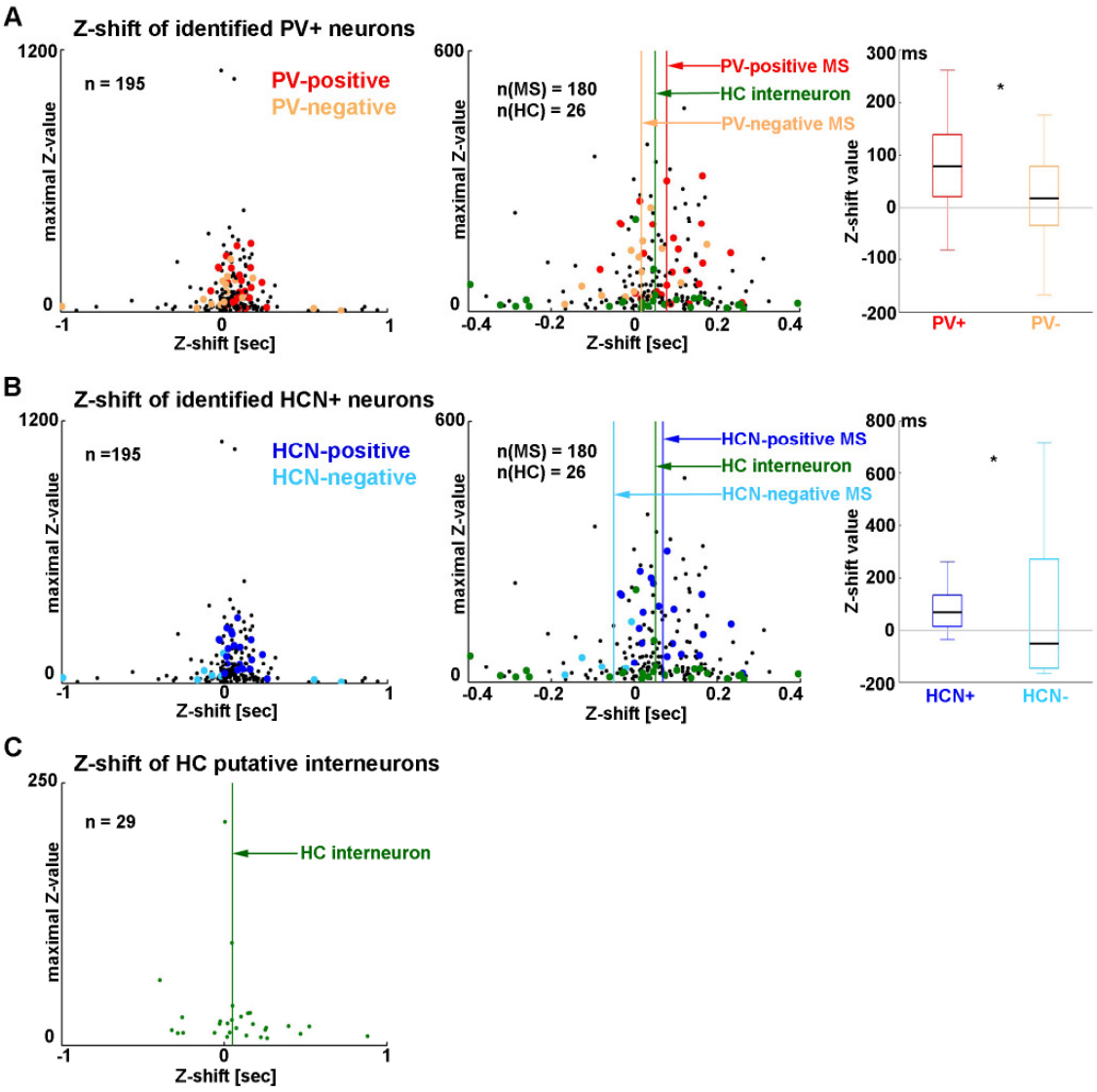

Figure 27. Z-shift values for theta segments with maximal phase locking. For each recording, theta segments with maximal Z-values were selected. Organization, notations and color-coding follow those of Figure 26.

Hippocampal interneurons precede hippocampal LFP by a shorter interval than PV/HCN cells

In order to compare the relationship of medial septal neurons and hippocampal interneurons to hippocampal local field oscillation, Z-shift was calculated for 27 putative hippocampal interneurons (5 of 27 theta-bursting; Fig. 24A-B). These cells preceded hippocampal theta oscillation by a median of 47 ms (Table 4). Thus, the delay

between hippocampal interneurons and LFP was 32 ms smaller than the time lag between PV- or HCN-IR MS cells and hippocampal LFP. This finding substantiates the results of the Z-shift analysis of the medial septal units and points to an MS - hippocampus direction of influence during theta activity.

Synchronization of PV- and HCN-IR medial septal neurons to hippocampal theta oscillation

Common information content (MI: mutual information) between MS unit and hippocampal LFP in the theta band reflects the strength of theta band synchrony between the two signals. Beyond linear correlation, MI is capable of detecting non-linear connections that are common among neural structures (Freiwald et al., 1999) and are underestimated or even not detected by linear methods. To unravel whether putative pacemaker neurons shown to precede hippocampal theta share different amounts of information with hippocampal LFP compared to immunonegative cells, MI during the longest theta and non-theta segments of recorded cells from these anatomical groups was calculated. Eighty-one cells were subjected to this analysis, among which 31 were anatomically characterized, whereas 50 cells were unidentified (n = 18 PV-IR (9 of 18 immunopositive for HCN as well), 11 non-PV, 15 HCN-IR (9 of 15 immunopositive for PV as well), 4 non-HCN; 50 unidentified; see Table 1 for the overlap between these groups).

Theta-associated increase of MI was characteristic to MS neurons

First, MI values from theta and non-theta segments were compared, in order to reveal theta-associated changes in the septo-hippocampal interaction. During non-theta segments, theta-band mutual information was significant only in a few neurons as compared to matched controls (5 of 81, 6%) ($p = 0.01$, Wilcoxon signed rank test, random Poisson control; see Materials and Methods). On the contrary, during theta episodes, the majority of MS units, especially theta-bursting neurons showed significant theta band synchrony with hippocampal LFP (59 of 81, 73%; 43 of 46 theta-bursters, 16

of 35 non-bursters) ($p = 0.01$, Wilcoxon signed rank test, random Poisson control; see Materials and Methods). Comparison of theta and non-theta segments uncovered significant theta-associated increase of MI in case of 58 of 81 MS neurons (72%) ($p = 0.01$, Mann-Whitney U test, see Materials and Methods), whereas MI decreased in only one case. Overall, MI values associated to theta segments were significantly higher than that of non-theta episodes ($p = 5.10 \times 10^{-37}$; Fig. 28C), reflecting the synchronization of MS units and hippocampal LFP on the course of theta formation.

Bursting neurons exhibit higher values of mutual information than non-bursting cells

Additionally, we tested whether theta-bursting MS neurons share higher amount of information with hippocampal LFP as opposed to non-bursters. Comparison of theta-associated MI values derived from 43 theta-bursting and 16 non-bursting MS cells showed that septal neurons with bursting activity are significantly more synchronous to hippocampal LFP than neurons without theta-bursts ($p = 6.96 \times 10^{-8}$; Figure 28D; only units with MI significantly higher than control were considered ($p = 0.01$, Wilcoxon signed rank test, random Poisson control; see Materials and Methods)).

PV/HCN neurons share high amount of information with hippocampal LFP

Next, we demonstrated that PV-IR cells shared a significantly higher amount of information with hippocampal LFP than non-PV neurons during theta episodes ($p = 6.52 \times 10^{-5}$, n = 15 PV-IR vs. 9 non-PV; neurons with higher than control MI during theta ($p = 0.01$, Wilcoxon signed rank test, random Poisson control; see Materials and Methods) were considered; Fig. 28A-B). Similarly, identified HCN-IR cells were proved to be significantly more synchronous to hippocampal LFP than HCN-immunonegative neurons ($p = 0.0176$, n = 13 HCN-IR vs. 3 non-HCN). MI values from the anatomically heterogeneous population of unidentified MS neurons were distributed over a wide range with a median between that of PV (HCN)-IR cells and PV (HCN)-immunonegative neurons. During non-theta episodes, only 5 neurons showed MI

significantly higher than control, from which one was identified as PV-IR. Because theta-bursting neurons were found to show higher mutual information compared to non-bursting cells (see Fig. 28D and above), one might hypothesize that the theta-related difference between PV (HCN)-IR and PV (HCN)-immunonegative neurons could be caused by the higher number of theta-bursting neurons in the immunopositive groups. Importantly, statistically significant difference in MI was also detectable between theta-bursting PV (HCN)-IR and theta-bursting immunonegative neurons, suggesting that higher synchrony with hippocampal theta is indicative of the above anatomical groups ($p = 0.00481$ for 14 PV-IR and 5 PV-immunonegative cells; $p = 0.00893$ for 11 HCN-IR and one HCN-immunonegative cell, Fig.28B right).

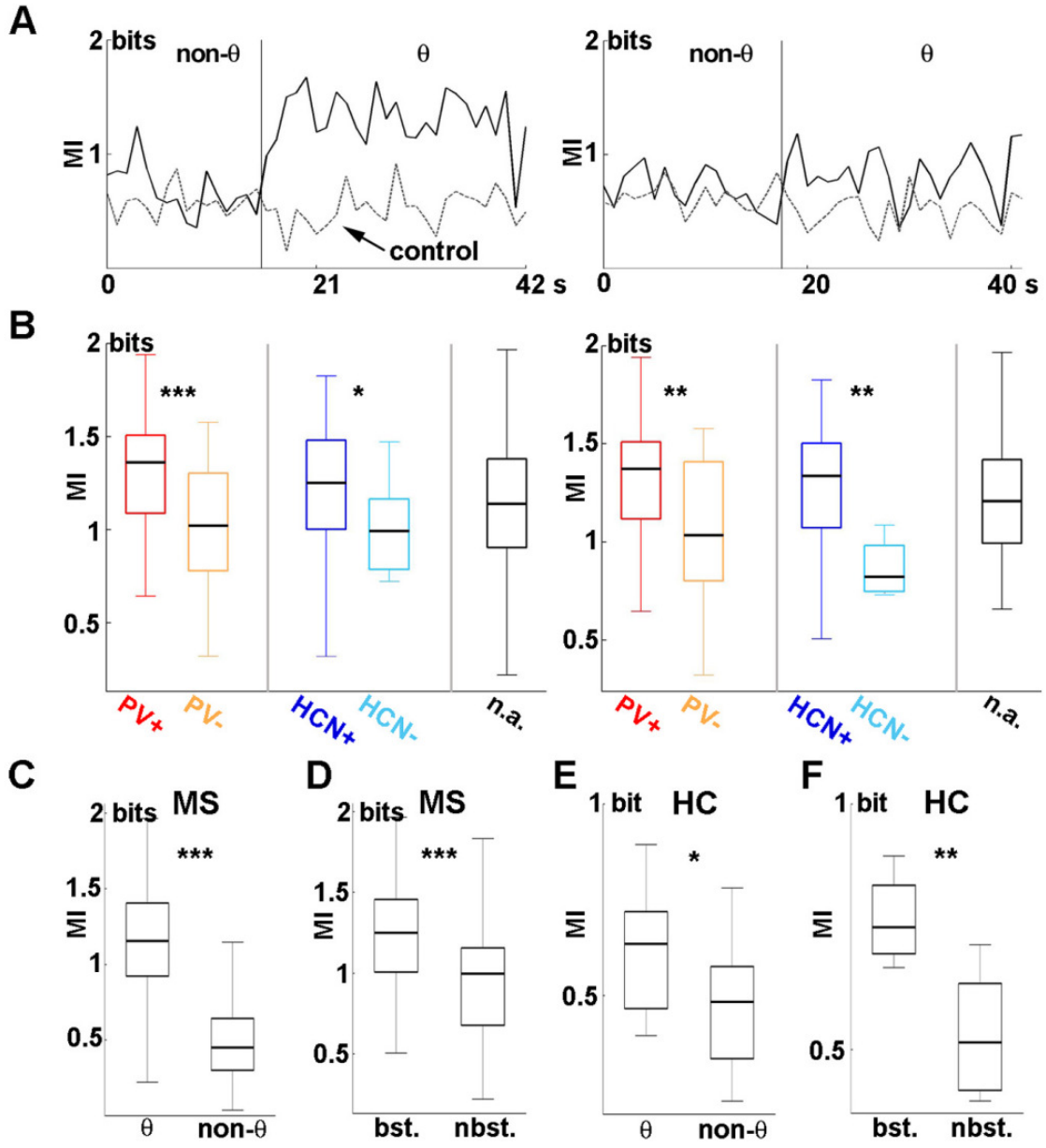

Figure 28. Medial septal PV/HCN-IR neurons are synchronous to hippocampal LFP. A: Left: MI during non-theta and theta activity from a medial septal neuron immunopositive for both PV and HCN. Black vertical line separates the longest theta and (usually non-adjacent) non-theta episode. MI was substantially increased during hippocampal theta oscillation compared with the non-theta segment (black solid line). Grey dashed line indicates random control. Right: MI from a non-PV non-HCN neuron (black solid line) with its matched control (grey dashed line). Only a mild theta-associated increase of MI was observed. **B**: Left: MI distributions of theta segments in anatomically identified groups of cells. Medial septal PV-IR neurons (red) showed

significantly higher MI values compared with non-PV cells (orange). Also, HCN-expressing MS cells (dark blue) exhibited significantly higher MI than non-HCN neurons (light blue). Black box displays the MI distribution from unidentified MS cells. Right: MI during theta segments including theta-bursting neurons only. The color-coding of the left panel applies. Differences among anatomical groups regarding theta-associated increases of MI were present despite excluding the non-bursting MS neurons. **C**: Comparison of MI values during theta and non-theta segments. MI values during hippocampal theta oscillation were significantly higher as compared to MI values of non-theta epochs. **D**: Comparison of MI values calculated for theta segments in theta-bursting and non-bursting MS neurons. Bursting neurons showed significantly higher MI. **E-F**: Mutual information was calculated between unit activity of putative interneurons of the hippocampus and hippocampal LFP. **E**: Comparison of MI distributions of theta and non-theta episodes. Significant theta-associated increase of MI could also be detected for hippocampal cells, albeit MI of putative hippocampal interneurons did not reach the level of MS cells during theta oscillation (compare the different scaling of C and E). **F**: Comparison of bursting and non-bursting hippocampal cells. Theta-bursting neurons showed significantly higher MI than non-burtsing cells. HC, hippocampus; bst, bursting; nbst, non-bursting.

Synchronization of hippocampal interneurons to theta oscillation

In order to compare the extent of synchronization of MS vs. hippocampal units to hippocampal theta oscillation, we calculated mutual information for the longest theta and non-theta segments of 7 putative hippocampal interneurons as well. Similar to MS neurons, MI values derived from theta episodes were significantly higher than MI values of non-theta segments ($p = 0.0261$, Fig. 28E). However, theta-associated MI values of the hippocampal neurons did not reach the level of similar values from medial septal cells. Again, we compared mutual information between the two signals in the case of one theta-bursting and two non-bursting hippocampal interneurons. The theta-bursting hippocampal neuron was found to be more synchronous to the ongoing local field activity than non-bursting cells ($p = 0.00404$, Fig. 28F; only units with MI significantly higher than random Poisson control ($p = 0.01$, Wilcoxon signed rank test)

were included; see Materials and Methods). Nevertheless, MI from the theta-bursting hippocampal cell was lower compared to MI values from MS neurons with bursting activity.

Controls for MI calculations

In order to evaluate the state-dependent changes in mutual information, three different types of controls were used. In all types, original hippocampal LFP was paired to an artificial action potential series. First, artificial unit was generated by a random Poisson process, with its frequency adjusted to the original MS (or hippocampal) unit. Second, original unit was cut into 1-1.2 second long segments that were shuffled with a random permutation. This type of control preserved the possibly rhythmic firing pattern of the unit. However, long range correlations could have an effect on this type of control, because hippocampal LFP is not certainly completely independent from the 1-second later/former MS unit segment. Third, interspike intervals of the original MS unit were shuffled using a random permutation. This type of control preserved the interspike interval histogram, but distorted possible long range correlations between hippocampal LFP and medial septum spiking. Results applying random Poisson units as controls are discussed above in details.

Qualitative results from the different types of controls were similar, albeit they could differ in particular statistical comparisons. Results from controls generated by the shuffling of segments or interspike intervals are shown on Figure 29 and 30, respectively. Significant differences depicted in Figure 28 could be detected by the use of the other types of controls, except that the difference between MI values of putative hippocampal interneurons during theta and non-theta episodes did not reach the level of significance ($p = 0.156$ and $p = 0.0957$ with segment-shuffled and interval-shuffled controls, respectively).

MS unit information content (entropy) cannot be completely independent from the frequency of action potentials, as a neuron firing on a very low rate is not able to transmit high amount of information in a short time period. It should be noticed however, that the observed significant changes of mutual information associated to hippocampal states could not be due to the change of firing frequency, as all three types

of controls preserved the state-dependent firing rate of the MS neuron. However, changes of firing frequency could account for subtle changes observed in the MI controls.

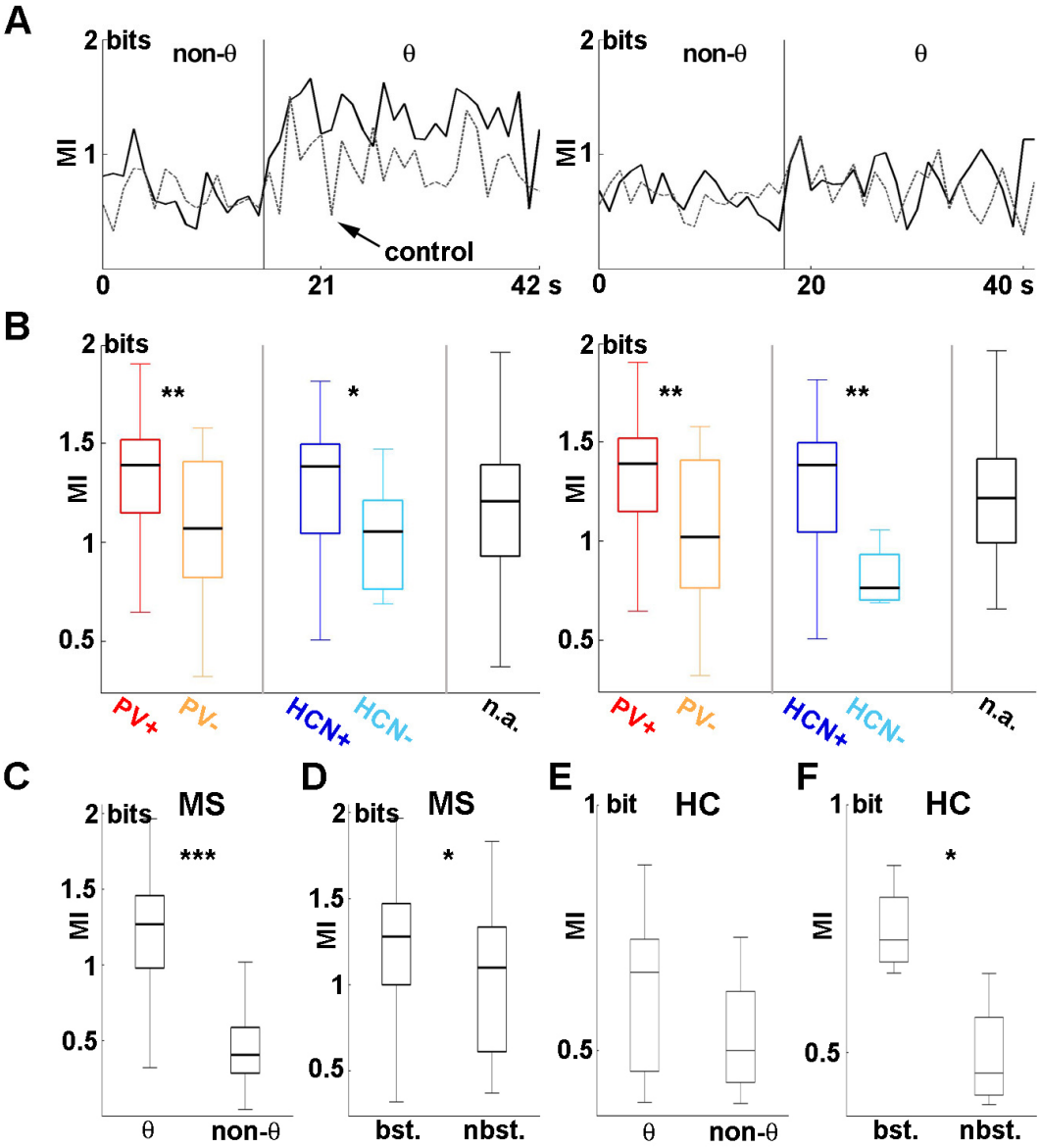

Figure 29. Repeating the MI analysis using segment-shuffled controls. Organization and all notations of this figure follow those of Figure 28. The difference between theta and non-theta segments in hippocampal unit - hippocampal LFP mutual information analysis was not significant.

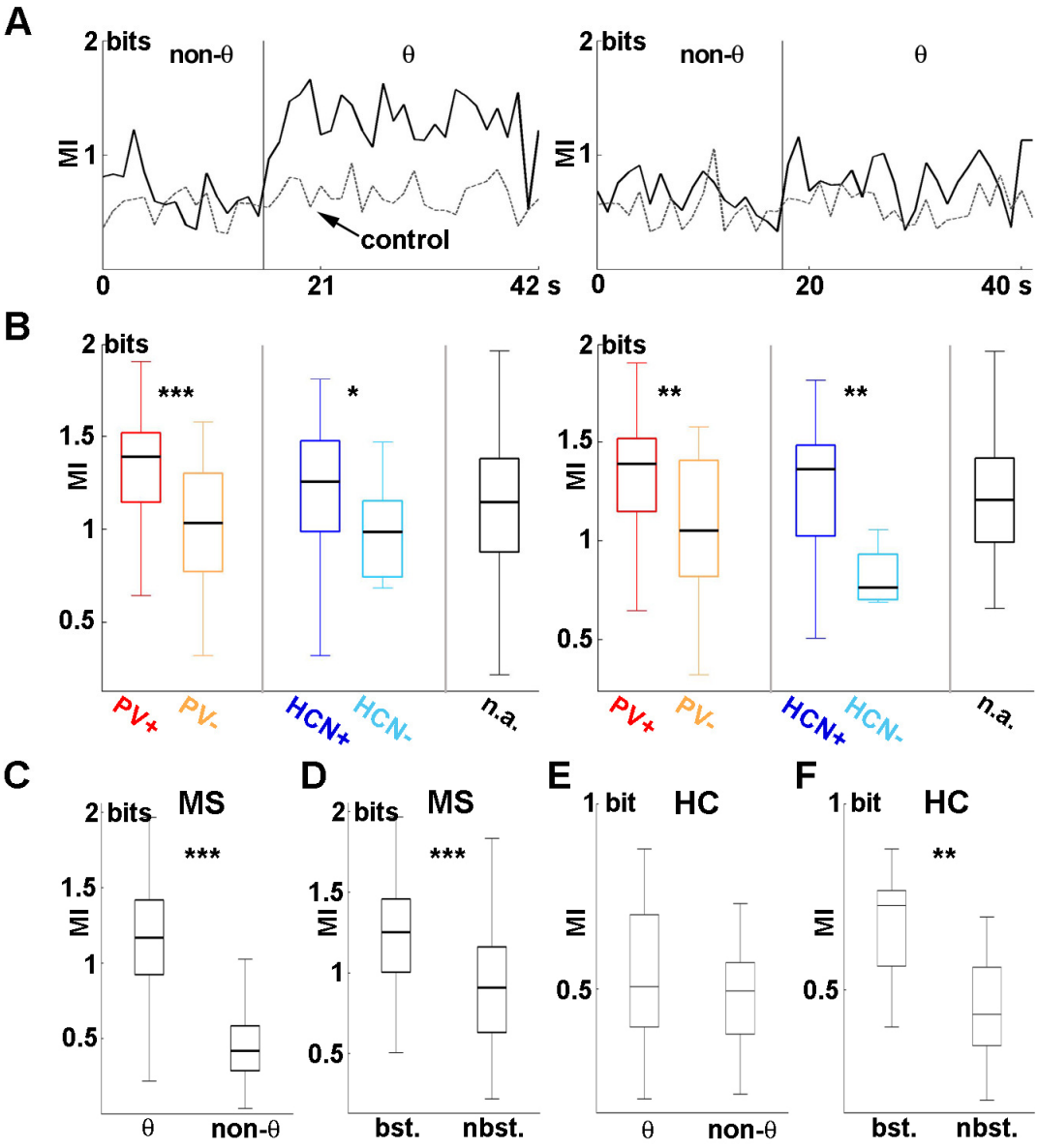

Figure 30. Repeating the MI analysis using interval-shuffled controls. Organization and notations of this figure follow those of Figure 28. Similar to the results of segment-shuffled controls, the difference on panel E did not reach the level of significance.

Analysis of the direction of information transmission reveals theta-associated septal dominance

The temporal lead of MS GABAergic neurons combined with the theta-associated increase of the information shared between these cells and the hippocampal

LFP strongly suggests a septo-hippocampal dominance of information flow during hippocampal theta oscillation. However, these methods do not provide any clue regarding the presence or extent of hippocampo-septal feedback. Indeed, pure unidirectional information flow and complex bidirectional transmission can lead to the same temporal delay between two signals, as reported in Cassidy and Brown (2003). In order to (1) directly test the hypothesis of theta-associated septo-hippocampal dominance of information transmission and to (2) decompose the information shared by the MS neurons and the hippocampal LFP to a septo-hippocampal and a hippocampo-septal component, we calculated normalized transfer entropy (NTE) and preferred direction of flow (DF) between septal cells and hippocampal LFP. Normalized transfer entropy from MS unit to hippocampal LFP gives the normalized amount of information that the past of the unit tells about the future of the LFP when the past of the LFP is already known; NTE in the opposite direction can be interpreted in a similar way. Using NTE, a normalized index taking its values between -1 and 1 called preferred direction of flow (DF) can be calculated. Negative values of DF correspond to septal lead over the hippocampus, whereas positive values indicate hippocampo-septal dominance (see Materials and Methods).

The interaction between the medial septum and hippocampus is dominated by the MS during theta oscillation

First, we compared DF values during theta and non-theta episodes in those medial septal neurons which shared a significant amount of information with hippocampal theta revealed by MI (analysis of 36 theta and 12 non-theta segments; ISI-shuffled control, $p = 0.01$, Wilcoxon signed rank test). As expected, most of the medial septal neurons (n = 27 out of 36; 22 of 27 theta-bursting, 5 of 9 non-bursting) showed a septo-hippocampal directional dominance during hippocampal theta oscillation with a median DF of -0.108 (Fig. 31A). In a sharp contrast, the dominant direction of influence changed in hippocampal non-theta state, during which most MS neurons (n = 10 out of 12; 5 of 7 bursting, 5 of 5 non-bursting) exhibited hippocampo-septal directionality (median: 0.178; significantly different from theta episodes: $p = 3.42 \times 10^{-4}$, Mann-Whitney U test).

Septo-hippocampal drive is accompanied by hippocampo-septal feedback

Thus, the investigation of DF values uncovered a theta-associated septal dominance, which turns to the opposite direction during non-theta epochs. We next analyzed NTE to reveal whether the above dominances originate from unidirectional information transmission or from a composition of a driver and a feedback influence. During hippocampal theta episodes, the septo-hippocampal direction of interaction was accompanied by a significantly smaller but still substantial hippocampo-septal component (Fig. 31B) (median of septo-hippocampal NTE: 0.379 median of hippocampo-septal NTE: 0.292; these were significantly different: $p = 5.52 \times 10^{-9}$, Wilcoxon signed rank test). Analysis of non-theta segments of the same neurons also revealed a two-component process with a dominant hippocampo-septal direction in parallel with a less pronounced septo-hippocampal influence (median of septo-hippocampal NTE: 0.119 median of hippocampo-septal NTE: 0.145; these were significantly different: $p = 0.023$, Wilcoxon signed rank test).

Medial septal HCN-IR neurons transmit a high amount of information to the hippocampus

Next, we investigated whether the strength of directional dominance during hippocampal theta segments are different between anatomically identified groups of cells. PV-containing MS neurons (n = 12) showed a marked asymmetry of interaction manifested in a dominant septo-hippocampal component (Fig. 31C) (median DF: -0.186). Non-PV neurons (n = 10) also exhibited medial septal directional dominance with a lower absolute median DF (-0.076). However, the difference between PV-expressing and PV-immunonegative neurons was not significant, showing a marginal p value of $p = 0.067$ (Mann-Whitney U test). Medial septal neurons immunopositive for HCN (n = 12) also belonged to the septal leading group (median DF: -0.140). Surprisingly, this was not the case for HCN-immunonegative cells (n = 3), which showed a positive median DF (0.046), indicating a hippocampo-septal dominance of communication. This difference between HCN-IR and non-HCN groups was found to

be significant (p = 0.0065, Mann-Whitney U test). Unidentified septal neurons (n = 33) showed an intermediate median DF value of -0.110.

Bursting neurons show stronger directionality than non-bursting cells

We compared theta-associated DF values in theta-bursting and non-bursting neurons. Bursting neurons showed significantly stronger septo-hippocampal directionality during hippocampal theta oscillation (Fig. 31D) (median of bursting neurons: -0.138; median of non-bursting neurons: -0.047; these were significantly different: p = 0.015, Mann-Whitney U test).

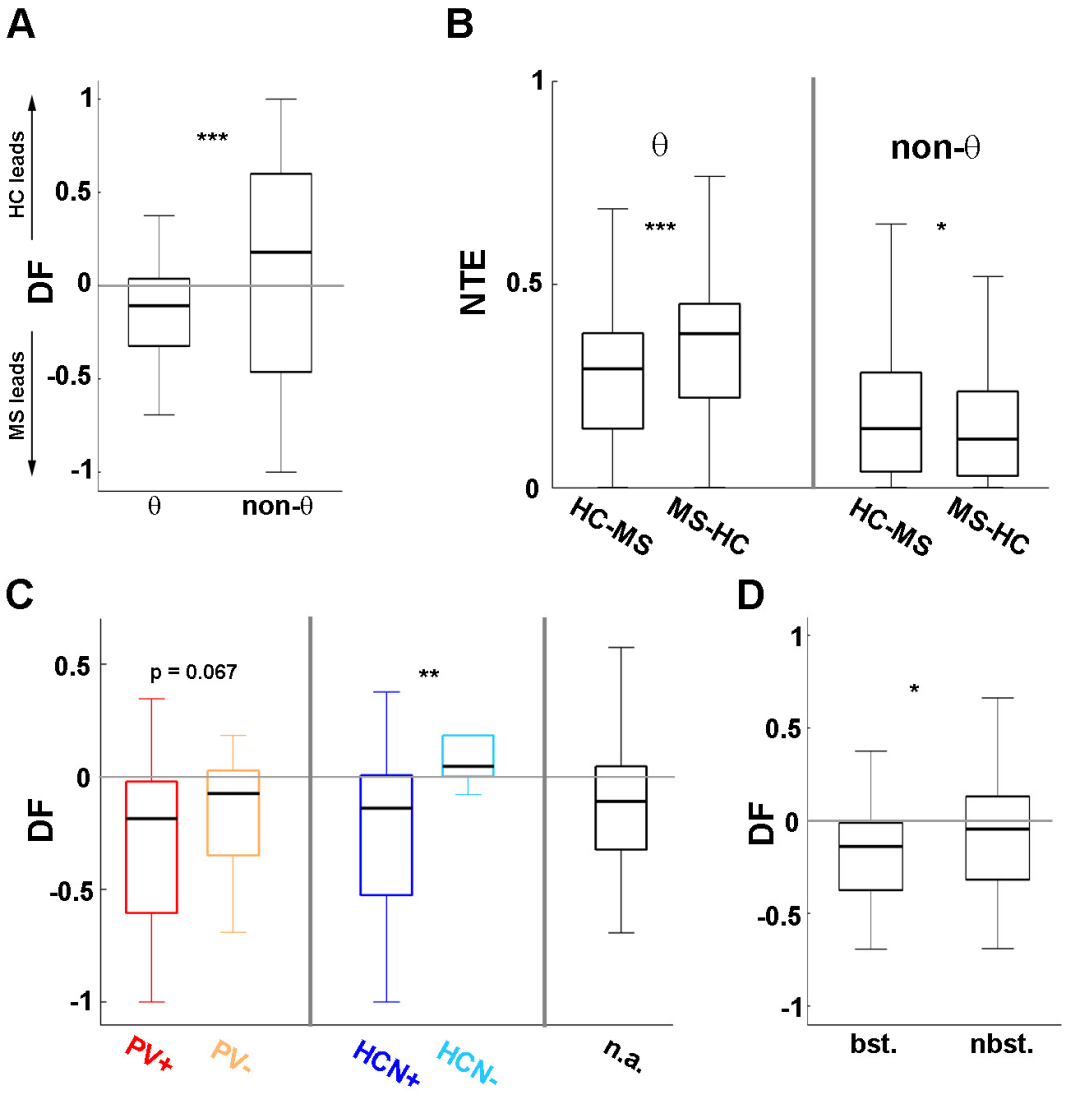

Figure 31. Theta-associated septo-hippocampal drive and hippocampo-septal feedback was uncovered by transfer entropy analysis. A: Comparison of DF values (characterizing preferred direction of influence) during hippocampal theta and non-theta segments. Theta-associated septal lead turned to hippocampal dominance during non-theta epochs. **B**: The analysis of normalized transfer entropy (NTE) values revealed that the dominant septo-hippocampal information transmission was accompanied by hippocampo-septal feedback during theta oscillation. During non-theta segments, also both directions of interaction were detected but with a significantly higher hippocampo-septal component. **C**: Comparison of DF values of theta segments among anatomically identified groups of neurons. PV-IR cells of the MS exhibited theta-associated septal directional dominance. Non-PV neurons showed similar directionality with a lower

absolute DF. However, the difference between these two groups did not reach the level of significance ($p = 0.067$). Medial septal neurons expressing HCN were characterized by a strong septo-hippocampal directional dominance, which was significantly different from the hippocampal dominance shown by the non-HCN cells. **D**: Comparison of direction of flow during theta oscillation in the groups of theta-bursting and non-bursting MS neurons. Bursting cells exhibited significantly higher absolute DF values, i.e., stronger septo-hippocampal directionality.

The amount of transmitted information correlates with the temporal delay

As the last step, we tested whether the results of Z-shift analysis is correlated with that of the information theory approach, that is, are the neurons that precede hippocampal theta the same as the ones that show septo-hippocampal directional dominance of information flow? When including all neurons with theta-associated MI significantly higher than control irrespective of anatomical identity ($n = 56$; $p = 0.01$, ISI-shuffled control, Wilcoxon signed rank test), a moderate but significant correlation between Z-shift and DF was observed ($R = -0.35$, $p = 0.038$, F test). Importantly, a strong Z-shift-DF correlation could be detected in the HCN-IR group ($n = 12$; $R = -0.78$, $p = 0.038$, F test). In the case of PV-IR cells, the correlation between Z-shift and DF values was not significant at $p = 0.05$ with a marginal p value of $p = 0.052$ (F test; $R = -0.88$). The negative R values indicate that positive Z-shift (septal antecedence) was accompanied by negative DF values (septo-hippocampal directional dominance).

Discussion

Main findings

Our data demonstrate that HCN-immunoreactivity in the medial septum strongly correlates with theta-rhythmic firing. All medial septal neurons containing the pacemaker channel HCN exhibit a dominant theta-component in their firing pattern, whereas only a minority of non-HCN neurons shows theta-rhytmicity. Additionally, HCN-IR neurons are precisely phase-locked to the ongoing theta oscillation at the individual level, whereas preferred phases of the population of HCN-containing neurons cover the entire theta cycle. By applying a circular statistical method, we show that the activity of the medial septal neurons containing parvalbumin and/or HCN precedes corresponding hippocampal field events. Importantly, this temporal antecedence is still clearly detectable when these putative pacemaker neurons are compared to hippocampal interneurons: the activity of the latter group also precedes LFP changes, but by a 32 ms shorter period compared with the PV/HCN-IR neurons, implying a PV/HCN-IR MS neuron - hippocampal interneuron - pyramidal neuron sequence of influence during theta formation. Moreover, the above neurons were found to share a high amount of information with the ongoing hippocampal field oscillation during theta rhythm, reflecting the central role of these cells in the theta-associated septo-hippocampal synchronization process. We used a recently documented approach of information theory to uncover the asymmetry of reciprocal interaction between the medial septum and the hippocampus. We were able to conclusively demonstrate that the medial septum dominates septo-hippocampal interactions during theta activity, but a significant hippocampo-septal component could also be observed.

Technical considerations

In previous studies, anatomical (Freund and Antal, 1988) and physiological (Borhegyi et al., 2004) observations pointed to those medial septal neurons containing the calcium-binding protein parvalbumin as a subnetwork of the MS optimally suited to be the rhythm generator of hippocampal theta oscillation. Additionally, our group

identified GABAergic neurons in the medial septum that contain the pacemaker channel HCN, making these cells capable of electronic rhythm generation. In order to investigate whether these two overlapping MS cell groups may function as the sources of theta rhythmic drive to the hippocampus, novel analysis tools had to be introduced to examine their relationship with the hippocampal network. Therefore, by using the recordings of these previously identified neurons in combination with hippocampal unit recording, we aimed to provide clues about their position in the process of septo-hippocampal theta genesis. Since the relationship of identified MS neurons to hippocampal activity was in the focus of our study and single cell labeling is still not possible at sufficiently high success rate in anesthetic-free animals, recordings were made under urethane anesthesia. Besides acknowledging the difference between natural and urethane-induced sleep (Leung, 1985; Simon et al., 2006), several characteristics of the latter including the spontaneous alteration of theta and non-theta state can be observed under urethane anesthesia (Clement et al., 2008).

The firing behavior of HCN-immunoreactive neurons

All HCN-containing neurons recorded in this study showed theta-rhythmic firing, whereas only the third of non-HCN cells' activity contained a theta-band component. The HCN channel was localized on the somadendritic membrane of the HCN-IR MS cells, suggesting that the H-current may play an important role in setting the membrane potential of those neurons (Sekirnjak and du Lac, 2002; Nolan et al., 2004a; Nolan et al., 2007; Tan et al., 2007), thus having a substantial impact on their firing pattern.

HCN channel was demonstrated to play an inevitable role in the generation of spontaneous rhythmic neuronal activity including rhythmic bursting and membrane potential oscillations (Bennett et al. 2000; Dickson et al. 2000; Wilson, 2005). We found that a substantial proportion of HCN-IR cells fire theta-bursts even in the absence of theta oscillation in the hippocampus, suggesting that these cells may exhibit an intrinsic mechanism of rhythm generation. None of the non-HCN cells were found to show theta-rhythmicity during hippocampal non-theta segments, strengthening the hypothesis that HCN distinguishes those neurons capable of theta generation.

Some of the non-HCN neurons also contained a theta-band activity component during hippocampal theta oscillation. This could originate from various sources, i.e. (1) rhythmic input from HCN-IR cells, (2) hippocampo-septal feedback input (Toth et al., 1993), (3) other potential pacemaker mechanisms or (4) other subunit type of the HCN channel, e.g. HCN4, not investigated in this study. False-negative staining for HCN1 or HCN2 of the juxtacellularly labeled neurons cannot be excluded either.

Phase relationship of HCN-IR neurons to the hippocampal theta oscillation

All HCN-IR neurons were found to be strongly phase-locked to hippocampal theta oscillation showing a narrow unimodal phase value distribution. Similar was reported concerning PV-IR septal neurons (Borhegyi et al., 2004). However, at the population level, a striking difference was observed between the two groups. PV-IR neurons could be separated to two distinct groups, one contained neurons phase-locked to the trough of the hippocampal theta cycle, while the other comprised cells phase-coupled to the ascending phase, near the peak of the theta wave (Borhegyi et al., 2004). Consistently with this finding, HCN-IR neurons containing PV also belonged to the above groups. In contrast, HCN-IR neurons as a whole did not show population level phase preference. Instead, mean phases of HCN-containing MS cells covered the entire theta cycle. A similar heterogeneity of the preferred theta phase can be observed among various hippocampal interneurons (Klausberger and Somogyi, 2008). Thus, it is possible that different subsets of MS HCN-expressing neurons preferring distinct phases entrain certain types of hippocampal interneurons.

Temporal order of activity changes: PV/HCN neurons are followed by hippocampal interneurons and then pyramidal cells

We aimed to reconstruct the temporal pattern of septo-hippocampal activity changes during theta-formation by implementing the recently developed Z-shift method

(Siapas et al., 2005). The observed 79 ms delay between the unit activity of septal HCN- and/or PV-immunoreactive neurons and hippocampal field oscillation could reflect the time taken by the transmission of the rhythmic output of MS GABAergic pacemaker neurons to hippocampal interneurons that ultimately results in the synchronization of the hippocampal network and a detectable field oscillation. Importantly, the 47 ms time delay between the hippocampal interneuron activity and LFP reflects (1) the delayed activation of interneurons compared to PV/HCN-IR MS cells (47 ms vs. 79 ms before LFP) and (2) the antecedence of interneuron activity changes compared to hippocampal pyramidal cells. However, it should be noted that although the majority of MS cells (139/189) appeared to precede hippocampal theta, a smaller population (50/189, see Results) showed negative Z-shift values (median: - 78 ms). This group (6 PV-negative/HCN-negative; 2 PV-positive/HCN-positive; 1 PV-positive/not tested for HCN; 1 PV-negative/HCN-positive; 40 unidentified) was characterized by weaker phase preference (i.e. lower median Z-values: 34 vs. 54) and lower proportion of bursting neurons (46% vs. 58%). We propose that these neurons form a septal "follower" group, receiving rhythmic input from hippocampal and/or from GABAergic medial septal neurons. They might contribute to the stabilization of synchronous activity by providing a fluctuating inhibitory tone to the pacemaker population.

The time lag between MS PV/HCN cells and hippocampal interneurons is substantially higher than the sum of the conduction time of septo-hippocampal axons (below 5 milliseconds; Jones et al., 1999), synaptic delays and latency of action potential genesis (Fricker and Miles, 2000). This finding can be paralleled by previous data showing that MS phasic theta-on neurons change their firing activity approximately 500 ms prior to the LIA to theta transition of the hippocampal LFP (Bland et al., 1999). Furthermore, in a hippocampal network model, delayed synchronization of its component subnetworks of basket, O-LM and pyramidal cells was demonstrated (Orbán et al., 2006). Thus, the delays in the septo-hippocampal system may reflect the time necessary for the gradual recruitment of the interconnected groups of neurons leading to the accumulation of synchronously firing oscillators and the appearance of the regular theta field activity. An additional implication of the above scenario is that the perturbation of one of the elements of the septo-hippocampal network initiates a chain

of events taking several tens of milliseconds to be manifested at the population level. It should be noted that Siapas et al. (2005) reported no significant temporal difference between hippocampal single unit and field activity, which was probably due to their mixed sample of principle cells and interneurons.

Hippocampal interneurons form an extremely heterogeneous cell population (Freund and Buzsaki, 1996). Various subgroups of interneurons were shown to fire at different phases of hippocampal theta field oscillation (Somogyi and Klausberger, 2005; Klausberger and Somogyi, 2008) and to be differentially innervated by medial septal neurons (Eyre et al., 2007). This diversity could account for the observed wide range of time lags for putative hippocampal interneurons and for the lower median MI values of hippocampal interneurons when compared to MS cells (see below). Thus, the differential contribution of anatomically identified interneuron subgroups to hippocampal theta formation needs to be further investigated on a larger sample of hippocampal cells.

High level of synchrony of PV/HCN neurons to hippocampal theta was detected by the calculation of mutual information

Differential contribution of anatomically identified medial septal cell groups to septo-hippocampal information transmission has been assessed by the calculation of mutual information. This well-established information theory approach is based on entropy, the classical measure of information content (Shannon, 1948). Entropy was applied to wavelet spectra of hippocampal local field potentials and medial septal or hippocampal unit recordings, in order to calculate the information content of time-frequency wavelet windows in the theta band (wavelet entropy: Yordanova et al., 2002). Subsequently, mutual information between corresponding wavelet windows of the LFP and unit was computed. This approach has numerous favorable properties. (1) The advantage of the MI method over classical linear correlation is its capability of detecting both the linear and non-linear aspects of synchronization (Kajikawa and Hackett, 2005), whereas the latter type of interactions are underestimated or even not detected by linear methods. Additionally, when calculating classical coherence measures, smoothing of the individual spectra as well as the cross-spectrum is necessary. However, the result

depends on the choice of the smoothing method and parameters, which problem does not occur in the MI method. (2) The application of wavelet entropy allowed us to bridge the qualitative difference of the LFP and single unit signal. (3) Also, decomposing the data in the frequency domain through wavelet calculation made us capable of investigating theta band separately. Importantly, theta-band was selected because (1) the medial septum principally affects the hippocampus through the generation of theta rhythm, (2) information in other frequency bands was relatively sparse during theta segments, whereas the theta-band still carried considerable amount of information during non-theta states (see Fig. 18B). However, other frequency bands could also carry significant information, and "cross-information" between different frequency bands of the two signals may also be relevant, which should be the aim of further investigations.

The high amount of shared information between medial septal neurons containing HCN and/or PV and hippocampal LFP compared to non-PV/non-HCN cells or to hippocampal interneurons indicates dominant contribution of the former MS cell groups to hippocampal theta genesis over the latter neurons.

Lower MI values of hippocampal interneurons compared with medial septal PV/HCN cells could be a consequence of interneuron diversity

A considerable proportion of medial septal GABAergic cells produce uniform bursts strongly coupled to the ongoing hippocampal theta oscillation, which is also reflected by the high MI values between the firing patterns of septal bursting neurons and hippocampal theta rhythm. On the other hand, hippocampal neurons are reported to show an extreme anatomical and functional heterogeneity (as mentioned above), which could account for the lower average MI values for hippocampal interneurons when compared to MS GABAergic cells. Various subtypes of interneurons are capable of theta-bursting, which subtypes could be differentially represented (if represented at all) in our sample. Thus, the diversity of interneurons could result in lower median MI even when only the bursting neurons were considered. The analysis of possible differences of MI values among the interneuron subtypes requires the registration of a large population of anatomically identified hippocampal interneurons. Our report principally focuses on

medial septal GABAergic neurons and the investigation of different hippocampal interneuron classes should be the aim of a further study. Additionally, it is possible that although individual interneurons show relatively lower MI values, a population of simultaneously active interneurons could share a high amount of information with the LFP (Quiroga and Panzeri, 2009). Testing this hypothesis would be possible via the concurrent recording of large populations of hippocampal cells by using multichannel recording techniques.

Firing pattern of hippocampal interneurons

The proportion of rhythmically bursting cells among hippocampal interneurons varies considerably in previous reports (for a review on this issue, see Vertes and Kocsis, 1997; especially pages 898-900). In addition, in recent studies from Klausberger and colleagues (Klausberger et al., 2003; Somogyi and Klausberger, 2005; Klausberger and Somogyi, 2008), different firing patterns of interneuron classes are characterized. These studies show a high variance in bursting properties among interneuron subtypes. For example, PV-positive basket cells and axo-axonic cells often fire in burst mode, whereas O-LM cells show a tendency for firing in a theta-modulated, but not theta-bursting manner (Klausberger et al., 2003; Somogyi and Klausberger, 2005). Moreover, a novel interneuron subgroup called “Ivy cells” has been described recently, which was reported to be the most abundant interneuron class of the hippocampus, and these cells do not show rhythmical bursting (Fuentealba et al., 2008). It is important to note that not all “theta cells” (neurons significantly phase-locked to theta oscillation) show bursting (clearly separable clusters of action potentials), but a large proportion of “theta cells” are only theta-modulated, that is, frequency changes preferentially located at specific theta phases can be detected. The discrepancy in the proportion of theta-bursting interneurons among studies can be resolved by (1) the differential representation of various interneuron subgroups in the samples or (2) the different methods of discrimination between theta-bursting and theta-modulated cells. The relatively low number of theta-bursting cells in our interneuron sample (5/27, 18.52%) could be explained by the relatively strict definition of theta-bursting neurons (see

Materials and Methods). All cells that were judged as "theta-bursting" showed clearly separable, highly regular bursts (see Figures 16A, 17A, 18A, 20A-B and 21B).

Analysis of transfer entropy indicates a septo-hippocampal direction of information flow during hippocampal theta oscillation

Synchrony between medial septum and hippocampus has long been in the focus of neurophysiological research (for detailed reviews, see Vertes and Kocsis, 1997 or Bland and Oddie, 2001). Symmetric measures of coupling between the medial septum and the hippocampus, such as cross-correlation (Green and Rawlins, 1979; Alonso et al., 1987; Colom and Bland, 1987; Colom and Bland, 1991), classical coherence (Buzsaki et al., 1983; Kinney et al., 1996) and joint peri-stimulus time histogram (Bland et al., 1999) has been applied to characterize the synchronization of the two regions. A specific aspect of synchrony is phase coupling, which has also been studied in details in the septo-hippocampal network (Dragoi et al., 1999; Borhegyi et al., 2004). In the recent years, both experimental (Toth et al., 1993; Toth et al., 1997) and modeling (Wang, 2002) studies have shown that, besides the septal drive via GABAergic and cholinergic septo-hippocampal projection, hippocampo-septal feedback is also essential for the genesis and maintenance of hippocampal theta oscillation. However, detailed directional dynamics of interaction through the septo-hippocampal channel remained unclear. In order to address the question of directionality of interaction between two brain regions, an asymmetric measure of interaction should be chosen. Conventional choices are (1) Partial Directed Coherence (Saito and Harashima, 1981; Baccalá and Sameshima, 1999; Sameshima and Baccalá, 2001), which is based on the general linear model and uses the concept of Granger-causality (Granger, 1969) or (2) Directed Transfer Function (DTF; Kaminski et al., 2001, Kocsis and Kaminski, 2006). The two algorithms are equivalent in the special case of two dimensions, that is, when measuring directionality between two different signals, as reported in Sameshima and Baccalá (2001). However, for different types of signals (e.g. field oscillation and unit activity), PDC has a major constraint, i.e. it is sensitive to normalization due to scaling-dependence of the method, which makes the comparison of the directional PDC values

ambiguous. An additional drawback of PDC (DTF) is linearity, which results in decreased sensitivity to complex non-linear interactions; however, the method is capable of accurately detecting linear connections among signals of the same type (e.g. field potentials, Sharott et al., 2005).

Information theoretical methods have a huge variety of applications in neuroscience (Hurtado et al., 2004; Kajikawa & Hackett, 2005; Panzeri et al., 2007). In our study, entropy and mutual information was applied to wavelet spectra of hippocampal field potentials and medial septal or hippocampal unit recordings, as discussed in previous parts of this study. Based on MI, the asymmetric measure of information transmission called transfer entropy can be introduced (Gourevitch and Eggermont, 2007; Schreiber, 2000; on wavelet: Imas et al., 2005), which is also capable of representing asymmetry of interaction, but lacks the above mentioned constraints of PDC (i.e. linearity and scaling-dependency). Nevertheless, it should be noted that neither PDC (see the discussion in Kocsis and Kaminski, 2006) nor transfer entropy analysis can exclude the possibility that the two brain regions are driven from a common source.

Our results demonstrated that MS neurons show theta-associated septo-hippocampal directional dominance, possibly due to large amount of transmitted information in the theta frequency range to the hippocampus during theta-oscillation. However, to a smaller but significant extent, hippocampo-septal feedback is also detectable in these cells. The preferred direction of flow changes during large amplitude irregular activity, in which the hippocampo-septal influences dominate. The behavior of these MS neurons is in agreement with previous results hypothesizing a septal pacemaker network transmitting rhythmic activity to the hippocampus during theta oscillation. Indeed, MS neurons showing theta-bursting activity were characterized by higher absolute DF values as compared with non-bursting cells. However, our results indicate that non-bursting septal neurons can also belong to the septal leading group. The presence of a hippocampo-septal component of interaction in MS cells strengthens the theory that strong hippocampal feedback to the medial septum operates during theta oscillation. Parallel with the above group characterized by theta-coupled septal lead, a small proportion of septal neurons (25%) received a dominant hippocampo-septal feedback, indicating that a part of the medial septal network is driven from the

hippocampus during theta activity. Although MS neurons are influenced only transiently during non-theta states by the hippocampus (Dragoi et al., 1999), non-theta-associated septal as well as hippocampal dominance could occur in a few cases. It implies that a certain level of coupling between the MS and the hippocampus in the theta-band is still detectable during non-theta activity. Identified medial septal HCN-IR neurons showed stronger directional asymmetry as compared with non-HCN cells, supporting the pivotal role of these neurons in driving hippocampal theta genesis. Both the analysis of temporal delays and that of preferred direction of flow indicated that while the HCN-IR neurons lead the hippocampal theta, non-HCN neurons of the MS compose a "follower" group. Additionally, temporal lags and DF values were strongly correlated among HCN-immunoreactive neurons. These data suggest that the HCN channel could serve as a marker of pacemaker neurons in the medial septum.

We could provide the first evidence indicating that the septo-hippocampal direction of influence is dominant, and acts in parallel with hippocampo-septal feedback during hippocampal theta oscillation in the intact brain. We propose that the medial septal neurons containing the HCN channel play a crucial role in the pacing of hippocampal theta oscillation.

Conclusions

Septo-hippocampal reciprocal inhibitory loop in the context of bottom-up sensory and top-down cortical influence

On the course of theta synchronization, septo-hippocampal GABAergic pacemaker neurons inhibit all known subtypes of hippocampal interneurons, which leads to the disinhibition of pyramidal cells (Freund and Antal, 1988; Toth et al., 1997; Fig. 32). The oscillating output of the hippocampal interneuron network produces the alternating charge flow along the somadendritic axis of pyramidal cells leading to the formation of field theta activity. Hippocampo-septal back-projection, targeting mostly septo-hippocampal GABAergic cells, could further enhance synchrony of MS GABAergic cells (Toth et al., 1993; Takacs et al., 2008). The above reciprocal inhibitory loop forms the core of the theta generating circuitry. In contrast with the GABAergic MS cells innervating interneurons exclusively, septal cholinergic neurons send diffuse projection to the hippocampus, influencing both interneurons and pyramidal cells (Frotscher and Leranth, 1985). Selective lesion of the MS cholinergic cells strongly reduces the number of rhythmically bursting neurons in the medial septum (Apartis et al., 1998) and also attenuates hippocampal field theta (Yoder and Pang, 2005). However, a recent study by Simon et al. (2006) demonstrated that anatomically identified cholinergic MS neurons display very slow, theta-unrelated firing *in vivo*. This suggests that these neurons might not act as pacemakers but rather play a permissive and modulatory role via the tonic excitation of MS GABAergic and glutamatergic neurons (Wu et al., 2000; Manseau et al., 2005) as well as hippocampal interneurons and principal cells (Frotscher and Leranth, 1985). Additionally, abrupt changes of cholinergic activity can also contribute to the resetting or blocking of the oscillation via ionotropic acetylcholine receptors. Recently, a substantial proportion of medial septal neurons was shown to be glutamatergic (Sotty et al., 2003). These cells innervate septal GABAergic and cholinergic neurons (Hajszan et al., 2004; Manseau et al., 2005), display slow firing or cluster firing discharge pattern *in vitro* (Sotty et al., 2003) and may also project to the hippocampus. These data suggest that septal

glutamatergic neurons may be involved in theta formation, which is also supported by a recent theoretical study (Ujfalussy et al., 2006). However, the *in vivo* activity pattern of MS glutamatergic cells and their exact role in theta genesis remains to be established. Thus, theta genesis in the septo-hippocampal reciprocal inhibitory loop may be triggered by excitatory inputs that convey incoming sensory load and modulated by cortical influence. Excitatory elements are also capable of setting the frequency and amplitude of the oscillation (Ujfalussy et al., 2006).

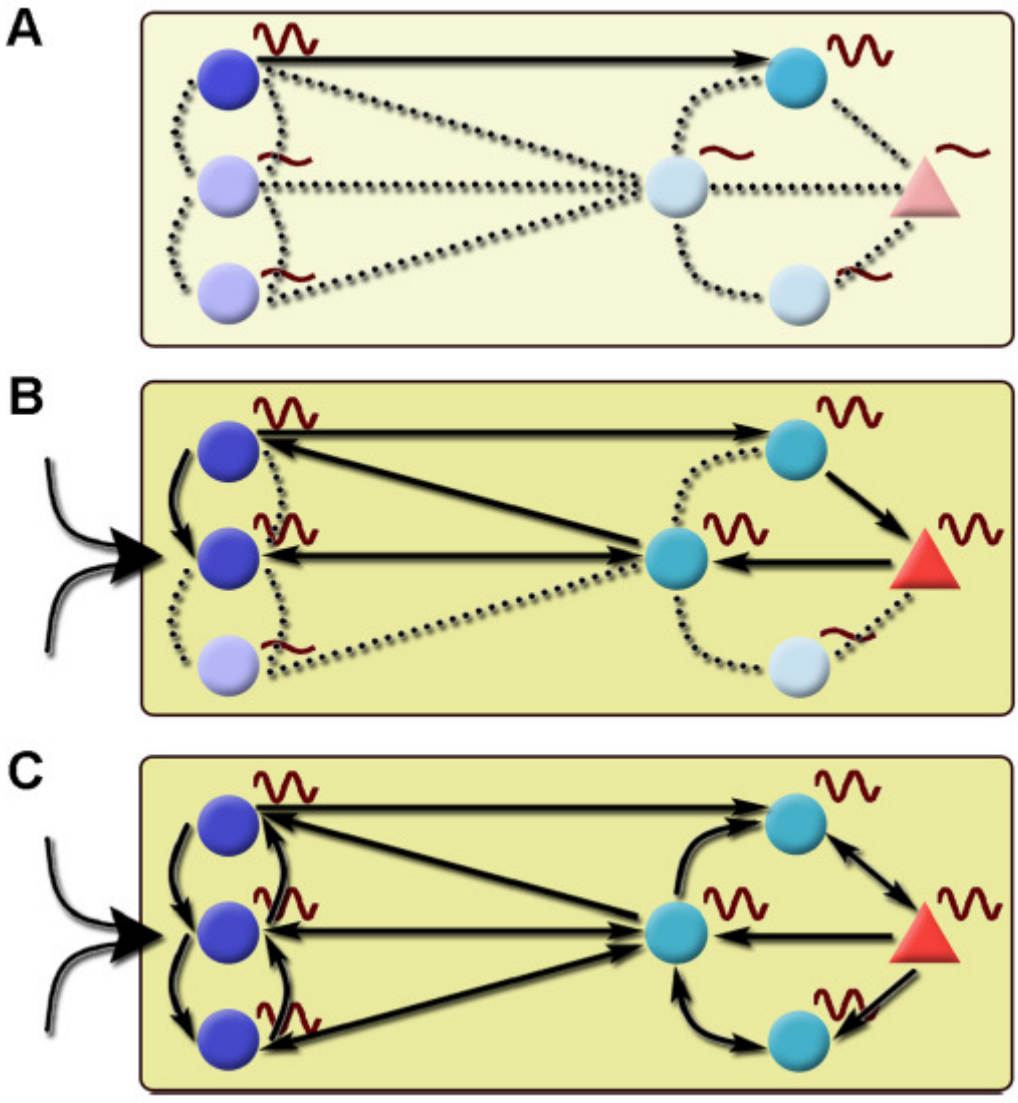

Figure 32. Gradual recruitment of oscillating units in the septo-hippocampal system leads to population level theta rhythm. In general, theta activity within the

septo-hippocampal system is formed by the build-up of synchrony among groups of interconnected oscillating units and spreads by recruiting non-oscillating components of the network. Reciprocal GABAergic inhibitory interactions under the control of tonic neuromodulatory action (muscarinic cholinergic and monoaminergic) and phasic rapid excitation (nicotinic cholinergic and glutamatergic) is indispensable for the operation of this rhythm-generating circuitry. Left side: MS; right side: hippocampus. Circle: GABAergic neuron, triangle: pyramidal cell. **A**: During non-theta states, only a subset of medial septal and hippocampal neurons exhibit theta frequency membrane potential oscillation (dark colored cells with sine waves; in the MS, the so called constitutive bursting cells in Borhegyi et al., 2004 and Varga et al., 2008). These oscillating units are only partly synchronized, most of them are functionally uncoupled. The out-of-phase activity can even weaken population-level synchrony. **B**: The elevation of ascending excitation (large arrow left to MS cells) pushes the septo-hippocampal system into a short transition state characterized by the abrupt elevation of GABAergic activity, the activation of pacemaker mechanisms and the rapid spread of synchronous activity via the coupling of activated medial septal and hippocampal oscillators. Tonic excitation of the septo-hippocampal GABAergic circuitry by septal cholinergic neurons (indicated by yellow background color of variable intensity) also contributes to this process. The reciprocal septo-hippocampal dialogue has a crucial role not only in connecting the two regions but also in orchestrating rhythmic units within them. **C**: The spread of synchrony leads to the formation of population level rhythm. The gradual build-up of oscillation is supported by the variance of temporal antecedence observed in this study: some rhythmic units precede hippocampal LFP more than others indicating that they might be involved in an earlier phase of the synchronization process. The overlap of MS and hippocampal Z-shift values and the significant bidirectional NTE components also points to the importance of the two-way interaction between the MS and hippocampus for both the formation and maintenance of the oscillation.

We conclude that PV- and/or HCN-immunopositive medial septal neurons play a key role in theta-band synchronization of the hippocampal network, being the first elements in the temporal pattern of activity, followed by hippocampal interneurons and then by the hippocampal LFP. In this process, increased excitation from local

cholinergic and/or glutamatergic neurons and ascending neuromodulatory inputs initiate the rhythmic firing and the synchronization process of MS GABAergic neurons (Fig. 32). Two scenarios are feasible: (1) septal units are synchronized via their local axon collateral system, possibly involving other subcortical areas such as the supramammillary nucleus. Then, a theta rhythmic output, mainly composed of inhibitory GABAergic fibers, is fed into the hippocampal GABAergic network where it entrains the activity of the various interneuron types. (2) Rhythmic activity of a few septal neurons leads to synchronization in small hippocampal domains. Activation of hippocampo-septal GABAergic neurons – either by local pyramidal cell activity, or by direct action of their septal input – synchronizes the medial septal pacemaker units. Even in the first scenario, hippocampo-septal back-projection, as hypothesized, would further enhance synchrony of MS GABAergic cells.

Summary

The hippocampal formation has long been considered as a main component of mnemonic processes. The regulation of these hippocampal functions strongly depends on subcortical connections, among which the reciprocal septo-hippocampal pathway plays a prominent role. The information processing in the septo-hippocampal system is substantially different during the two major hippocampal activity states, the regular 4 to 10 Hz theta oscillation and the large amplitude irregular activity. Synchronization between the medial septum and in the hippocampus was demonstrated by a large body of research. However, the timing of events in this process and the state-dependent changes of directional influences remains elusive.

To address these questions, we analyzed dual recordings of hippocampal local field potential and medial septal (or hippocampal) single cell activity from urethane anesthetized rats. Single cell recordings were performed by the juxtacellular technique, which made the immunocytochemical identification of the recorded neurons possible. We used novel circular statistical and information theory analysis tools to gain insight into the regulation of the septo-hippocampal communication.

Our data revealed the temporal antecedence of activity changes in a subgroup of medial septal neurons containing the calcium binding protein parvalbumin (PV) and/or the putative pacemaker channel HCN (hyperpolarization activated and cyclic nucleotide gated non-selective cation channel) compared with hippocampal interneurons and pyramidal cells. The information theory analysis revealed a dominant septo-hippocampal direction of information transfer during theta oscillation that was accompanied by a hippocampo-septal feedback influence. These data suggest the pacemaker role of medial septal PV/HCN neurons in the formation of hippocampal theta oscillation.

Összefoglaló

Régóta ismert, hogy a hippocampus fontos szerepet tölt be a különböző memóriafolyamatokban. A hippocampalis memóriafunkciók szabályozásában kulcsszerepet töltenek be különböző kéregalatti területek, elsősorban a hippocampus-szal kétirányú anatómiai kapcsolatban álló medialis septum (MS). A MS és a hippocampus közötti információátvitel fontos különbségeket mutat a két legjellemzőbb hippocampalis aktivitásmintázat, a 4-10 Hz-es theta ritmus és a nagy amplitúdójú irreguláris aktivitás alatt. Számos kísérletes és elméleti tanulmány mutat a MS elengedhetetlen szerepére a hippocampalis hálózat szinkronizációjában theta oszcilláció alatt. Ennek ellenére a folyamat különböző eseményeinek időzítése és az információáramlás irányának állapotfüggő változásai ismeretlenek.

A fenti kérdések megválaszolásához uretánnal altatott patkányokból származó hippocampalis helyi mezőpotenciál és egyidejű medialis septalis (vagy hippocampalis) egysejt-aktivitás felvételeket elemeztünk. Az egysejt-aktivitást juxtacelluláris technikával rögzítettük, mely lehetővé tette az elvezetett sejtek immuncitokémiai azonosítását. A septo-hippocampalis kommunikáció szabályozásának vizsgálatához új cirkuláris statisztikai és információelméleti módszereket használtunk.

Sikerült kimutatnunk, hogy a parvalbumint (PV) és/vagy a feltételezett ritmusgeneráló HCN csatornát (hiperpolarizáció által aktivált, ciklikus nukleotidok által szabályozott nem-szelektív kation csatorna) kifejező medialis septalis idegsejtek aktivitásváltozásai megelőzik a hippocampalis interneuronok és piramissejtek perturbációit. Az információelméleti elemzés segítségével theta szakaszok alatt domináns septo-hippocampalis irányú információáramlást mutattunk ki, mellyel egyidejűleg jelentős hippocampo-septalis visszacsatolást észleltünk. Adataink a medialis septum PV és/vagy HCN fehérjéket kifejező sejtjeinek a hippocampalis theta oszcilláció létrehozásában betöltött ritmusgeneráló szerepére utalnak.

References

Accili EA, Proenza C, Baruscotti M, DiFrancesco D (2002) From funny current to HCN channels: 20 years of excitation. News Physiol Sci 17:32-37.

Acsady L, Kamondi A, Sik A, Freund T, Buzsaki G (1998) GABAergic cells are the major postsynaptic targets of mossy fibers in the rat hippocampus. J Neurosci 18:3386-3403.

Alonso A, Gaztelu JM, Buno W Jr, Garcia-Austt E (1987) Cross-correlation analysis of septohippocampal neurons during theta-rhythm. Brain Res 413:135-146.

Amaral DG, Dolorfo C, Alvarez-Royo P (1991) Organization of CA1 projections to the subiculum: a PHA-L analysis in the rat. Hippocampus 1:415-436.

Andersen P, Morris R, Amaral D, Bliss T, O'Keefe J (2007) The hippocampus book. Oxford University Press, New York

Apartis E, Poindessous-Jazat FR, Lamour YA, Bassant MH (1998). Loss of rhythmically bursting neurons in rat medial septum following selective lesion of septo-hippocampal cholinergic system. J Neurophysiol 79:1633-1642.

Bennett BD, Callaway JC, Wilson CJ (2000) Intrinsic membrane properties underlying spontaneous tonic firing in neostriatal cholinergic interneurons. J Neurosci 20:8493–8503.

Baccala LA, Sameshima K (2001) Partial directed coherence: a new concept in neural structure determination. Biol Cybern 84:463-474.

Blackstad TW (1956) Commisural connections of the hippocampal region in the rat, with special reference to their mode of termination. J Comp Neurol 105:417-537.

Bland, BH, Oddie SD, Colom LV (1999) Mechanisms of neural synchrony in the septohippocampal pathways underlying hippocampal theta generation. J Neurosci 9: 3223-3237.

Bland BH, Oddie SD (2001) Theta band oscillation and synchrony in the hippocampal formation and associated structures: the case for its role in sensorimotor integration. Behav Brain Res 127:119-136.

Bódizs R, Kántor S, Szabó G, Szûcs A, Erõss L, Halász P (2001) Rhythmic hippocampal slow oscillation characterizes REM sleep in humans. Hippocampus 11:747-753.

Borhegyi Z, Varga V, Szilágyi N, Fabo D, Freund TF (2004) Phase segregation of medial septal GABAergic neurons during hippocampal theta activity. J Neurosci 24:8470-8479.

Brazhnik ES, Fox SE (1999) Action potentials and relations to the theta rhythm of medial septal neurons in vivo. Exp Brain Res 127:244-258.

Brown HF, DiFrancesco D, Noble SJ (1979) How does adrenaline accelerate the heart? Nature 280:235-236.

Buzsaki G, Leung LW, Vanderwolf CH (1983) Cellular bases of hippocampal EEG in the behaving rat. Brain Res 287:139-171.

Buzsaki G, Czopf J, Kondakor I, Kellenyi L (1986) Laminar distribution of hippocampal rhythmic slow activity (RSA) in the behaving rat: current-source density analysis, effects of urethane and atropine. Brain Res 365:125-137.

Buzsáki G (1989) Two-stage model of memory trace formation: a role for "noisy" brain states. Neuroscience 31:551-570.

Buzsaki G (2002) Theta oscillations in the hippocampus. Neuron 33:325-340.

Buzsaki G (2006) Rhythms of the Brain. Oxford Univesity Press, New York

Calandreau L, Jaffard R, Desmedt A (2007) Dissociated roles for the lateral and medial septum in elemental and contextual fear conditioning. Learn Mem 14:422-429.

Cantero JL, Atienza M, Stickgold R, Kahana MJ, Madsen JR, Kocsis B (2003) Sleep-dependent theta oscillations in the human hippocampus and neocortex. J Neurosci 23:10897-10903.

Caplan JB, Madsen JR, Schulze-Bonhage A, Aschenbrenner-Scheibe R, Newman EL, Kahana MJ (2003) Human theta oscillations related to sensorimotor integration and spatial learning. J Neurosci 23:4726-4736.

Cassidy M, Brown P (2003) Spectral phase estimates in the setting of multidirectional coupling. J Neurosci Meth 127:95-103.

Cheung THC, Cardinal RN (2005) Hippocampal lesions facilitate instrumental learning with delayed reinforcement but induce impulsive choice in rats. BMC Neuroscience 6:36

Csicsvari J, Hirase H, Czurko A, Buzsáki G (1998) Reliability and state dependence of pyramidal cell-interneuron synapses in the hippocampus: an ensemble approach in the behaving rat. Neuron 21:179-189.

Csicsvari J, Hirase H, Czurko A, Mamiya A, Buzsaki G (1999) Fast network oscillations in the hippocampal CA1 region of the behaving rat. J Neurosci 19:RC20.

Csicsvari J, Hirase H, Mamiya A, Buzsáki G (2000) Ensemble patterns of hippocampal CA3-CA1 neurons during sharp wave-associated population events. Neuron 28:585-594.

Csicsvari J, Jamieson B, Wise KD, Buzsáki G (2003) Mechanisms of gamma oscillations in the hippocampus of the behaving rat. Neuron 37:311-322.

Clemens Z, Mölle M, Eross L, Barsi P, Halász P, Born J (2007) Temporal coupling of parahippocampal ripples, sleep spindles and slow oscillations in humans. Brain. 130:2868-2878.

Clement EA, Richard A, Thwaites M, Ailon J, Peters S, Dickson CT (2008) Cyclic and sleep-like spontaneous alternations of brain state under urethane anaesthesia. PLoS ONE 3:e2004.

Colom LV, Bland BH (1987) State-dependent spike train dynamics of hippocampal formation neurons: evidence for theta-on and theta-off cells. Brain Res 422:277-286.

Colom LV, Bland BH (1991) Medial septal cell interactions in relation to hippocampal field activity and the effects of atropine. Hippocampus 1:15-30.

Craig LA, Hong NS, Kopp J, McDonald RJ (2008) Emergence of spatial impairment in rats following specific cholinergic depletion of the medial septum combined with chronic stress. Eur J Neurosci 27:2262-2271.

Cutsuridis V, Cobb S, Graham BP (2009) Encoding and retrieval in a model of the hippocampal CA1 microcircuit. Hippocampus *Epub ahead of print*

de Almeida RM, Giovenardi M, da Silva SP, de Oliveira VP, Stein DJ (2005) Maternal aggression in Wistar rats: effect of 5-HT2A/2C receptor agonist and antagonist microinjected into the dorsal periaqueductal gray matter and medial septum. Braz J Med Biol Res 38:597-602.

De Garengeot RJC (1742) Splanchnologie ou l'anatomie des visceres, 2nd Edition. C. Osmond, Paris, pp. 250-251.

Dekhuijzen AJ, Bagust J (1996) Analysis of neural bursting: nonrhythmic and rhythmic activity in isolated spinal cord. J Neurosci Methods 67:141-147.

Destexhe A, Bal T, McCormick DA, Sejnowski TJ (1996) Ionic mechanisms underlying synchronized oscillations and propagating waves in a model of ferret thalamic slices. J Neurophysiol 76:2049-2070.

Dickson CT, Magistretti J, Shalinsky MH, Fransen E, Hasselmo ME, Alonso A (2000) Properties and role of Ih in the pacing of subthreshold oscillations in entorhinal cortex layer II neurons. J Neurophysiol 83:2562–2579.

DiFrancesco D (1986) Characterization of single pacemaker channels in cardiac sino-atrial node cells. Nature 324:470–473.

Dragoi G, Carpi D, Recce M, Csicsvari J, Buzsaki G (1999) Interactions between hippocampus and medial septum during sharp waves and theta oscillation in the behaving rat. J Neurosci 19:6191-6199.

Ekstrom AD, Caplan JB, Ho E, Shattuck K, Fried I, Kahana MJ (2005) Human hippocampal theta activity during virtual navigation. Hippocampus 15:881-889. Erratum in: Hippocampus 16:101.

Ekstrom A, Viskontas I, Kahana M, Jacobs J, Upchurch K, Bookheimer S, Fried I (2007) Contrasting roles of neural firing rate and local field potentials in human memory. Hippocampus 17:606-617.

Eyre MD, Freund TF, Gulyas AI (2007) Quantitative ultrastructural differences between local and medial septal GABAergic axon terminals in the rat hippocampus. Neuroscience 149:537-548.

Farge M (1992) Wavelet transforms and their applications to turbulence. Annu Rev Fluid Mech 24:395–457.

Fisher, N. (1993) Statistical Analysis of Circular Data. Cambridge Univerity Press, Cambridge

Fonyó A (2002) Principles of medical physiology. Medicina, Budapest

Freiwald WA, Valdes P, Bosch J, Biscay R, Jimenez JC, Rodriguez LM, Rodriguez V, Kreiter AK, Singer W (1999) Testing non-linearity and directedness of interactions between neural groups in the macaque inferotemporal cortex. J Neurosci Methods 94:105-119.

Freund TF, Antal M (1988) GABA-containing neurons in the septum control inhibitory interneurons in the hippocampus. Nature 336:170-173.

Freund TF (1989) GABAergic septohippocampal neurons contain parvalbumin. Brain Res 478:375-381.

Freund TF, Buzsáki G (1996) Interneurons of the hippocampus. Hippocampus 6:347-470.

Freund TF (2003) Interneuron diversity series: rhythm and mood in perisomatic inhibition. Trends Neurosci 26:489–495.

Freund TF, Katona I (2007) Perisomatic inhibition. Neuron 56:33–42.

Fricker D, Miles R (2000) EPSP amplification and the precision of spike timing in hippocampal neurons. Neuron 28:559-569.

Frotscher M, Leranth C (1985) Cholinergic innervation of the rat hippocampus as revealed by choline acetyltransferase immunocytochemistry: a combined light and electron microscopic study. J Comp Neurol 239:237-246.

Fuentealba P, Begum R, Capogna M, Jinno S, Márton LF, Csicsvari J, Thomson A, Somogyi P, Klausberger T (2008) Ivy cells: a population of nitric-oxide-producing, slow-spiking GABAergic neurons and their involvement in hippocampal network activity. Neuron 57:917-929. Erratum in: Neuron 58:295.

Gabor D (1946) Theory of communication. Proc IEE 93:429-457.

Geisler C, Robbe D, Zugaro M, Sirota A, Buzsáki G (2007) Hippocampal place cell assemblies are speed-controlled oscillators. Proc Natl Acad Sci USA. 104:8149-8154.

George MS, Abbott LF, Siegelbaum SA (2009) HCN hyperpolarization-activated cation channels inhibit EPSPs by interactions with M-type K(+) channels. Nat Neurosci 12:577-584.

Gourévitch B, Eggermont JJ (2007) Evaluating information transfer between auditory cortical neurons. J Neurophysiol 97:2533-2543.

Granger CWJ (1969) Investigating causal relations by econometric models and cross-spectral methods. Econometrica 37:424-438.

Grastyán E, Lissák K, Madarász I, Donhoffer H (1959) Hippocampal Electrical Activity during the Development of Conditioned Reflexes. Electroencephalogr Clin Neurophysiol Suppl 11:409-430.

Green KF, Rawlins JN (1979) Hippocampal theta in rats under urethane: generators and phase relations. Electroencephalogr Clin Neurophysiol 47:420-429.

Hajszan T, Alreja M, Leranth C (2004) Intrinsic vesicular glutamate transporter 2-immunoreactive input to septohippocampal parvalbumin-containing neurons: Novel glutamatergic local circuit cells. Hippocampus 14:499–509.

Hasselmo ME (2005) What is the function of hippocampal theta rhythm? Linking behavioral data to phasic properties of field potential and unit recording data. Hippocampus 15:936-949.

Henderson Z, Boros A, Janzso G, Westwood AJ, Monyer H, Halasy K (2005) Somato-dendritic nicotinic receptor responses recorded in vitro from the medial septal diagonal band complex of the rodent. J Physiol 562:165-182.

Hu H, Vervaeke K, Storm JF (2002) Two forms of electrical resonance at theta frequencies, generated by M-current, h-current and persistent Na+ current in rat hippocampal pyramidal cells. J Physiol 545:783-805.

Hurtado JM, Rubchinsky LL, Sigvardt KA (2004) Statistical method for detection of phase-locking episodes in neural oscillations. J Neurophysiol 91:1883-1898.

Imas OA, Ropella KM, Ward BD, Wood JD, Hudetz AG (2005) Volatile anesthetics disrupt frontal-posterior recurrent information transfer at gamma frequencies in rat. Neurosci Lett 387:145-150.

Ishizuka N, Weber J, Amaral DG (1990) Organization of intrahippocampal projections originating from CA3 pyramidal cells in the rat. J Comp Neurol 295:580-623.

Jarosiewicz B, Skaggs WE (2004) Level of arousal during the small irregular activity state in the rat hippocampal EEG. J Neurophysiol 91:2649-2657.

Jinno S, Klausberger T, Marton LF, Dalezios Y, Roberts JD, Fuentealba P, Bushong EA, Henze D, Buzsáki G, Somogyi P (2007) Neuronal diversity in GABAergic long-range projections from the hippocampus. J Neurosci 27:8790-8804.

Jones GA, Norris SK, Henderson Z (1999) Conduction velocities and membrane properties of different classes of rat septohippocampal neurons recorded in vitro. J Physiol 517:867-877.

Jung R, Kornmüller AE (1938) Eine Methodik der ableitung lokalisierter Potentialschwankungen aus subcorticalen Hirngebieten. Arch Psychiat Nervenkr 109:1–30.

Kahana MJ, Sekuler R, Caplan JB, Kirschen M, Madsen JR. (1999) Human theta oscillations exhibit task dependence during virtual maze navigation. Nature 399:781-784.

Kajikawa Y, Hackett TA (2005) Entropy analysis of neuronal spike train synchrony. J Neurosci Methods 149:90-93.

Kaminski M, Ding M, Truccolo WA, Bressler SL (2001) Evaluating causal relations in neural systems: granger causality, directed transfer function and statistical assessment of significance. Biol Cybern 85:145-157.

Kamondi A, Acsady L, Wang XJ, Buzsaki G (1998) Theta oscillations in somata and dendrites of hippocampal pyramidal cells in vivo: activity-dependent phase-precession of action potentials. Hippocampus 8:244-261.

Karson MA, Tang AH, Milner TA, Alger BE (2009) Synaptic cross talk between perisomatic-targeting interneuron classes expressing cholecystokinin and parvalbumin in hippocampus. J Neurosci 29:4140-4154.

King C, Recce M, O'Keefe J (1998) The rhythmicity of cells of the medial septum/diagonal band of Broca in the awake freely moving rat: relationships with behaviour and hippocampal theta. Eur J Neurosci 10:464-477.

Kinney GG, Kocsis B, Vertes RP (1996) Medial septal unit firing characteristics following injections of 8-OH-DPAT into the median raphe nucleus. Brain Res 708:116-122.

Kiss J, Patel AJ, Freund TF (1990a) Distribution of septohippocampal neurons containing parvalbumin or choline acetyltransferase in the rat brain. J Comp Neurol 298:362-372.

Kiss J, Patel AJ, Baimbridge KG, Freund TF (1990b) Topographical localization of neurons containing parvalbumin and choline acetyltransferase in the medial septum-diagonal band region of the rat. Neuroscience 36:61-72.

Kiss J, Magloczky Z, Somogyi J, Freund TF (1997) Distribution of calretinin-containing neurons relative to other neurochemically identified cell types in the medial septum of the rat. Neuroscience 78:399-410.

Klausberger T, Magill PJ, Marton LF, Roberts JD, Cobden PM, Buzsaki G, Somogyi P (2003) Brain-state- and cell-type-specific firing of hippocampal interneurons in vivo. Nature 421:844-848.

Klausberger T, Somogyi P (2008) Neuronal diversity and temporal dynamics: the unity of hippocampal circuit operations. Science 321:53-57.

Koch U, Grothe B (2003) Hyperpolarization-activated current (Ih) in the inferior colliculus: distribution and contribution to temporal processing. J Neurophysiol 90:3679-3687.

Kocsis B, Kaminski M (2006) Dynamic changes in the direction of the theta rhythmic drive between supramammillary nucleus and the septohippocampal system. Hippocampus 16:531-540.

Kramis R, Vanderwolf CH, Bland BH (1975) Two types of hippocampal rhythmical slow activity in both the rabbit and the rat: relations to behavior and effects of atropine, diethyl ether, urethane, and pentobarbital. Exp Neurol 49:58-85.

Lacaille JC, Mueller AL, Kunkel DD, Schwartzkoin PA (1987) Local circuit interactions between oriens/alveus interneurons and CA1 pyramidal cells in hippocampal slices: electrophysiology and morphology. J Neurosci 8:1400-1410.

Lawson VH, Bland BH (1993) The role of the septohippocampal pathway in the regulation of hippocampal field activity and behavior: analysis by the intraseptal microinfusion of carbachol, atropine, and procaine. Exp Neurol 20:132-144.

Leung LW (1985) Spectral analysis of hippocampal EEG in the freely moving rat: effects of centrally active drugs and relations to evoked potentials. Electroencephalogr Clin Neurophysiol 60: 65-77.

Li X-G, Somogyi P, Ylinen A, Buzsaki G (1994) The hippocampal CA3 network: an in vivo intracellular labeling study. J Comp Neurol 339:181-208.

Lorente de Nó (1934) Studies on the structure of the cerebral cortex. II. Continuation of the study of the ammonic system. J Physiol Neurol 46:113-177.

Lytton WW, Destexhe A, Sejnowski TJ (1996) Control of slow oscillations in the thalamocortical neuron: a computer model. Neuroscience 70:673-684.

Maglóczky Z, Acsády L, Freund TF (1994) Principal cells are the postsynaptic targets of supramammillary afferents in the hippocampus of the rat. Hippocampus 4:322-334.

Manns ID, Mainville L, Jones BE (2001) Evidence for glutamate, in addition to acetylcholine and GABA, neurotransmitter synthesis in basal forebrain neurons projecting to the entorhinal cortex. Neuroscience 107:249-263.

Manns ID, Alonso A, Jones BE (2003) Rhythmically discharging basal forebrain units comprise cholinergic, GABAergic, and putative glutamatergic cells. J Neurophysiol 89:1057-1066.

Manseau F, Danik M, Williams S (2005) A functional glutamatergic neurone network in the medial septum and diagonal band area. J Physiol 566: 865–884.

Manseau F, Goutagny R, Danik M, Williams S (2008) The hippocamposeptal pathway generates rhythmic firing of GABAergic neurons in the medial septum and diagonal bands: an investigation using a complete septohippocampal preparation in vitro. J Neurosci 28:4096-4107.

McCormick DA, Pape HC (1990) Properties of a hyperpolarization-activated cation current and its role in rhythmic oscillation in thalamic relay neurones. J Physiol 431:291-318.

Meibach RC, Siegel A (1977) Efferent connections of the septal area in the rat: an analysis utilizing retrograde and anterograde transport methods. Brain Res 119:1-20.

Merchenthaler I, Gorcs T, Setalo G, Petrusz P, Flerko B (1984) Gonadotropin-releasing hormone (GnRH) neurons and pathways in the rat brain. Cell Tissue Res 237:15-29.

Mironov SL, Langohr K, Richter DW (2000) Hyperpolarization-activated current, Ih, in inspiratory brainstem neurons and its inhibition by hypoxia. Eur J Neurosci 12:520-526.

Misiti M, Misiti Y, Oppenheim G, Poggi, JM (2000) Wavelet toolbox user's guide (for use with Matlab). The Mathworks Inc., Natick, USA

Mölle M, Yeshenko O, Marshall L, Sara SJ, Born J (2006) Hippocampal sharp wave-ripples linked to slow oscillations in rat slow-wave sleep. J Neurophysiol 96:62-70.

Montagnese CM, Székely AD, Adám A, Csillag A (2004) Efferent connections of septal nuclei of the domestic chick (Gallus domesticus): an anterograde pathway tracing study with a bearing on functional circuits. J Comp Neurol 469:437-456.

Montagnese CM, Zachar G, Bálint E, Csillag A (2008) Afferent connections of septal nuclei of the domestic chick (Gallus domesticus): a retrograde pathway tracing study. J Comp Neurol 511:109-150.

Montgomery SM, Buzsáki G (2007) Gamma oscillations dynamically couple hippocampal CA3 and CA1 regions during memory task performance. Proc Natl Acad Sci USA 104:14495-14500.

Morris NP, Harris SJ, Henderson Z (1999) Parvalbumin-immunoreactive, fast-spiking neurons in the medial septum/diagonal band complex of the rat: intracellular recordings in vitro. Neuroscience 92:589-600.

Muthuswamy J, Thakor NV (1998) Spectral analysis methods for neurological signals. J Neurosci Methods 83:1-14.

Naber PA, da Silva FHR, Witter MP (2001) Reciprocal connections between the entorhinal cortex and hippocampal fields CA1 and the subiculum are in register with the projections from CA1 to the subiculum. Hippocampus 11:99-104.

Nakashiba T, Buhl DL, McHugh TJ, Tonegawa S (2009) Hippocampal CA3 output is crucial for ripple-associated reactivation and consolidation of memory. Neuron 62:781-787.

Nakashiba T, Young JZ, McHugh TJ, Buhl DL, Tonegawa S (2008) Transgenic inhibition of synaptic transmission reveals role of CA3 output in hippocampal learning. Science 319:1260-1264.

Nolan MF, Dudman JT, Dodson PD, Santoro B (2007) HCN1 channels control resting and active integrative properties of stellate cells from layer II of the entorhinal cortex. J Neurosci 27:12440–12451.

Nolan MF, Malleret G, Dudman JT, Buhl DL, Santoro B, Gibbs E, Vronskaya S, Buzsaki G, Siegelbaum SA, Kandel ER, Morozov A (2004a) A behavioral role for dendritic integration: HCN1 channels constrain spatial memory and plasticity at inputs to distal dendrites of CA1 pyramidal neurons. Cell 119:719–732.

Nolan MF, Tsay D, Siegelbaum SA, Kandel, ER (2004b) A novel role for HCN1 channels: suppression of rhythmic low-frequency network oscillations in cerebellar basket cells. In: SFN2004. San Diego, USA.

Notomi T, Shigemoto R (2004) Immunohistochemical localization of Ih channel subunits, HCN1-4, in the rat brain. J Comp Neurol 471:241-276.

O'Keefe J (1976) Place units in the hippocampus of the freely moving rat. Exp Neurol 51:78-109

O'Keefe J, Nadel L (1978) The hippocampus as a cognitive map. Clarendon Press, Oxford.

O'Keefe J, Recce ML (1993) Phase relationship between hippocampal place units and the EEG theta rhythm. Hippocampus 3:317-330.

Orbán G, Kiss T, Erdi P (2006) Intrinsic and synaptic mechanisms determining the timing of neuron population activity during hippocampal theta oscillation. J Neurophysiol 96:2889-2904. Erratum in: J Neurophysiol 97:1869.

Panzeri S, Senatore R, Montemurro MA, Petersen RS (2007) Correcting for the sampling bias problem in spike train information measures. J Neurophysiol 98:1064-1072.

Pastalkova E, Itskov V, Amarasingham A, Buzsaki G (2008) Internally generated cell assembly sequences in the rat hippocampus. Science 321:1322-1327.

Paxinos G (2004) The rat nervous system, 3rd Edition. Elsevier, Amsterdam

Paxinos G, Watson C (1998). The Rat Brain in Stereotaxic Coordinates, 4th edn. Academic Press, New York.

Pikkarainen M, Rönkkö S, Savander V, Insausti R, Pitkänen A (1999) Projections from the lateral, basal, and accessory basal nuclei of the amygdala to the hippocampal formation in rat. J Comp Neurol 403:229-260.

Pinault D (1996) A novel single-cell staining procedure performed in vivo under electrophysiological control: morpho-functional features of juxtacellularly labeled thalamic cells and other central neurons with biocytin or Neurobiotin. J Neurosci Methods 65:113-136.

Pitkänen A, Pikkarainen M, Nurminen N, Ylinen A (2000) Reciprocal connections between the amygdala and the hippocampal formation, perirhinal cortex, and postrhinal cortex in rat. A review. Ann NY Acad Sci 911:369-391.

Quiroga RQ, Panzeri S (2009) Extracting information from neuronal populations: information theory and decoding approaches. Nat Rev Neurosci 10:173-185.

Raman IM, Bean BP (1999) Ionic currents underlying spontaneous action potentials in isolated cerebellar Purkinje neurons. J Neurosci 19:1663–1674.

Ramón Y Cajal S (1893) Estructura del asta de Ammon y fascia dentata. Ann Soc Esp Hist Nat 22

Ranck JB Jr (1984) Head direction cells in the deep layer of dorsal presubiculum in freely moving rats. Soc Neurosci Abstr 10:599.

Rao JS (1972) Bahadur efficiencies of some tests for uniformity on the circle. Ann Math Stat 43:468-479.

Rao JS (1976) Some tests based on arc-lengths for the circle. Sankhya 38:329-338.

Rawlins JN, Feldon J, Gray JA (1979) Septo-hippocampal connections and the hippocampal theta rhythm. Exp Brain Res 37:49-63.

Robinson RB, Siegelbaum SA (2003) Hyperpolarization-activated cation currents: from molecules to physiological function. Annu Rev Physiol 65:453-480.

Rosenbaum T, Gordon SE (2004) Quickening the pace: looking into the heart of HCN channels. Neuron 42:193-196.

Rosenblum MG, Pikovsky AS, Kurths J (1996) Phase synchronization of chaotic oscillators. Phys Rev Lett 76:1804-1807.

Rosenblum MG, Pikovsky AS, Kurths J, Schafer C, Tass PA (2001) Phase synchronization: from theory to data analysis, In: Neuro-Informatics, edited by Moss F and Gielen S, Elsevier, Amsterdam, pp. 279-321.

Saito Y, Harashima H (1981) Tracking of information within multichannel EEG record - causal analysis in EEG. In: Recent advances in EEG and EMG Data Processing, edited by Yamaguchi N and Fujisawa K, Elsevier, Amsterdam, pp. 133-146

Sameshima K, Baccala LA (1999) Using partial directed coherence to describe neuronal ensemble interactions. J Neurosci Methods 94:93-103.

Sava S, Markus EJ (2008) Activation of the medial septum reverses age-related hippocampal encoding deficits: a place field analysis. J Neurosci 28:1841-1853.

Schafer C, Rosenblum MG, Abel HH, Kurths J (1999) Synchronization in the human cardiorespiratory system. Phys Rev E Stat Phys Plasmas Fluids Relat Interdiscip Topics 60:857-870.

Schreiber T (2000) Measuring information transfer. Phys Rev Lett 85:461-464.

Sekirnjak C & du Lac S (2002) Intrinsic firing dynamics of vestibular nucleus neurons. J Neurosci 22:2083–2095.

Shannon C (1948) A mathematical theory of communication. BellSystTech J, 27:379-423, 623-656.

Sharott A, Magill PJ, Bolam JP, Brown P (2005) Directional analysis of coherent oscillatory field potentials in the cerebral cortex and basal ganglia of the rat. J Physiol 562: 951-963.

Sherman SM, Guillery RW (2000) Exploring the thalamus. Academc Press, New York.

Siapas AG, Wilson MA (1998) Coordinated interactions between hippocampal ripples and cortical spindles during slow-wave sleep. Neuron 21:1123-1128.

Siapas AG, Lubenov EV, Wilson MA (2005) Prefrontal phase locking to hippocampal theta oscillations. Neuron 46:141-151.

Simon AP, Poindessous-Jazat F, Dutar P, Epelbaum J, Bassant MH (2006) Firing properties of anatomically identified neurons in the medial septum of anesthetized and unanesthetized restrained rats. J Neurosci 26:9038-9046.

Skaggs WE, McNaughton BL (1996) Replay of neuronal firing sequences in rat hippocampus during sleep following spatial experience. Science 271:1870-1873.

Smythe JW, Cristie BR, Colom LV, Lawson VH, Bland BH (1991) Hippocampal theta field activity and theta-on/theta-off cell discharges are controlled by an ascending hypothalamo-septal pathway. J Neurosci 11:2241-2248.

Somogyi P, Klausberger T (2005) Defined types of cortical interneurone structure space and spike timing in the hippocampus. J Physiol 562:9-26.

Sotty F, Danik M, Manseau F, Laplante F, Quirion R, Williams S (2003) Distinct electrophysiological properties of glutamatergic, cholinergic and GABAergic rat septohippocampal neurons: novel implications for hippocampal rhythmicity. J Physiol 551:927-943.

Speed HE, Dobrunz LE (2009) Developmental changes in short-term facilitation are opposite at temporoammonic synapses compared to Schaffer collateral synapses onto CA1 pyramidal cells. Hippocampus. 19:187-204.

Squire LR (1992) Memory and the hippocampus: a synthesis from findings with rats, monkeys, and humans. Psychol Rev 99:195-231.

Srividya R, Mallick HN, Kumar VM (2007) The medial septum acts through the medial preoptic area for thermoregulation and works with it for sleep regulation. Indian J Physiol Pharmacol 51:261-273.

Swanson LW, Wyss JM, Cowan WM (1978) An autoradiographic study of the organization of intrahippocampal association pathways in the rat. J Comp Neurol 181:681-716.

Swanson LW, Cowan WM (1979) The connections of the septal region in the rat. J Comp Neurol 186:621-655.

Szabadics J, Soltesz I (2009) Functional specificity of mossy fiber innervation of GABAergic cells in the hippocampus. J Neurosci 29:4239-4251.

Takács VT, Freund TF, Gulyás AI (2008) Types and synaptic connections of hippocampal inhibitory neurons reciprocally connected with the medial septum. Eur J Neurosci 28:148-164.

Tan ML, Theeuwes HP, Feenstra L, Borst JG (2007) Membrane properties and firing patterns of inferior colliculus neurons: an in vivo patch-clamp study in rodents. J Neurophysiol 98:443–453.

Torrence C, Compo GP (1998) A Practical Guide to Wavelet Analysis. Bull Amer Meteor Soc 79:61-78.

Toth K, Borhegyi Z, Freund TF (1993) Postsynaptic targets of GABAergic hippocampal neurons in the medial septum-diagonal band of broca complex. J Neurosci 13:3712-3724.

Toth K, Freund TF, Miles R. (1997) Free in PMC Disinhibition of rat hippocampal pyramidal cells by GABAergic afferents from the septum. J Physiol 500:463-474.

Ujfalussy B, Kiss T (2006) How do glutamatergic and GABAergic cells contribute to synchronization in the medial septum? J Comput Neurosci 21:343–357.

Vanderwolf CH, Kramis R, Robinson TE (1977) Hippocampal electrical activity during waking behaviour and sleep: analyses using centrally acting drugs. Ciba Found Symp 58:199-226.

Vanderwolf CH (2001) The hippocampus as an olfacto-motor mechanism: were the classical anatomists right after all? Behav Brain Res 127:25-47.

van Strien NM, Cappaert NL, Witter MP (2009) The anatomy of memory: an interactive overview of the parahippocampal-hippocampal network. Nat Rev Neurosci 10:272-282.

Vertes RP, Kocsis B (1997) Brainstem-diencephalo-septohippocampal systems controlling the theta rhythm of the hippocampus. Neuroscience 81:893-926.

Vinogradova OS (1995) Expression, control, and probable functional significance of the neuronal theta-rhythm. Prog Neurobiol 45:523-583.

Wang J, Chen S, Nolan MF, Siegelbaum SA (2002) Activity-dependent regulation of HCN pacemaker channels by cyclic AMP: signaling through dynamic allosteric coupling. Neuron 36:451-461.

Wang XJ (2002) Pacemaker neurons for the theta rhythm and their synchronization in the septohippocampal reciprocal loop. J Neurophysiol 87:889-900.

Watson GS (1961) Goodness of fit tests on a circle. Biometrika 48:109-114.

Whishaw IQ, Vanderwolf CH (1973) Hippocampal EEG and behavior: changes in amplitude and frequency of RSA (theta rhythm) associated with spontaneous and learned movement patterns in rats and cats. Behav Biol 8:461-484.

Wilent WB, Nitz DA (2007) Discrete place fields of hippocampal formation interneurons. J Neurophysiol 97:4152-4161.

Wilson CJ (2005) The mechanism of intrinsic amplification of hyperpolarizations and spontaneous bursting in striatal cholinergic interneurons. Neuron 45:575–585.

Wolansky T, Clement EA, Peters SR, Palczak MA, Dickson CT (2006) Hippocampal slow oscillation: a novel EEG state and its coordination with ongoing neocortical activity. J Neurosci 26:6213-6229.

Wu M, Shanabrough M, Leranth C, Alreja M. (2000) Cholinergic excitation of septohippocampal GABA but not cholinergic neurons: implications for learning and memory. J Neurosci 20:3900-3908.

Yoder RM, Pang KC (2005) Involvement of GABAergic and cholinergic medial septal neurons in hippocampal theta rhythm. Hippocampus 15:381-392.

Yordanova J, Kolev V, Rosso OA, Schurmann M, Sakowitz OW, Ozgoren M, Basar E (2002) Wavelet entropy analysis of event-related potentials indicates modality-independent theta dominance. J Neurosci Methods 117:99-109.

Zagotta WN, Olivier NB, Black KD, Young EC, Olson R, Gouaux E (2003) Structural basis for modulation and agonist specificity of HCN pacemaker channels. Nature 425:200-205.

List of publications

List of publications related to the dissertation

Articles

1. Varga V, **Hangya B**, Kránitz K, Ludányi A, Zemankovics R, Katona I, Shigemoto R, Freund TF, Borhegyi Z (2008) The presence of pacemaker HCN channels identifies theta rhythmic GABAergic neurons in the medial septum. J Physiol 586:3893-3915. (impact factor: 4.605)
2. **Hangya B**, Borhegyi Z, Szilágyi N, Freund TF, Varga V (2009) GABAergic neurons of the medial septum lead the hippocampal network during theta activity. J Neurosci 29:8094-8102 (latest published impact factor: 7.452)

Abstracts

1. Varga V, **Hangya B**, Szilágyi N, Borhegyi Z, Freund TF (2004) Firing pattern analysis of medial septal neurons. IBRO International workshop on neuronal circuits: from elementary to complex functions, Budapest, Hungary
2. Varga V, **Hangya B**, Szilágyi N, Borhegyi Z, Freund TF (2004) Analysis of septo-hippocampal information flow. 33th annual meeting of Society for Neuroscience in San Diego, USA
3. Varga V, Borhegyi Z, **Hangya B**, Szilágyi N, Freund TF (2005) Firing pattern analysis of the HCN1 pacemaker ion channel expressing neurons in the medial septum in vivo. 11th Meeting of the Hungarian Neuroscience Society, Pécs, Hungary
4. Varga V, Borhegyi Z, **Hangya B**, Szilágyi N, Freund TF, (2005) Anatomical and electrophysiological characterization of HCN1-expressing neurons of the medial septum. Gordon Research Conferences, Inhibition in the CNS, New London, USA
5. Borhegyi Z, Varga V, **Hangya B**, Szilágyi N, Freund TF (2005) The role of medial septal HCN1 immunoreactive neurons in the regulation of hippocampal

theta rhythm. 35th annual meeting of Society for Neuroscience in Washington DC, USA

6. Varga V, **Hangya B**, Kránitz K, Borhegyi Z (2005) HCN-immunoreactive neurons in the medial septum: possible pacemakers of hippocampal theta rhythm. Pharmacology Seminar at School of Pharmacy, University of London, UK
7. Borhegyi Z, Varga V, **Hangya B**, Szilágyi N, Freund TF (2006) The role of medial septal HCN1 immunoreactive neurons in the regulation of hippocampal theta rhythm. IBRO International Workshop on Regulatory mechanisms of synaptic transmission in the central nervous system, Budapest, Hungary
8. **Hangya B**, Borhegyi Z, Freund TF, Varga V (2006) Directionality of communication in the septo-hippocampal system. IBRO International Workshop on Regulatory mechanisms of synaptic transmission in the central nervous system, Budapest, Hungary
9. Varga V, **Hangya B**, Kránitz K, Shigemoto R, Freund TF, Borhegyi Z (2006) Physiological parameters distinguishes HCN1-immunoreactive neurons in the medial septum. FENS 5th Forum of Europian Neuroscience, Vienna, Austria
10. **Hangya B**, Borhegyi Z, Freund TF, Varga V (2006) Directionality of interaction in the septo-hippocampal system. FENS 5th Forum of European Neuroscience, Vienna, Austria
11. **Hangya B**, Varga V, Freund TF, Borhegyi Z (2007) Analysis of interaction between medial septum and hippocampus. 11th Meeting of the Hungarian Neuroscience Society, Szeged, Hungary
12. **Hangya B**, Varga V, Borhegyi Z, Freund TF (2007) Information flow in the septo-hippocampal system. PhD Conference of the Semmelweis University, Budapest, Hungary
13. **Hangya B**, Varga V, Freund TF, Borhegyi Z (2007) Analysis of interaction between medial septum and hippocampus. 37th annual meeting of Society for Neuroscience in San Diego, USA
14. **Hangya B**, Borhegyi Z, Freund TF, Varga V (2008) An information theoretical approach to analyze interaction between two neuronal networks. PENS Hertie Winter School, Obergurgl, Austria

List of other publications

Articles

1. Jelinek I, László V, Buzás E, Pállinger É, **Hangya B**, Horváth Z, Falus A (2007) Increased antigen presentation and Th1-polarization in genetically histamine-free mice. Int Immunol 19:51-58. (impact factor: 3.290)

Abstracts

1. László V, Jelinek I, **Hangya B** (2002) Increased in vitro antigen presentation in genetically histamine-free mice. 32nd Meeting of the Hungarian Immunology Society, Kaposvár, Hungary
2. László V, **Hangya B**, Jelinek I, Buzás E, Falus A (2002) Increased antigen presentation in genetically histamine free mice. 31st Meeting of the European Histamine Research Society, Eger, Hungary
3. Varga V, Kránitz K, **Hangya B**, Domonkos A, Freund TF, Borhegyi Z (2007) Very short latency, temporally focused responses of hippocampal interneurons to the stimulation of the median raphe nucleus. 37th annual meeting of Society for Neuroscience in San Diego, USA
4. **Hangya B**, Slézia A, Bokor H, Ulbert I, Varga V, Acsády L, Freund TF (2008) Semi-automatic burst detection in thalamic relay cells. IBRO International Workshop on Complex Neural Networks „From synaptic transmission to seeing the brain in action", Debrecen, Hungary
5. Slézia A, **Hangya B**, Ulbert I, Bokor H, Acsády L (2008) Influence of extrareticular GABAergic inhibition on higher order thalamic relays. IBRO International Workshop on Complex Neural Networks „From synaptic transmission to seeing the brain in action", Debrecen, Hungary
6. Plattner VM, Bokor H, Slézia A, Bodor ÁL, **Hangya B**, Deschenes M, Acsády L (2008) Convergence of ascending and descending driver afferents on the same thalamic relay cells in the rat. IBRO International Workshop on Complex Neural

Networks „From synaptic transmission to seeing the brain in action", Debrecen, Hungary

7. **Hangya B**, Czurkó A, Freund TF, Varga V (2008) Complementary Spatial Firing Pattern between Hippocampal Interneurons and Place Cells. PhD Conference of the Semmelweis University, Budapest, Hungary
8. **Hangya B**, Slézia A, Bokor H, Ulbert I, Varga V, Acsády L (2008) Burst identification in thalamocortical neurons by the means of hierarchical cluster analysis. FENS 6th Forum of European Neuroscience, Geneva, Switzerland
9. Slézia A, **Hangya B**, Bokor H, Ulbert I, Barthó P, Acsády L (2009) Differences in firing pattern of first order and higher order thalamocortical relays in anesthetized rats - burst properties and phase relationship to cortical EEG. 12th Meeting of the Hungarian Neuroscience Society, Budapest, Hungary
10. Stefanics G, **Hangya B**, Ulbert I, Lakatos P, Winkler I, Hernádi I (2009) Attentive anticipation modulates phase-entrainment of human delta EEG oscillations – a single trial analyis. 12th Meeting of the Hungarian Neuroscience Society, Budapest, Hungary
11. **Hangya B**, Varga V, Erőss L, Entz L, Fabó D, Ulbert I (2009) Exploring the propagation of human cortical slow waves: an information theory method. 12th Meeting of the Hungarian Neuroscience Society, Budapest, Hungary
12. Varga V, Domonkos A, Borhegyi Z, **Hangya B**, Freund TF (2009) Glutamate is involved in mediating the fast activation of hippocampal interneurons in response to median raphe stimulation. 12th Meeting of the Hungarian Neuroscience Society, Budapest, Hungary
13. **Hangya B**, Varga V, Erőss L, Entz L, Fabó D, Tihanyi B, Freund TF, Ulbert I (2009) Exploring the propagation of human cortical slow waves: an information theory method. PhD Conference of the Semmelweis University, Budapest, Hungary

Acknowledgement

First of all I have to thank to my supervisors, Drs. Viktor Varga and Zsolt Borhegyi for their invaluable help and support during my work as a student research assistant and subsequently as a PhD student. I thank Prof Tamas Freund for providing me the possibility to work in the Laboratory of Cerebral Cortex Research of the Department of Cellular and Network Neurobiology in the Institute of Experimental Medicine of the Hungarian Academy of Sciences. (The work was supported by the grants OTKA K60927, the Howard Hughes Medical Institute and NIH MH54671; Viktor Varga was János Bólyai Research Fellow.) I thank to Dr. Nóra Szilágyi (Department of Physiology and Neurobiology, Eötvös Loránd University, Budapest, Hungary) for her initial help in the implementation of wavelet and mutual information calculations.

Additionally, I would like to thank Drs. Szabolcs Káli, László Acsády, Andrea Slézia, Hajnalka Bokor, Péter Barthó, Edit Papp and all other members of the Department of Cellular and Network Neurobiology and the participants of the Budapest Computational Neuroscience Forum for the lively scientific discussions and for creating an extremely inspiring environment. I thank Ms. Katalin Iványi, Mrs. Katalin Lengyel, Mrs. Emőke Szépné Simon, Mr. Győző Goda and the administrators of the János Szentágothai School of Ph.D. Studies for the excellent technical assistance.

Finally, I would like to thank the continuous support of my family, particularly my wife, Anna Hangyáné Benkovics; my parrents, Márta Hangyáné Szalkai and László Hangya; my uncle, István Szalkai and my brothers, Miklós Hangya and Dániel Hangya.